UNCLASSIFIED

AD 403890

Reproduced
by the

DEFENSE DOCUMENTATION CENTER

FOR

SCIENTIFIC AND TECHNICAL INFORMATION

CAMERON STATION, ALEXANDRIA, VIRGINIA

UNCLASSIFIED

NOTICE: When government or other drawings, specifications or other data are used for any purpose other than in connection with a definitely related government procurement operation, the U. S. Government thereby incurs no responsibility, nor any obligation whatsoever; and the fact that the Government may have formulated, furnished, or in any way supplied the said drawings, specifications, or other data is not to be regarded by implication or otherwise as in any manner licensing the holder or any other person or corporation, or conveying any rights or permission to manufacture, use or sell any patented invention that may in any way be related thereto.

CATALOGED BY ASTIA
AS AD NO. 403890

63-3-4

ASD-TDR-62-1044

CARBON ELECTRODE FUEL CELL

TECHNICAL DOCUMENTARY REPORT NO. ASD-TDR-62-1044

March 1963

DDC
RECEIVED
MAY 17 1963
TISIA A

Directorate of Aeromechanics
Aeronautical Systems Division
Air Force Systems Command
Wright-Patterson Air Force Base, Ohio

403890

Project No. 8173, Task No. 817303

(Prepared under Contract No. AF 33(616)-7256 SA/5
by Union Carbide Consumer Products Company,
Cleveland, Ohio)

NOTICES

When Government drawings, specifications, or other data are used for any purpose other than in connection with a definitely related Government procurement operation, the United States Government thereby incurs no responsibility nor any obligation whatsoever; and the fact that the Government may have formulated, furnished, or in any way supplied the said drawings, specifications, or other data, is not to be regarded by implication or otherwise as in any manner licensing the holder or any other person or corporation, or conveying any rights or permission to manufacture, use, or sell any patented invention that may in any way be related thereto.

Qualified requesters may obtain copies of this report from the Armed Services Technical Information Agency, (ASTIA), Arlington Hall Station, Arlington 12, Virginia.

This report has been released to the Office of Technical Services, U.S. Department of Commerce, Washington 25, D.C., in stock quantities for sale to the general public.

Copies of this report should not be returned to the Aeronautical Systems Division unless return is required by security considerations, contractual obligations, or notice on a specific document.

B

27-648M, 200, 5-8-63

FOREWORD

This report was prepared by the Union Carbide Consumer Products Company, Cleveland, Ohio under Contract No. AF 33(616)-7256 SA/5. This contract was initiated under Project No. 8173, "Energy Conversion Technology", Task No. 817303, "Fuel Cells". The work was administered under the direction of the Flight Accessories Laboratory, Directorate of Aeromechanics, Aeronautical Systems Division with Mr. R. L. Kerr acting as project engineer.

This report covers work conducted from April, 1961 to December, 1962.

ABSTRACT

The work summarized in this report supplements and extends effort previously described in Report ASD-TR-61-342 (ASTIA AD No. 271971) "Experimental Properties of Carbon Electrode Fuel Cells". Experimental studies have been conducted on methods of water removal in space, problems of zero-gravity operation, improved construction materials and techniques and improvement of auxiliary components. Based on these studies, a 500 watt net electrical output fuel cell battery has been assembled and tested. The battery was assembled from 4 - 140 watt modules with necessary auxiliaries and controls for fully automatic operation. The complete system was operated for 25 days continuous operation, with testing of individual modules extending from 735 hours to 2830 hours. The gross power of the 500 watt battery was 535 watts initially and 520 watts after 720 hours. Auxiliary power requirements varied from 34 watts to 28 watts. Gross thermal efficiency (based on the high heat of combustion of hydrogen) for the system varied from 55.3 per cent initially to 51 per cent at 720 hours. Results of the experimental program are applied to the conceptual design of a flyable fuel cell power system.

TABLE OF CONTENTS

LIST OF FIGURES

LIST OF TABLES

Carbon Electrode Fuel Cell

Technical Documentary Report No. ASD-TDR-62-1044
Project No. 8173, Task No. 817303
Contract AF 33(616)-7256 SA/5

I. Summary of Program

1. Objectives

A. Initial Contract Effort

The original contract AF 33(616)-7256 was awarded by the Aeronautical Systems Division, Wright-Patterson Air Force Base, Ohio,to Union Carbide Consumer Products Company, Edgewater Development Laboratory at Cleveland, Ohio on 31 March 1960. The objective of the program was to package and test for 50 hours a 500 watt state-of-the-art carbon fuel cell battery to determine adaptability of the UNION CARBIDE Fuel Cell to Air Force aerospace requirements.

The results of this effort covering the development and final contractual 50 hour plus test were submitted to United States Air Force, Aeronautical Systems Division. It was published and distributed by United States Air Force, Aeronautical Systems Division under the title "Experimental Properties of Carbon Electrode Fuel Cells" ASD-TR-61-342 (ASTIA AD No. 271971).

The original contract was extended to develop and incorporate advances in the state-of-the-art into a 500 watt test battery to demonstrate long-term unattended laboratory performance.

B. Contract Extension Effort

The objectives of Contract AF 33(616)-7256 SA/5 extension were to:

(1) Conduct initial sustained performance tests to identify the major problems revealed by long-term operation of multicell batteries;

(2) Incorporate design changes resulting from the initial sustained performance testing;

(3) Conduct final sustained performance tests on the modified system (500 watt 28 volt long-term);

(4) Recommend design changes necessary to adapt the UNION CARBIDE Fuel Cell to space, and

---

Manuscript released by authors November 1962 for publication as an ASD Technical Documentary Report.

(5) Design a 500 watt 28 volt power system using carbon electrode fuel cells compatible with a hostile space environment.

In parallel with the above program, development work was conducted on problems revealed by the basic program and later disclosed in the second phase development. These included:

(1) Space vacuum water evaporation;

(2) Leakage current phenomenon;

(3) Electrolyte flow in modules;

(4) Framing materials and techniques;

(5) Cell leakage;

(6) Electrolyte pump improvement and optimization;

(7) Electrode thickness reduction;

(8) Bubble control at '0' gravity;

(9) Cryogenic fuel supply;

(10) Transpiration of water vapor, and

(11) Electrolyte contamination.

Effort under contract extension AF 33(616)-7256 SA/5 covered two distinguishable types of work: (a) Engineering study on the laboratory bench of critical component problems, such as water removal, electrolyte flow patterns, pump design, bubble removal, etc., and (b) design, construction and operational testing of the 500 watt test battery. In view of the lead time required to design and procure components for the 500 watt test battery, not all of the engineering advances in state-of-the-art achieved in the engineering study could be incorporated in the test battery. As a result, the state-of-the-art acquired through the present contract effort goes beyond the type of performance demonstrated in the 500 watt test battery. In particular, the engineering study has demonstrated the feasibility of water removal via the gas streams, permitting the collection and storage of water on board and eliminating the need for KOH makeup as was practiced in the 500 watt test. Analysis of test data has led to design changes in the electrode frames and modules which will increase the reliability of future fuel cell batteries. Problems of electrolyte contamination, leakage, electrode wetting, frame materials, electrode framing stresses and others have been identified and solved during the contract program and will greatly improve the performance of future systems. A new type of completely sealed electrolyte pump has been designed and tested for over 3000 maintenance-free hours, test still in progress, and is now available for future systems.

On the basis of these engineering advances which are detailed in the body of this report, it has been possible to establish the conceptual design of a space-flyable UNION CARBIDE Fuel Cell system. In a 100 watt size, as might be appropriate for a preliminary space test, the total system will weigh less than 75 pounds and occupy less than 2 cubic feet. Enough cryogenic fuel can be included for one week of operation at an average power of 100 watts, with excursions for experimental purposes to higher and lower powers under fully automatic controls. In a nonredundant design, the

reliability (based on the observed performance of cells and batteries studied in the present contract) for such an experimental module is 0.99 for a duration of 8 orbits and approximately 0.89 for a period of one week.

Further design studies based on data acquired in the present contract show that a future 500 watt battery including fuel and oxidant for 7 days' operation should weigh less than 200 pounds and occupy less than 9 cubic feet for a nonredundant design. By incorporating suitable redundancy (e.g., 1.5) in the battery design for a 6 volt system, a reliability of about 0.99999 for the battery itself can be predicted for a period of two weeks, assuming performance similar to that recorded during the present contract.

Sufficient engineering information has been acquired during the course of Contract Extension AF 33(616)-7256 SA/5 to allow scheduling of a flight test of a 100 watt prototype of the UNION CARBIDE Fuel Cell in 1963, with operation of a practical 0.5 to 2 kw power plant feasible in 1964.

2. Technical Approach

The broad definitions of the Air Force, Aeronautical Systems Division Phase II Objectives were selected to permit an orderly program of development and investigations based on problems known at the time of Phase II funding, with provisions for optimization of the distribution of effort as required to solve problems disclosed during the development effort.

Effort under Contract Extensions AF 33(616)-7256 SA/5 has covered the following general studies.

(1) The performance of single cells and electrodes has been studied to define more accurately the proper conditions (of temperature, gas and electrolyte flow rate, current density, etc.), for use in the design of the required 500 watt power system.

(2) The design of the electrode frames has been studied to optimize gas and electrolyte flow distributions, together with attention to problems of simple and reliable manufacturing processes, freedom from leakage or gas mixing, adequate strength and thermal stability.

(3) Materials of construction have been selected and tested to permit reliable and effective production of injection molded frames, with particular attention to problems of cold flow, thermal distortion, hoop stress, impact strength and thoughness.

(4) Techniques of bonding porous carbon to plastic have been studied to develop methods of producing rugged gas tight joints capable of withstanding vibration and shock.

(5) Studies of fuel cell module performance during the course of Contract AF 33(616)-7256 revealed a rate of anode wetting higher than that predicted by earlier single cell test data. Effort was supplied under the present contract extension to identify and eliminate the source of this extraordinary wetting, which was found in part to be related to establishing proper temperature and relative humidity of the input hydrogen gas. Electrodes for

the AF/ASD batteries are cut from standard 12" x 14" production size fuel cell electrodes to a size of about 5-1/2" x 6", yielding 4 electrodes per original plate. The outer edge of the 12" x 14" plate is inactive, since the plate is held by the edges during processing. This results in at least one inactive edge on each of the final AF/ASD electrodes, which was found during the experimental program to be highly susceptible to wetting. The difficulty was alleviated by coating the inactive edge with epoxy cement, preventing electrolyte contact with inactive carbon. This problem could be corrected in future electrode manufacture by redesign of the production mold so that the inactive edge would not be included in the cut electrode.

(6) Studies were conducted on the physical and electrochemical properties of carbon electrodes as a function of electrode thickness. It was found that 0. 187 inch is the minimum thickness consistent with good mechanical strength at the present state-of-art, based on techniques developed for application to the AF/ASD type fuel cell battery. On the basis of this work, in reducing the nominal electrode thickness from 0. 250" to 0. 187", the design weight of a one kilowatt battery will be reduced 9 lbs. Further reduction in thickness to 0. 125" appears to be a reasonable development goal for "standard" baked carbon electrodes. Research work supported on Company funds in parallel with the present contract shows promise of yielding tough, flexible electrodes as thin as 0. 015"-0. 020" which will become available for future ASD batteries.

(7) The engineering design of 18-cell fuel cell modules was studied to optimize module performance. Particular attention was devoted to uniformity and reproducibility of electrolyte and gas flow patterns, using specially designed test modules. Design of the electrolyte manifolds was studied to minimize power loss resulting from electrolytic conductance through the manifolds, while still retaining low pumping power requirements. Test modules were operated using both series and parallel flow of electrolyte and gases to select the optimum mode of operation for the 500 watt test battery.

(8) A complete fuel cell module was assembled and bench tested to select the proper parameters of temperature and current density for the 500 watt test.

(9) Based on the previously collected data, the 500 watt test battery was designed and constructed. Electrical load and control circuits were designed and installed. Instrumentation was provided for automatic data recording of all parameters capable of rapid variation, with frequent manual recording of all significant but slowly varying parameters.

(10) Laboratory studies were conducted to measure the rate of transpiration of water through porous media as a means of water removal. Two modes of operation were shown to be feasible: (a) Water can be removed from warm electrolyte by transpiration through a porous barrier to space vacuum. This provides a compact mode of operation, but involves the ejection of gas (water vapor) from the system which in some applications may be a disadvantage. (b) Water can be removed by transpiration through the carbon electrodes directly into the reactant gas streams. Water can be condensed from the circulating gases and stored for use, for example,as potable

water on a manned vehicle. The necessary auxiliary devices, specifically a condenser capable of zero-g operation, were not available to permit operation of the 500 watt test battery in this mode of operation.

(11) The problem of removing any fortuitous gas bubbles from the electrolyte was analyzed, resulting in establishing a design for a compact gas-electrolyte separator. Actual testing of the 500 watt test battery indicates that under proper conditions of operation such a separator may not be necessary. The decision of whether to incorporate a gas-liquid separator in the electrolyte loop for a future space power plant design will depend upon the total power level, power density, required lifetime and required reliability.

(12) Based on the water transpiration studies, system designs were developed for a space power plant operating on either of two modes: (a) rejection of water by evaporation to space; (b) rejection of water by transpiration into the circulating gas streams, with collection and storage of potable water aboard.

(13) A feasibility study based on engineering analysis and vendor's information was conducted to assess the problems of cryogenic reactant supply. It was concluded that a supercritical cryogenic supply of hydrogen and oxygen is suitable for space application, but the lead-time and engineering cost of the cryogenic supplies precluded trial of the 500 watt test battery in this mode of operation.

(14) The 500 watt test battery was placed in operation, and operated for a period of 735 hours as a complete system. Separate 125 watt modules were removed from the test stand and continued on test for periods up to 1730 hours, with operation of one module to 2832 hours at reduced performance.

II. Fuel Cell Design and Construction

1. Basic Cell Design

A bipolar electrode unit cell design made up with multiple components stacked together comprises the basic building block of the 500 watt formal test battery. Figure 1 (A) shows the various components of a unit cell.

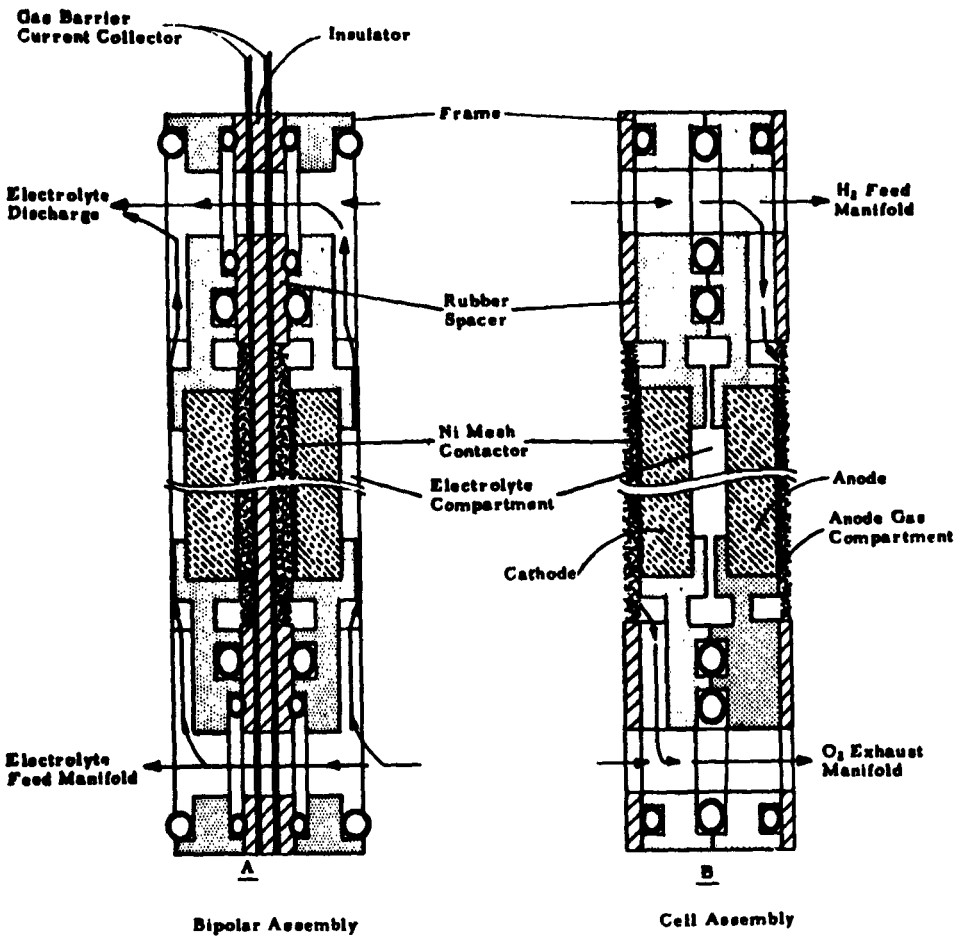

D-95

Figure 1 - Unit Cell Design

The bipolar electrode structure consists of two carbon electrodes, each having approximate dimensions of 1/4" x 6" x 6", surrounded by injection-molded polystyrene plastic frames. Appropriate passages and

porting were molded into the frame members to handle the necessary electrolyte, hydrogen and oxygen feed and discharge streams. The gas and electrolyte are sealed through the use of "O" rings placed around each port and each frame member. The framed electrode at the left of Figure 2

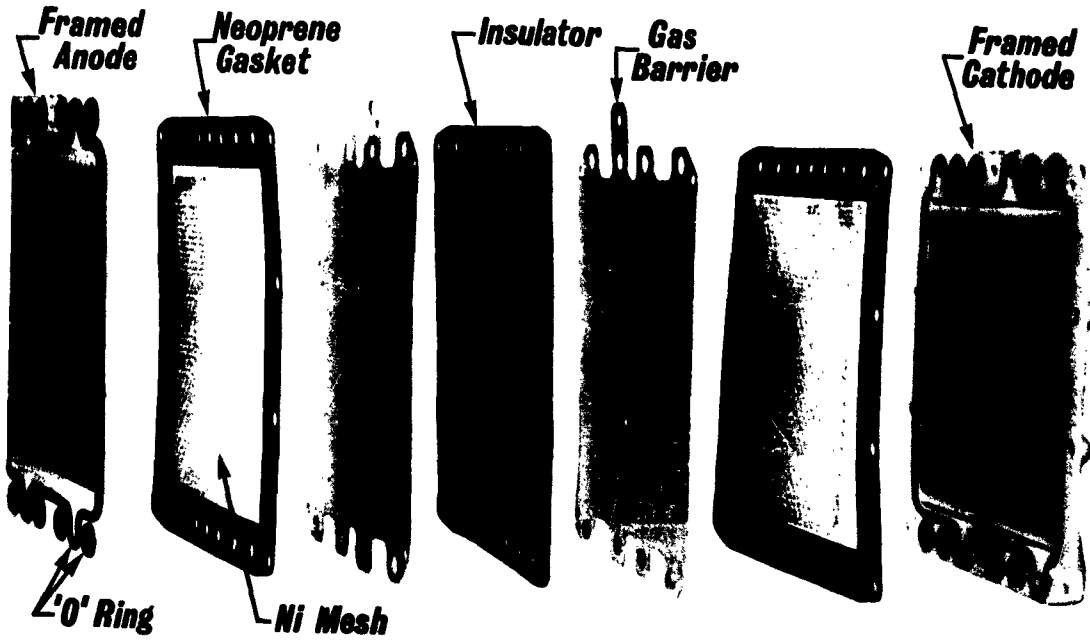

D-96

Figure 2 - Fuel Cell Components

shows the electrolyte face to which the electrolyte enters the cell through two small ports located inside of protruding loops in the large "O" ring, passes upward through a series of small slots and across the electrode face, then out an identical configuration at the top of the frame. The entry and exit holes visible in the frame form a manifold down the length of a multicell battery when a number of electrodes are placed together as a battery structure.

The second cell component appearing in Figure 2 is a nickel wire woven mesh, surrounded by a 1/16" thick neoprene rubber gasket. The nickel mesh provides a gas permeable electrical contact between the back of the carbon electrode and the metal gas barrier, separating the hydrogen from the oxygen gas. Improvement in current distribution across electrode surfaces and minimized contact resistance losses between the carbon electrode and metal mesh contactor was achieved by the application of a porous nickel coating to the electrode gas entry surface.

The gas barrier is a sandwiched assembly comprised of two nickel plated copper sheets separated by a rubber insulator. The sandwich is appropriately ported to permit gas and electrolyte flow to the cell, and

designed to avoid metal contact with the electrolyte. A woven nickel wire mesh contactor is located on either side of the gas barrier.

The entire assembly is held together in compression. The compressive forces seal the fluid compartments to prevent intermingling and leakage. The same forces achieve the necessary low resistance pressure contacts for electrical continuity from one electrode gas face through the metal mesh and gas barrier to the opposite electrode.

Six fluid ports shown in the right hand framed electrode of Figure 2 are located across both the top and bottom. From left to right the first and fourth port are common and carry hydrogen to the anode. Inerts and/or recirculated hydrogen exits at the bottom of the frame through the third and sixth ports, diagonally across the gas face of the electrode. Conversely, oxygen is fed to the cathode through the third and sixth port at the top and is discharged through the first and fourth port - bottom.

Both anode and cathode frames are identical, but when placed with gas faces toward each other as shown in Figure 1 (B) with a separating gas barrier each electrode is fed through separate gas ports without intermingling of the reactant gases.

Electrolyte flows in ports two and four at the bottom of the electrode frame and out the same ports two and four at the top.

The same general fluid flow exists in all cells.

A. Unit Cell Operation

The electrochemical operation of the basic carbon electrode cell is described with reference to Figure 1 (B). Hydrogen gas enters through the gas manifold shown at the top of the cell and is distributed via a porous nickel mesh contact member to the gas surface of the anode. Excess hydrogen gas for recirculation exits from the cell via a cell manifold which is not shown, occurring in a cell section parallel to the plane section shown.

Oxygen gas enters the cell through a manifold not shown (in a plane section parallel to that shown), is distributed to the cathode surface via the nickel mesh contact member shown, and exits from the cell through the oxygen exit manifold shown at the bottom of the cell. Electrolyte is circulated through the cell via electrolyte inlet and exit ports, which are shown more clearly in the section chosen to illustrate the bipolar assembly, Figure 1 (A).

Hydrogen in the anode gas compartment diffuses through the porous carbon electrode to a three-phase reaction zone located close to the electrolyte-carbon interface. The hydrogen gas is adsorbed on a catalyst surface and dissociated to adsorbed hydrogen atoms. The hydrogen atoms then react with hydroxyl ions in the electrolyte, releasing an electron which is conducted through the carbon electrode, the porous nickel contact member, and the metallic intercell gas barrier to the adjoining cell and thus eventually to the negative terminal of the battery. The corresponding electrode reaction is

$$H\ (adsorbed) + OH^-\ (aq) \rightarrow H_2O + e^-$$

The water produced in the anode reaction may be retained in the electrolyte, simply diluting the KOH, as occurred under the operating conditions of the AF/ASD 500 watt test battery. At higher temperatures and higher gas flow rates, all of the water produced can be transpired through the anode and be swept away by the recirculating gas.

The oxygen in the cathode gas compartment diffuses through the porous cathode to a three-phase reaction zone located close to the carbon-electrolyte interface. The oxygen is adsorbed and reacts in molecular form, producing peroxyl ions. In the presence of the catalysts used, the peroxyl ions decompose as rapidly as they are produced, forming hydroxyl ions and additional oxygen which immediately enters the electrode reaction.

The electrode reactions are:

$$2e^- + O_2\ (adsorbed) + H_2O \rightarrow HO_2^- + OH^-$$

$$2HO_2^- \rightarrow 2OH^- + O_2\ (adsorbed)$$

Since any oxygen produced through peroxyl ion decomposition is consumed in the over-all electrode reaction, the net coulombic efficiency is nearly 100 per cent. The electrons entering the cathode reaction are drawn from the carbon electrode, being supplied by the nickel mesh contact member, the metallic intercell gas barrier, and thus (ultimately) the positive terminal of the battery.

The net cell reaction is

$$2H_2 + O_2 \rightarrow 2H_2O$$

The reversible EMF of the cell, for the conditions of temperature and concentration employed, is approximately 1.20 volts. In operation at the rated current density of about 9 amperes per cell, the on-load cell voltage of the AF/ASD type cell is about 0.8 volt.

The so-called electrochemical efficiency, therefore, is 0.8/1.2 = 67 per cent under the conditions of operation imposed by the 500 watt test.

The total heat of combustion of hydrogen gas, based on the formation of pure liquid water under standard conditions is 34.16 Kcal/g atom. The electrical equivalent of this heat at 9 amperes current is 13.3 watts. Since the cell delivers 9 amperes x 0.8 volt = 7.2 watts of electricity, the thermal efficiency, (based on the high heat of combustion) is 54 per cent. (See conversion of energy units in Table I.) The remaining 46 per cent of the fuel energy, 6.1 watts/cell in the present example, occurs as heat. Of this energy, 3.6 watts of heat result from operation at 67 per cent electrochemical efficiency rather than 100 per cent electrochemical efficiency; this energy loss can be divided further into two approximately equal parts arising from internal resistance (primarily of the electrolyte) and polarization. About 2 watts of heat result from the condensation of water at the 9 ampere rate of production. The remaining 0.5 watt of heat is released in the battery and results from the difference, $T\Delta S$, between the enthalpy and

TABLE I

FUEL CELL ($H_2 + O_2$ FORMING H_2O LIQ.)

Thermodynamic Energy Equation:

$Q = \Delta H + nfE_{Term.}$

where Q = K Cals.

ΔH = Standard heat of formation - H_2O (liquid) at 25°C = -68.3174 K Cals. per mole (heat evolved)

n = Electron change in reaction - in this case 2

f = Faraday - Coulombs (ampere seconds)

$E_{Term.}$ = Terminal Voltage

nfE = Watt seconds ÷ 3600 = Watt hours x 0.86001 = K Cals. x 3.9685 = B.t.u.

Thermodynamic Electrical Efficiency:

$$\frac{nfE_{Term.}}{\Delta H} \frac{\text{(watt-hrs.)} \times 0.86001 \times 100}{} = \text{(in this case) } 67.48383\ E_{Term.}$$

Thermal Efficiency of a Fuel Cell Operating at 0.80 volt Terminal

% Eff. = (67.48) (0.8 volt)

= 54 %

free energy of the cell reaction. In summary, at 9 amperes, 13.3 watts (total heat value of fuel) = 7.2 watts (net electrical output) plus 3.6 watts (resistive plus polarization loss) plus 2 watts (heat of condensation of water) plus 0.5 watt ($T\Delta S$ correction).

In operation of the fuel cell battery with transpiration of water vapor via the gas streams to an external condenser, the 2 watts of heat originating in the heat of condensation of water will be delivered to the external condenser rather than to the fuel cell battery, reducing the heat rejection load by 2/6.1 = 33 per cent. The bulk of the heat loss occurs in the electrolyte, since the electrolyte resistance and polarization losses are the largest terms in the heat loss equations.

B. Unit Cell Performance

A typical polarization curve of a unit cell is shown in Figure 3. The majority of 6" x 6" cell testing has centered around the 50 ASF current density level. A total continuous life performance of 2300 hours at 50 ASF has been achieved on single cell units constructed as described above without any attempt to preheat gases or remove water, except by electrolyte absorption and reconcentration. Nominal operating conditions were:

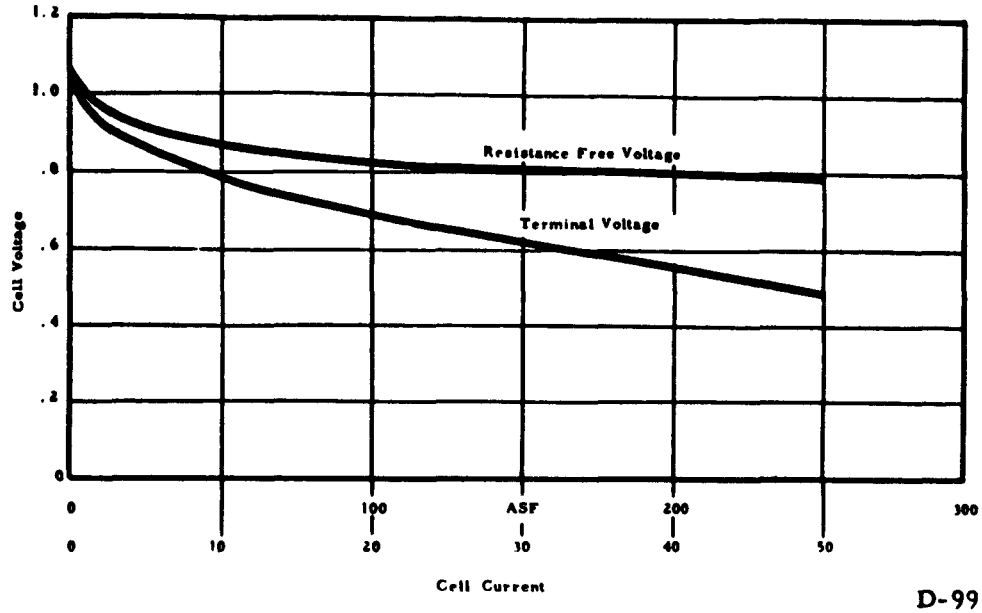

D-99

Figure 3 - Typical Polarization Curves 6" x 6" Plastic Framed Electrodes

1) Average cell temperature - 45°C;
2) Electrolyte concentration - 12 N aqueous KOH, and
3) Steady bubbled purge of gases w/o recirculation.

Additional detailed records of single cell test data are included in Appendix A.

C. Cell Construction Problems

Problems related to cell construction have arisen in the course of the program. Electrode framing material selection and frame adhesion to the electrode edges have been surmounted by development and testing. Extraordinary anode wetting experienced in long-term operation of cells has been eliminated. Progress has been made in electrode thickness reduction. The epoxy fillet seal of the plastic frame and electrode assembly plus temperature controlled inlet hydrogen effectively limits extraordinary anode wetting.

1) Electrode Framing

Carbon electrodes for low temperature operation (up to 120°F) have been successfully framed with injection molded polystyrene thermoplastics. Styrenes were selected for caustic resistance and molding ease. A rubber-modified styrene plastic with properties of high impact, high elongation and medium strength was selected with adequate success in the final performance test. This material was Union Carbide Plastics Company's high impact rubber-modified polystyrene TMD 2100.

Hoop stress was the principal problem associated with injection molding a thermoplastic around a flat carbon plate. The plastic has a high shrink factor induced by mold cooling. The carbon plate has a low coefficient of thermal expansion by comparison - about 1/20 of the plastic. The dimensional change of the carbon plate upon cooling from the injection mold temperature is practically nil. The plastic frame is constrained from shrinking and tensile stresses develop in the plastic. As a result, the carbon is compressively stressed across its width and length. It was necessary to select a frame material to yield low stressed parts.

The frame could not be over stressed in tension to cause (1) splitting at high stress points of the frame, or (2) buckling of the carbon in compression.

Figure 4 shows four samples of styrene framed electrodes. Sample A frame was used for electrodes in the final sustained performance tests. The other three samples illustrate the behavior of unsuitable materials.

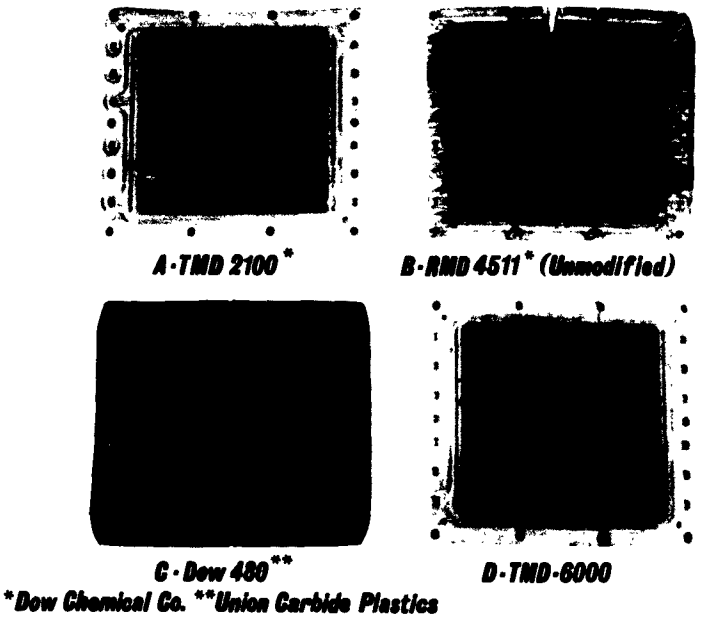

D-100

Figure 4 - Fuel Cell Carbon Electrode Frame Materials
Thermoplastic Polystyrenes

The comparison of the four materials is shown in Table II. The frame in Sample B is notch sensitive. The frame split was induced by a light tap from a sharp instrument. Frame cracking of Sample C was caused by high stress across the knit line of the plastic. The frame in D failed because of high stress across the bolt hole.

TABLE II

COMPARISON OF STYRENE MATERIALS USED FOR ELECTRODE FRAMING

	Sample	A Extra High Impact Rubber Modified TMD 2100	B High Strength Unmodified RMD 4511	C Extra High Impact Gen. Pur. Rub. Mod. Styron 480	D High Impact Gen. Pur. Rub. Mod. TMD 6000
**	Source	UCC Plastics	UCC Plastics	Dow Chemical Co.	UCC Plastics
**	Tensile Strength - psi	4,000	11,000	3,500	3,900
**	Mold Shrinkage - in/in	.005	.004	.0045	.005
**	Elastic Modulus - psi in Tension	240,000	540,000	250,000	340,000
**	Working Stress - psi Based on Mold Shrinkage	1,200	2,160	1,125	1,700
**	Safety Factor	3.3	5.1	3.1	2.3
**	Impact Resistance Ft-lb/in of Notch ASTM D 256	8.0	0.55	7.0	2.0
**	% Elongation in Tension ASTM D 638	60	2.5	30	34
**	Deflection Temp. °F ASTM D 648 (Unannealed)	178	200	165	170
/	Elastic Recovery of 6x6 Frames After 500 hrs. Room Temp. Storage - in/in	.0016	.0006	.0013	*
/	Residual Stress After psi 500 hrs. of Storage Based on Elastic Recovery	363	324	325	*
/	Safety Factor with Storage 6x6 Frames	11	34	10.8	

*Values indeterminate for specific frames. Plastic either cracked or upset in tension at bolt holes.
**Manufacturers' Catalog Data.
/Actual measurements.

The table shows material in Frame A has less than half the tensile strength of the clear styrene in B but it is 30 times as extensible (to absorb hoop stress) and is almost 15 times as impact resistant.

The frame material in Sample C is closely comparable to material of A; it is only half as extensible but it was rejected in this application because of inability to achieve good joining of the plastic at the knit-lines. Material in Sample D has the same tensile strength as A but in this design the working stress is about 50 per cent greater. Hence a safety factor:

$$\text{Safety Factor, } \frac{\text{Tensile Strength}}{\text{Working Stress}} = \frac{3900 \text{ psi}}{1700 \text{ psi}} = 2.3 \ .$$

An estimate showed tensile stress due to the abrupt change in section at the two bolt holes along the frame length to be approximately three times the cross-sectional stress between holes. This would indicate the safety factor of the material should be at least greater than 3. Failure due to cracking in sample D was due to an over-stressed condition around the bolt holes at molding.

Higher safety factors are used in general design; however, the hoop stresses induced by molding a 6" x 6" electrode are maximum

immediately after molding but decay with time. If the injection molded electrode assembly survives the molding operation without failure from overstressing, it will relax its internal stresses with time. Factor of safety is 3.3 (only 10 per cent above estimated minimum) for material in Sample A at time of molding but achieves a factor of 11 after several hundred hours. Although TMD 4511 achieves a high safety factor after storage, it still remains relatively fragile - hence undesirable.

Attempts to anneal the strains in stressed thermoplastic frames have resulted in distorted parts. Elongation per cent of TMD 2100 is double that of TMD 6000 or Dow 480 and is sufficient to yield with shrinkage strains of mold cooling, thus achieving tolerably stressed parts. Present 6" x 6" electrode framing technique employing TMD 2100 polystyrene has produced highly reliable, mildly stressed parts for low temperature service.

2) Plastic to Carbon Bonding Problem

A secondary problem existed after solving the primary one of frame material selection. Intimate adhesion of the plastic frame to the carbon electrode peripheral edge was needed to prevent fortuitous leakage of electrolyte between the carbon electrode edge and the frame during service.

Simple injection molding of the plastic around the electrode did not wholly insure a complete and continuous bond of electrode and plastic. Loose carbon particles on the carbon edges acted much like mold-release dust and made the interface subject to separation. The practice of edge treatment prior to molding surmounted the problem.

Preheated electrodes were withdrawn from an oven singly and edge treated with a solvent dispersed polystyrene cement. This treatment accomplished a twofold effect: (1) it provided an intimate bond to the carbon pores of a 'tacky' film for the hot styrene to 'strike' into as it flowed in the mold, and (2) it functioned to tie-up loose carbon particles. Adhesive encapsulation of loose carbon particles avoids interference of the particles with the bond. Edge leakage from bonding was brought under control and attention was focused on leakage or abnormal wetting of electrodes due to other causes.

3) Elimination of Extraordinary Anode Wetting (Caustic)

Multiple tests made after edge bonding was brought under control showed anodes to still suffer a large degree of wetting while cathode wetting under normal discharge conditions was virtually eliminated.

Further tests and observations showed that anode wetting persisted although cathode wetting disappeared regardless of the fact that both electrodes are framed under identical conditions. This anode wetting was traced to at least two causes: (1) cold (room temperature) inlet hydrogen gas, and (2) exposure of unactivated anode edges to electrochemical action.

Compared with two other cell constructions anodes showed some similar wetting patterns. All anodes exhibited a wet pattern condition (highly caustic) on the gas faces of carbon electrodes around the inlet ports

particularly when they are fed with room temperature hydrogen. The severity of the wetting (apparently a migration of electrolyte to the gas face of the anode through fine pores) at the hydrogen faced port was significantly reduced by preheating the gas before admitting it onto the electrode face. The preheating was accomplished by placing a small nichrome wire coil in the hydrogen feed manifold of each battery. Parasitic power required to raise the inlet hydrogen temperature above the cell temperature was 10 watts for a 500 watt battery, or about 2 per cent parasitic power consumption - a quantity less than the electrolyte manifold leakage current losses.

Wetting of anodes was also traced to the presence of unactivated carbon zones at some edges of the anodes. This phenomenon was earlier confused with the frame bonding problem. However, after frame bonding and hydrogen preheating were brought under control, the wetting patterns occurring due to unactivated edge were clearly discernible. Existence and location of the unactivated zones were known. Masking and impregnation of epoxy cement into these zones eliminated wetting through them.

Anode wetting still occurs to a slight degree, but is a long-term phenomenon which under proper conditions of temperature and relative humidity does not appear to limit utility of the anode (for periods less than a few thousand hours). Further attention is being devoted to the problem for a clearer understanding of this behavior.

4) Thinner Electrodes

Present carbon electrodes are nominally 1/4" thick. Thinner electrodes are more desirable to reduce diffusion resistance of gas and vapor in and out of the electrode pores, and to reduce the amount of material (weight) required to package a cell.

Hoop stresses created by injection molding of electrode frames around 1/4" or 3/16" thick carbon fuel cell electrodes present no mechanical problems. However, hoop stress buckling of 1/8" carbon plates has limited present development of thinner plastic framed electrodes to 3/16". Present carbon electrode manufacture is yielding stock with approximately 80 per cent strength increase. One-eighth inch framed electrodes may be achieved in the near future. Parallel effort on framing materials and frame design has also led to designs with lowered hoop stress, reducing the stress to which a thin carbon electrode is subjected in assembly operations.

5) Contact Resistance

Current is transmitted from one electrode to another in a series-connected fuel cell of the Figure 1 design by means of pressure contact from the electrode gas face through the woven nickel mesh (second from left in Figure 2) and gas barrier to same members in the adjacent electrode.

The security and resistance level of contact is related to the resiliency of the woven Ni mesh. It was necessary to uniformly squeeze and confine the mesh to approximately 1/16" thickness to preserve good low resistance current-carrying ability.

Table III shows a relationship between pressure thickness and resistance for this particular nickel mesh of the 500 watt test battery cell construction. The nickel mesh is shown framed in Figure 2 by its 1/16" rubber gasket. Thickness of 1/16" chosen from Table III.

TABLE III

INFLUENCE OF PRESSURE ON THICKNESS OF THE NICKEL MESH CONTACT

Pressure psi	Compressed Thickness Inches	Contact Resistance Milliohms/in^2
Uncompressed Mesh*		
.5	.108	14.4
1.0	.102	9.0
1.5	.097	6.3
2.0	.095	4.5
2.5	.070	3.4
16.5	.015	2.0
Precompressed Mesh**		
.5	.080	15.0
1.0	.072	8.3
1.5	.059	5.7
2.0	.055	4.0
2.5	.052	3.5
16.5	.015	2.0

*Nickel mesh as received.
**Nickel mesh precompressed at 16 and 20 psi.

2. Battery Module

The fuel cell per se is a high current low voltage electrochemical device. High voltage fuel cell batteries are made by arranging several cells in series. The specific number of cells is governed by the required voltage at a particular level of current density. The basic cell design (Figure 2) provides for flexible assembly of multicell batteries (modules). The output voltage of a given battery may be adjusted by merely adding or subtracting cells.

A. Module Assembly and Design

Figure 5 illustrates the assembly of a module made up of 18 unit cells. The assembler is stacking the bipolar sandwiches on a simple stacking fixture. Each layer is fitted with the necessary gasketing "O" rings.

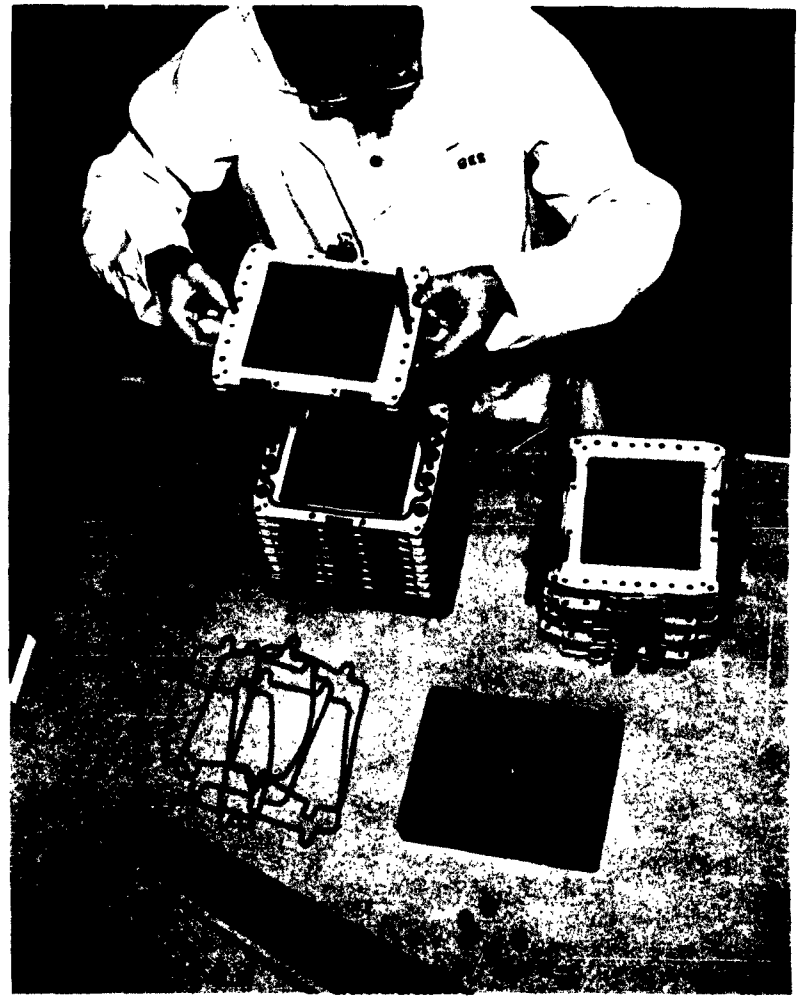

D-101

Figure 5 - Module Assembly

A fully assembled module is shown in Figure 6. The filter-press array of 18 cells is held together in compression by two plastic endplates and ten tie rods. Each tie rod is spring loaded to compensate for thermal expansion when the battery achieves normal operating temperature.

The endplates of the module are ported appropriately and fitted for fluid connections to deliver the gases and electrolyte to their respective header manifolds in the cell stack. Fluids are delivered to the proper cell compartments through the frame porting and manifold contours.

B. Module Operation

A module operates in essentially the same manner as a single cell except for the total voltage delivered at the terminals. Gas is fed to all electrodes simultaneously in a parallel manner as shown in Figure 1 (B).

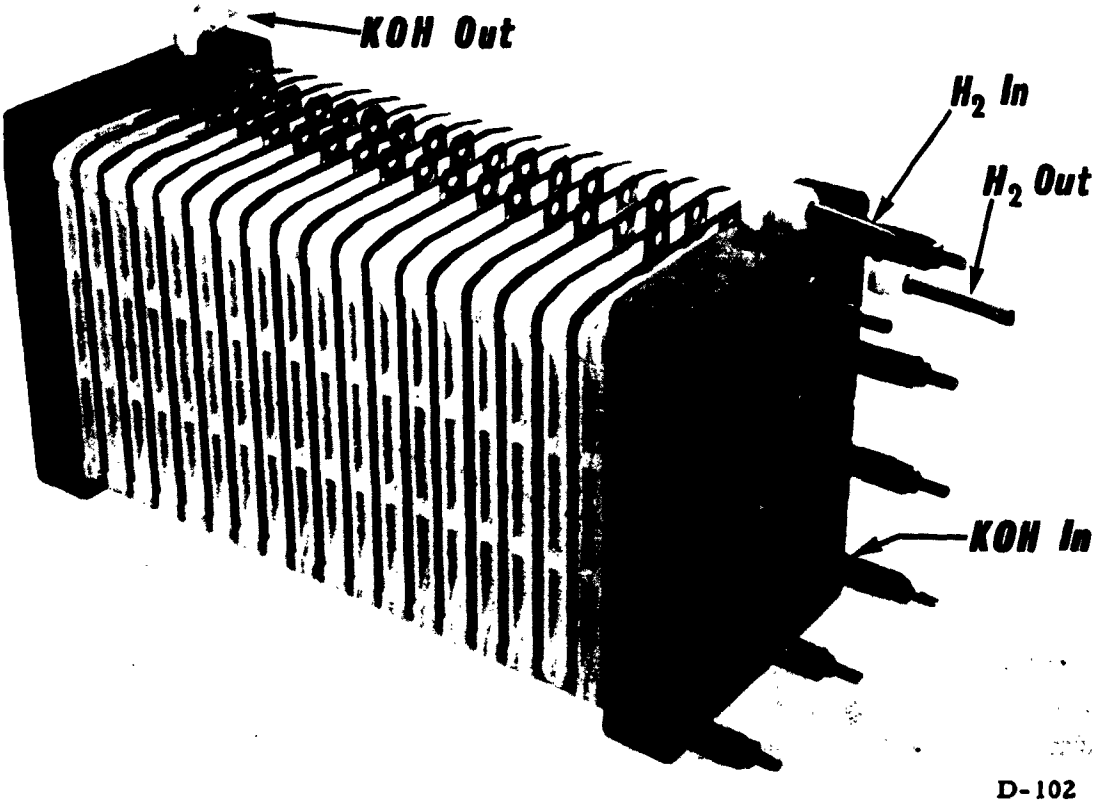

Figure 6 - 18-Cell Module

1) Fluid Flow in Modules

Fluid flow past each electrode in all cells of the module is similar. All cells in a module are fed with parallel streams of gas and electrolyte.

The total number of cells per module is limited by the ability to proportionally feed all cells adequately by a parallel manifolding of electrolyte and gases. Experience indicates that an 18-cell module (Figure 6) made up of the basic 6" x 6" cell described above approaches the limit for good proportionate feed of the battery fluids because of limiting manifold conditions for this particular cell frame design.

2) Electrolyte Circulation

Flow rate of KOH in a carbon fuel cell may vary widely without apparent ill effects. Flow of electrolyte sufficient to carry away excess heat of formation and control a 20°F temperature rise inlet to outlet through the battery is more than ample to eliminate effects of by-product water dilution.

A reasonable disproportionate flow from one cell to another in a parallel fed module is tolerable. Should the flow rate from one cell to the next differ, it does not necessarily follow that the condition is intolerable. If the cell having the least flow rate is adequately serviced, it follows that all those having higher flow rates will also be adequately serviced. Experience

has shown that carbon electrode fuel cells will operate over rather wide ranges of electrolyte concentrations, gas pressure, gas purities, and temperatures. However, if varying rate differences are on the order of 50 per cent, corrective design should be applied.

Measurements of cell temperature distribution throughout an 18-cell module with proper electrolyte flow do not vary more than 15°F from the end to the middle cells. Table IV shows a tabulation of actual gas barrier temperature values in two operating modules at 450 hours of operating life.

TABLE IV

CELL TEMPERATURE VARIATIONS

Modules # I and # 2 of 500 Watt Battery at 460 Hours of Life

Module # 1					Module # 2				
Module #	1,	Tab #	1* -	114°F	Module #	2,	Tab #	1* -	116°F
"	1	"	2 -	116°F	"	2	"	2 -	116°F
"	1	"	3 -	117°F	"	2	"	3 -	115°F
"	1	"	4 -	119°F	"	2	"	4 -	117°F
"	1	"	5 -	121°F	"	2	"	5 -	118°F
"	1	"	6 -	124°F	"	2	"	6 -	121°F
"	1	"	7 -	125°F	"	2	"	7 -	123°F
"	1	"	8 -	127°F	"	2	"	8 -	123°F
"	1	"	9 -	126°F	"	2	"	9 -	122°F
"	1	"	10 -	125°F	"	2	"	10 -	121°F
"	1	"	11 -	122°F	"	2	"	11 -	120°F
"	1	"	12 -	122°F	"	2	"	12 -	119°F
"	1	"	13 -	121°F	"	2	"	13 -	118°F
"	1	"	14 -	119°F	"	2	"	14 -	118°F
"	1	"	15 -	117°F	"	2	"	15 -	117°F
"	1	"	16 -	117°F	"	2	"	16 -	116°F
"	1	"	17 -	114°F	"	2	"	17 -	115°F

*Tab Numbers are Gas Barrier Tab Positions

Experience has shown that when serious disturbance of the electrolyte flow distribution occurs in a battery, the temperature of the gas barrier is a close indication of flow condition of the cell because its temperature is very nearly electrolyte temperature. Maldistribution of electrolyte reflects in a maldistribution of gas barrier temperatures.

C. Module Testing

Small multicell modules were tested to establish the load design and specifications for the 500 watt formal test battery. Cells used in the small modules were identical to those for the 500 watt battery, except for total number. Pretest modules contained less than 10 cells.

Pretest modular performance at 50 ASF (design current density for 500 watt battery) logged over 900 hours of continuous life with better than 90 per cent terminal voltage maintenance.

After 720 hours of continuous performance (target test period for 500 watt battery) a partial polarization curve was generated to determine average cell terminal voltage at higher current densities. This gave some indication of overload capacity of 50 ASF modules after a month of operation. Figure 7 shows the average cell polarization of the terminal voltage to be a straight line curve of normal Tafel slope and that 160 per cent of normal load at 757 hours is a comfortable overload condition.

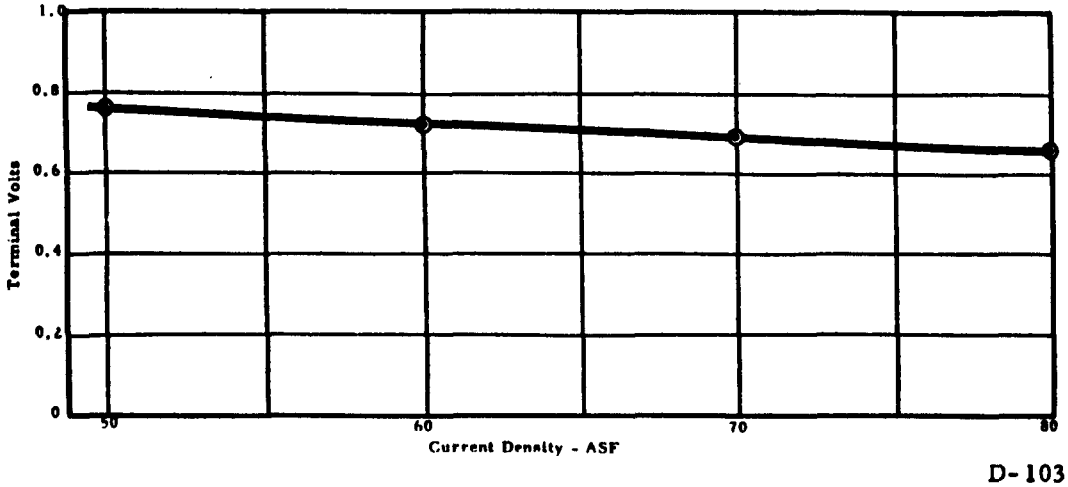

D-103

Figure 7 - Terminal Voltage vs Current Density. Avg. per Cell (3 Cell Module) after 757 Cont. Hrs. at 50 ASF. 6" x 6" Plastic Framed Cells.

Performance at 80 ASF in one other module achieved more than 475 hours of life without noticeable voltage depression. Unfortunately, this test was lost due to an electrolyte system malfunction.

D. Module Problems

Leakage current problems are peculiar to any multicell battery employing a common electrolyte system. Interconnection of the electrolyte from one cell to the next constitutes a high resistance, low current short. This problem can complicate storage of a fuel cell battery in the ready

condition because of fuel consumption due to the small current. Corrective measures have been employed to reduce leakage current during battery discharge and to interrupt leakage current during storage.

Two types of electrolyte flow through a multicell fuel battery are possible - parallel or series flow. In parallel flow, all cells are fed from a common supply header. In series flow, each cell is connected in series with each previous or succeeding cell. Parallel flow was judged to be more practical based on minimum pumping requirements.

A fuel cell module requires electrolyte recirculation to

1) overcome any local dilution which may occur in cell compartments,

2) maintain an average electrolyte system concentration, and

3) transfer heat from the battery when necessary caused by lowered efficiency or heavy overload conditions.

Power, cost and size considerations imply that for a given pumping requirement, a single pump employed for recirculation is more economical than several smaller pumps. All modules were serviced from a single pump in the 500 watt test system. Power expended for pumping was approximately 25 watts.

1) Leakage Current

Leakage current is caused by the flow of electrons (by virtue of the potential difference) from anode to cathode of a bipolar sandwich (Figure 1 (A)) through the electrolyte path common to both. The magnitude of the leakage current is a function of the port sizes of the interconnecting electrolyte loops. The cross-sectional area and the length of the connecting paths constitute the amount of resistance to the leakage current. The quantity of leakage current is minimized by employing port sizes just large enough to permit adequate flow through connecting electrolyte paths or tubes designed as long as practicable. The amount of leakage current in the present design is on the order of 0.3 to 0.5 amp depending upon the electrode position in the battery and upon the load it is carrying. An analysis of the leakage current associated with the modules used in the 500 watt test battery is contained in Appendix B.

Leakage current does not exist in single cells. A method of eliminating leakage current in a battery with common electrolyte is to disconnect all cells of the battery electrically. This has been provided in the present design. All cells can be disconnected simply without dismantling the battery.

Figure 1 (A) shows the assembly of the bipolar cell components. Anode to cathode contact can be eliminated by disconnecting the jumper bar across the two gas barriers which are shown insulated from each other. This interrupts any electrical circuit associated with the cell whether it be load current or leakage current. This operation can be used only for placing an activated module on complete open circuit as required for storage. It cannot be used to eliminate leakage current under load.

2) Parallel vs Series Electrolyte Flow in a Fuel Cell Module

Pumping power economy is the overriding consideration governing mode of electrolyte flow selected to service a fuel cell module. Series flow through each cell is one mode. Parallel flow is another.

Series flow in a multicell module is costly in terms of power. Total flow resistance is directly proportional to the number of cells in the module. The resistance to flow is cumulative as more cells are added to the battery.

Parallel manifolding of battery cells offers the least resistance to flow, if the manifolds insure adequate service.

If N is number of fuel cells in module, then for series flow of a fixed quantity of fluid flow, the flow resistance R

$$R \propto N$$

for parallel flow

$$R \propto \frac{1}{N} \quad .$$

Direct analogy to Ohm's and Kirchhoff's laws for parallel and series electrical resistances circuit can be applied.

Total flow resistance of the series flow battery is

$$R_s = r_{\text{cell } 1} + r_{\text{cell } 2} \cdots + r_{\text{cell } N} \quad .$$

Assume all flow resistances equal

$$R_s = r \cdot n \text{ cells}.$$

Total flow resistance R_p of parallel flow battery is:

$$\frac{1}{R_p} = \frac{1}{r \text{ cell}_1} + \frac{1}{r \text{ cell}_2} \cdots\cdots + \frac{1}{r \text{ cell } N} \quad .$$

Assume all flow resistance equal

$$\frac{1}{R_p} = \frac{N \text{ cells}}{r} \qquad R_p = \frac{r}{N} \quad .$$

For a given flow of liquid in and out of a 10-cell battery:

$$\frac{R_s}{R_p} = \frac{10\ r}{\frac{r}{10}} = \frac{100}{1} \quad .$$

Resistance of a series flow battery of 10 cells is 100 times that of a parallel fed battery. Parallel flow was employed in the 500 watt battery

modules. Manifold resistance of any parallel fed battery is assumed to be negligible in the above analysis.

Actual measurements of electrolyte flow versus pressure drop are compared on the graph of Figure 8. The pressure drop through the 18-cell

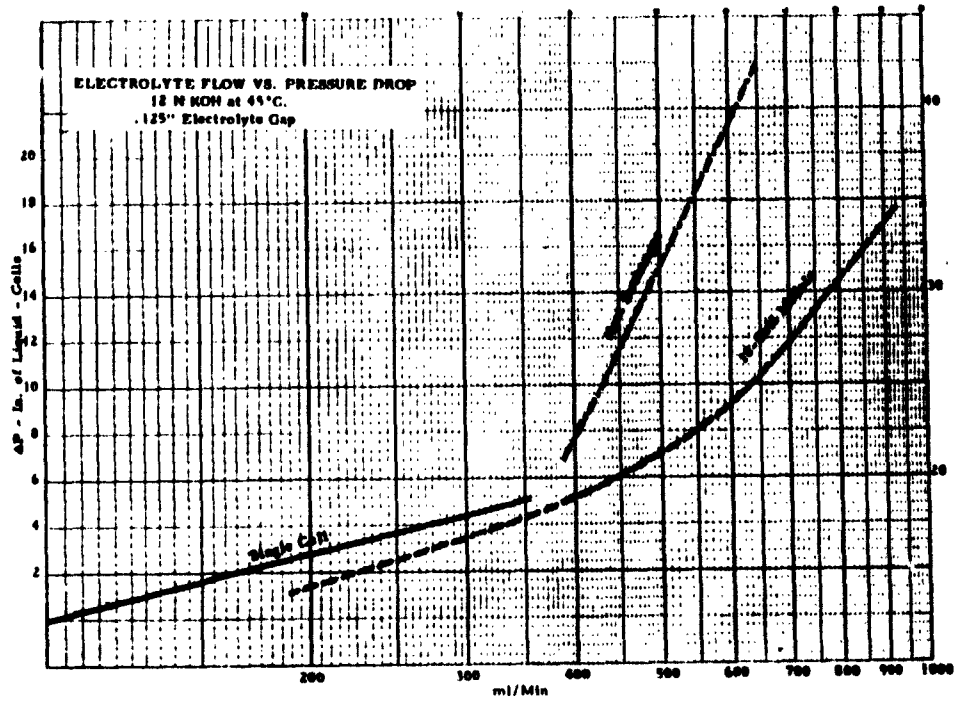

D-104

Figure 8 - 6"x 6" Plastic Framed Carbon Fuel Cell Battery Electrolyte

module is slightly less at low flow than through the single cell for a given flow rate below 400 ml/min. The differential implied in the above analysis does not exist in the comparative graphs. Manifold and port resistance is significant in the 18-cell battery. The increase in slope of the module flow resistance shows that the ports and manifolds of the module have controlling significance at flow rates above 550 ml/min.

Flow rate throughout the test was varied from approximately 550 ml/min to 850 ml/min/module or 30 to 50 ml/min per cell. This was sufficient to control temperature rise ΔT of 6 - 10°F.

III. Carbon Fuel Cell Battery Systems

At least three types of carbon fuel cell systems may be employed to meet various electric power requirements in space. Depending on mission restrictions, a single system or combination may satisfy power and ecological specifications.

All three systems are similar. They differ principally in the method of handling by-product water. Water of formation in a carbon fuel cell battery may be:

1) Absorbed in the electrolyte system;

2) Transpired from the system, condensed and stored outside the fuel battery, and

3) Evaporated by space vacuum through a porous system located in the recirculating electrolyte loop.

Absorption has been employed in the 500 watt test battery system to satisfy the 30 day operating requirement of the contract. Transpiration has been recently tested to survey its operating parameters and capabilities on a closed system basis. Evaporation has not yet been employed with an operating laboratory battery test system, but study of the porous septum design has been conducted.

1. System Design - 500 Watt Test Battery

The 500 watt carbon fuel cell battery system (Figure 9) was designed, built and tested for 30 days' operation to demonstrate self-sufficient unattended 30 day performance in compliance with contract specifications.

The portion of the contract covering this test specified that a fuel cell system resulting from the basic contract shall be modified to incorporate advances in the state-of-the-art and shall be made self-sufficient prior to the start of sustained performance tests.

The 500 watt system was designed to incorporate the absorption method for handling water of formation. The system has low temperature (up to 50°C),low pressure (less than 1 psig),utilizes commercially pure fuel, oxidant and highly concentrated aqueous potassium hydroxide electrolyte (47 per cent). These conditions were chosen to allow the battery every opportunity to demonstrate good performance over long-term loading with high reliability.

The system was composed of 5 main subsystems:

1) The 500 watt battery complex;

2) An electrolyte subsystem;

3) Gas subsystems;

4) Electrical load and control circuits, and

5) Data recording.

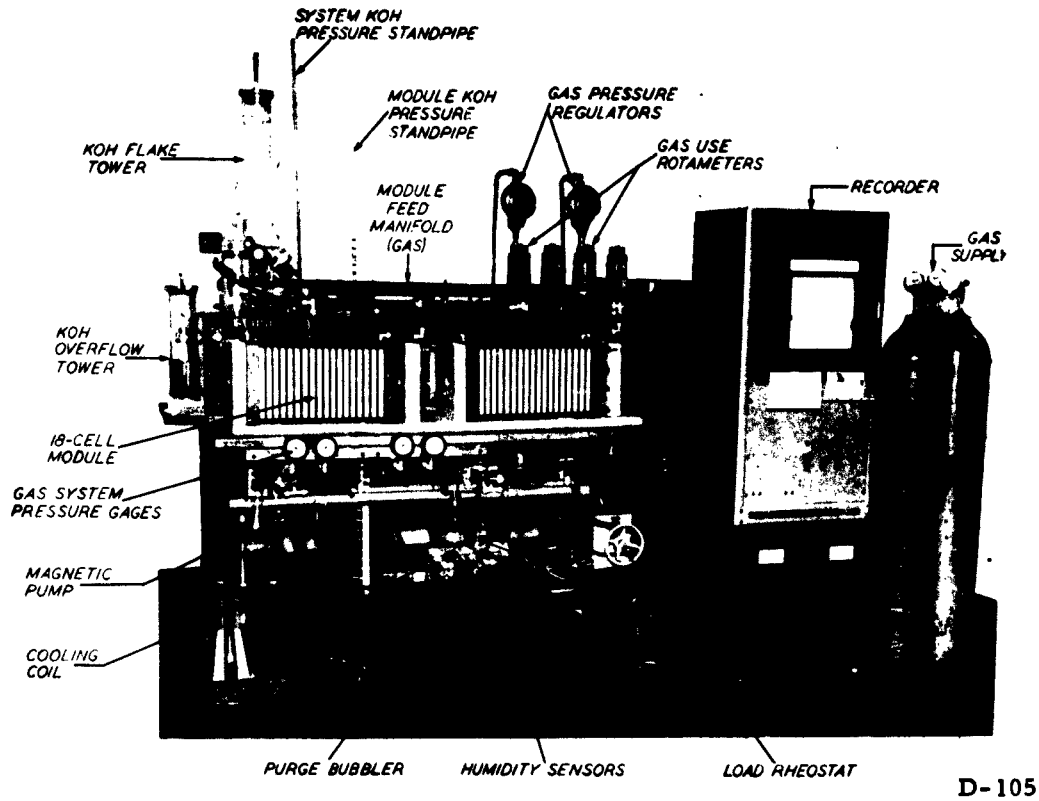

Figure 9 - 500 Watt Test Skid

A. The 500 Watt Battery Complex

Five hundred (500) watts of net power during the formal test were supplied to a carbon pile resistor by a 72-cell complex of 4 multicell modules containing 18 cells per module. Each module shared 25 per cent of the total load. The complex was wired electrically in a parallel series array.

Gas and electrolyte service to all modules was delivered by parallel feed and discharge manifolds. Figure 10 shows one module in the system (others deleted for clarity) with subsystem connections.

B. Electrolyte Subsystem

The electrolyte system of a carbon fuel cell battery functions to render electrochemical mobility to the action of the cells; to serve as a heat exchange medium when necessary; to aid vapor diffusion control of water through the porous electrodes into the gas systems; and to absorb by-product water if or when necessary.

The electrolyte system of the 500 watt battery functioned as the primary means of temperature control by excess heat rejection. It served to absorb essentially all water of formation. System electrolyte concentration preserved a water vapor pressure condition of 15 mm Hg on the average (18 per cent relative humidity within the battery proper) which is

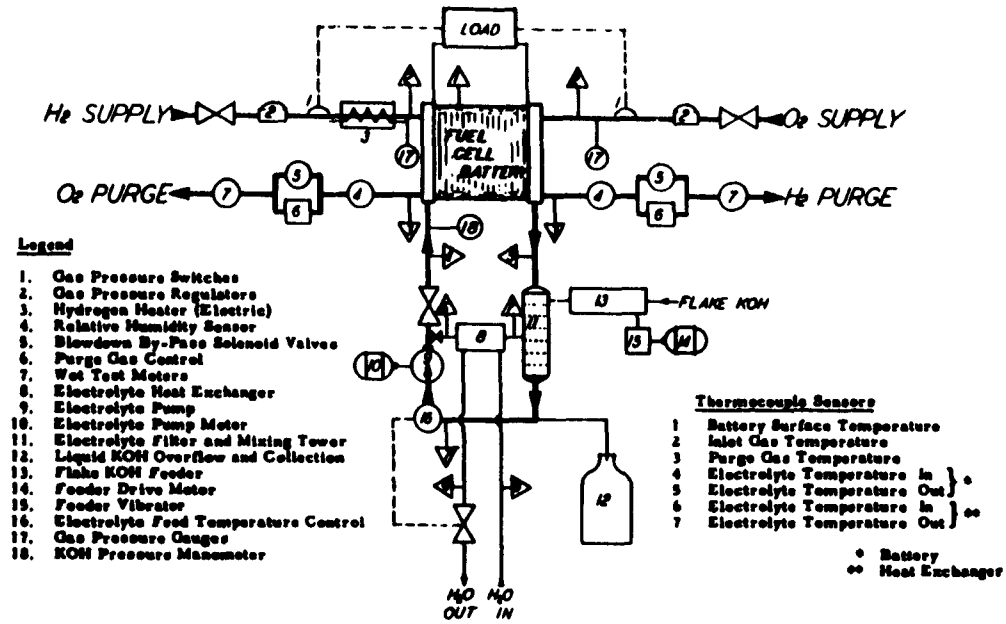

D-106

Figure 10 - Fluid System Schematic - 500 Watt Fuel Cell Battery System. Sustained Performance Test.

slightly less than the 18 mm Hg vapor pressure of the 12.5 N (47 per cent) aqueous KOH battery electrolyte at 45°C - small difference due to purge rate of gases.

Design of electrolyte system for the 500 watt sustained performance battery was restricted to materials chemically inert to KOH. Plastic materials were generously employed; nylon, rigid polyvinyl chloride, polystyrene and clear acrylics. No metals were in contact with electrolyte except a very small amount of nickel. Stainless steels were avoided categorically because of fortuitous trace-metal-poisoning of the electrode catalysts.

The diagram of the fluid system schematic of Figure 10 shows electrolyte entering one end plate of the battery module (single module shown for simplicity) and discharging at the other end plate through a manifold into the mixing tower. At this point, flake KOH was added once each half hour automatically from the hopper of the KOH feeder by means of a motor driven auger controlled by a program timer. Duration of the on-time for feed was selected on the basis of ampere-hour battery performance to reconcentrate electrolyte against dilution by water of formation. Appendix A shows the estimate of periodic flake addition to the 500 watt battery system to be 0.535 lb/hr. KOH flake was added in small increments to avoid any

wide swings in battery temperature due to heat of solution. Periodic data gathered on KOH concentration uniformity were taken directly from a hydrometer located in the mixing tower.

Electrolyte was drawn from the outlet of the mixing tower filter by the electrolyte pump and delivered to the feed manifold of the modules. Some of the KOH flow (approximately 20 per cent) was by-passed through the heat exchanger, cooled and recirculated back through the mixing tower. Eighty (80) per cent was circulated through the battery modules. Flow through modules was regulated manually by a valve.

1) Electrolyte Pump Optimization

The optimum pump for recirculating highly concentrated aqueous KOH in carbon electrode fuel cell batteries must:

a) Be highly efficient to minimize parasitic power required for pumping and maintain high over-all efficiency;

b) Not cause electrolyte contamination;

c) Be leakproof. KOH solutions are highly fugitive. Creepage past dynamic seals is prevalent, and

d) Be reliable. Overheating under load due to loss of recirculation may be intolerable. Pump failure must be less probable than battery failure. The pump shown in Figures 11 and 12 designed for the 500 watt sustained performance test has met most of these criteria. It has logged in

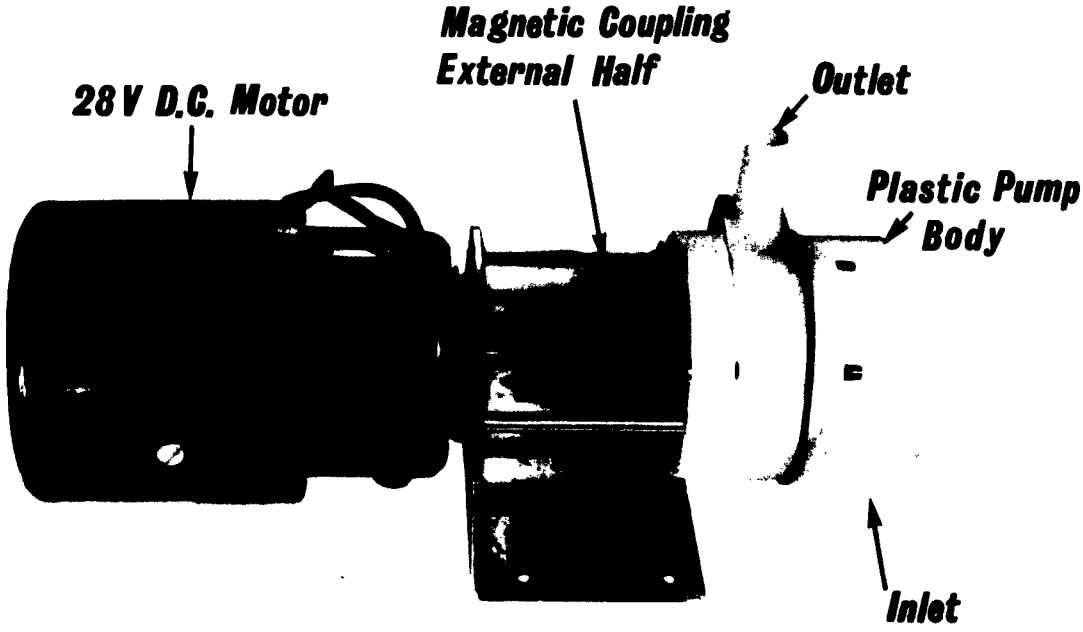

D-107

Figure 11 - Electrolyte Pump

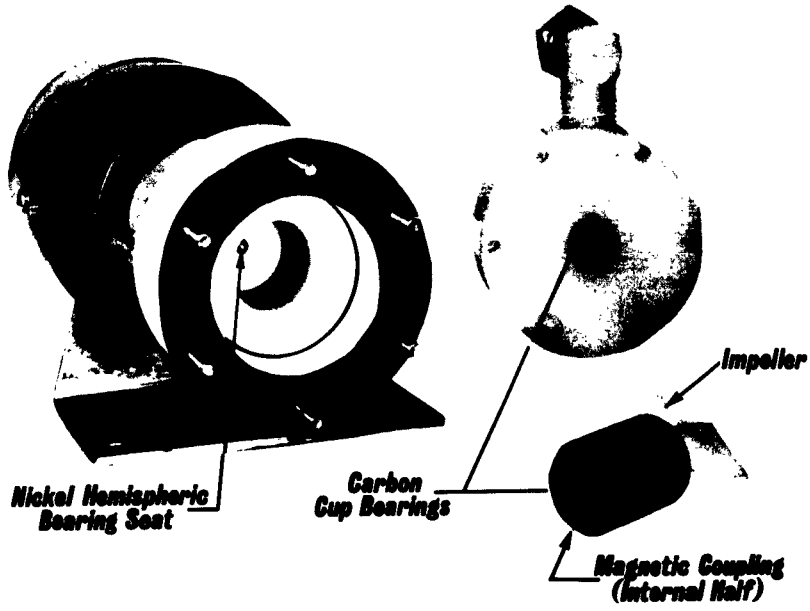

D-108

Figure 12 - Electrolyte Pump Components

excess of 3000 hours of service-free performance with negligible wear on the nickel- to graphite-bearing surfaces. Reliability of the pump approaches that of the drive motor itself, only long-term testing will confirm. The pump is thoroughly leakproof. It is d. c. motor driven through a magnetic coupling, thus dynamic seals are eliminated. A static gasket seal permits simple assembly. Contamination of electrolyte is avoided by employing all plastic parts except for the ceramic magnet, plus small carbon-to-nickel bearings. Some lubrication is provided by the recirculating caustic which also serves as coolant to the bearings of the impeller shaft. The operation of the pump unit has been a success.

One problem remains to be solved. Pump efficiency must be increased by proper redesign. Present over-all pump efficiency is less than 25 per cent. Not only does the pump design require improved efficiency but it must be miniaturized. Estimated pumping requirements for the 500 watt system were 5. 1 watts. Actual power expended for pumping was 20-25 watts during the formal 500 watt sustained performance test, 4 to 5 times the necessary requirement. An estimate of the pumping power requirement is in Appendix A.

A fuel cell module requires electrolyte recirculation to overcome any local dilution which may occur in cell compartments; maintain an average electrolyte system concentration; remove excess heat from the battery caused by lowered efficiency or heavy overload conditions.

Power, cost and size considerations imply that for a given pumping requirement, a single pump employed for recirculation is more economical than several smaller pumps. Therefore, it has been decided that all cells would be serviced from a single pump.

2) KOH Flake Feeder

Figure 13 shows the device employed on the 500 watt battery system to reconcentrate the electrolyte against dilution. The unit is constructed of clear plastic which is passive to the electrolyte. The nickel plated auger is the only metal part in contact with KOH.

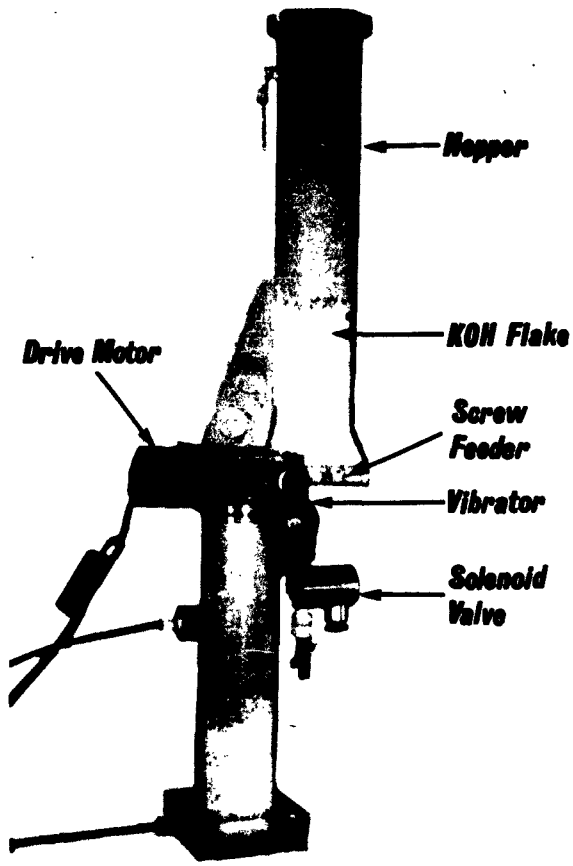

D-109

Figure 13 - Electrolyte Reconcentrator

The operation of the feeder is accomplished by simply transferring the flake from the hopper to the reconcentration tower by a slow turning auger. The maximum feed rate is 3000 g/hr. This rate will adjust against dilution for a fuel cell power system up to 11 kw or any portion thereof by proper setting. Control of feed rate is attained merely by adjusting the dwell period of a cam timer to a given portion of "on-time" per 1/4 hour to match the average current level of the battery.

3) KOH Heat Exchanger

The waste heat of the 500 watt battery which was not conducted away by ambient environment was rejected in a liquid to liquid shell and tube heat exchanger. Its outer shell was simply a 15 ft. length of 5/8" O. D. copper tube around a 3/16" O. D. polyethylene tube. Tap water passed through the copper shell and electrolyte recirculated through the polyethylene tube. Counter-flow of both liquids was employed for effective heat transfer. The rate of cooling water through the heat exchanger was controlled by an adjustable temperature regulator. The unit operated to modulate the flow of tap water to preserve a constant temperature at the sensing bulb located in recirculating electrolyte loop.

C. Gas Subsystems

1) Supply

Hydrogen and oxygen gases were fed to the battery from commercial high pressure tanks. Delivery of the gases at the operating pressure of the battery (15"W. C.) was done in two pressure stages - 2200 psi to 30 psi and 30 psi to 15" W. C. - with commercial pressure regulators. Gas bottles were connected in parallel to afford replacement of empties without test interruption. Pressure switches were employed to protect the battery modules. In case of gas supply depletion or failure, the pressure switches opened the load circuit of the battery.

All four modules of the 500 watt battery were manifolded in parallel similar to cell gas distribution in a module. Movement of gas through the modules was continuous at a low rate (10 per cent or more above use rate) to prevent excessive accumulation of inert gas impurities. Once per hour each module was blown down successively and separately on each gas.

2) Purge Method

It was felt that periodic flushing of the cell compartments with fresh gas at high rate for a brief period (30 sec. per hour per module) would create enough turbulence to guard against inert concentration in remote zones within a module from becoming excessive. This method of combined purge and blow-down was judged more than adequate to prevent inert build-up based on purge estimates for nominal commercial tank gas purities, but was employed to allow the fuel battery every chance to perform. The use of commercial tank gas had been substituted for cryogenic supply and, therefore, high purge rates of gas to ensure purity, so excessive purge was not chargeable to the 500 watt test battery performance. Battery performance was being demonstrated and not gas purge adequacy. Tolerable minimums of purge rate for a fixed battery design have yet to be established, and will vary with particular sizes of fuel cell batteries and gas supply sources. Theoretical purge rates vs equilibrium gas composition have been established for commercial H_2 and O_2.

The total gas usage in fuel cell operation under constant load is determined by the current output of the system and the purge rate required to maintain the gas concentration at desired levels. The purge rate

required is a direct function of the impurity content of the respective gases; typically 0. 5 per cent for commercial tank oxygen and 0. 05 per cent for commercial tank hydrogen. Material balances at steady-state conditions show the following relationship:

$$\% \text{ Inerts in System} = \frac{\% \text{Inerts in Feed Gas} \times \text{Feed Rate}}{\text{Purge Rate}}$$

where the feed rate equals the use rate plus the purge rate.

Using the inert concentration present in tank gas supplies, Figure 14 relating equilibrium gas composition to per cent purge based on electrochemical use rate has been developed. Here the influence of the impurity

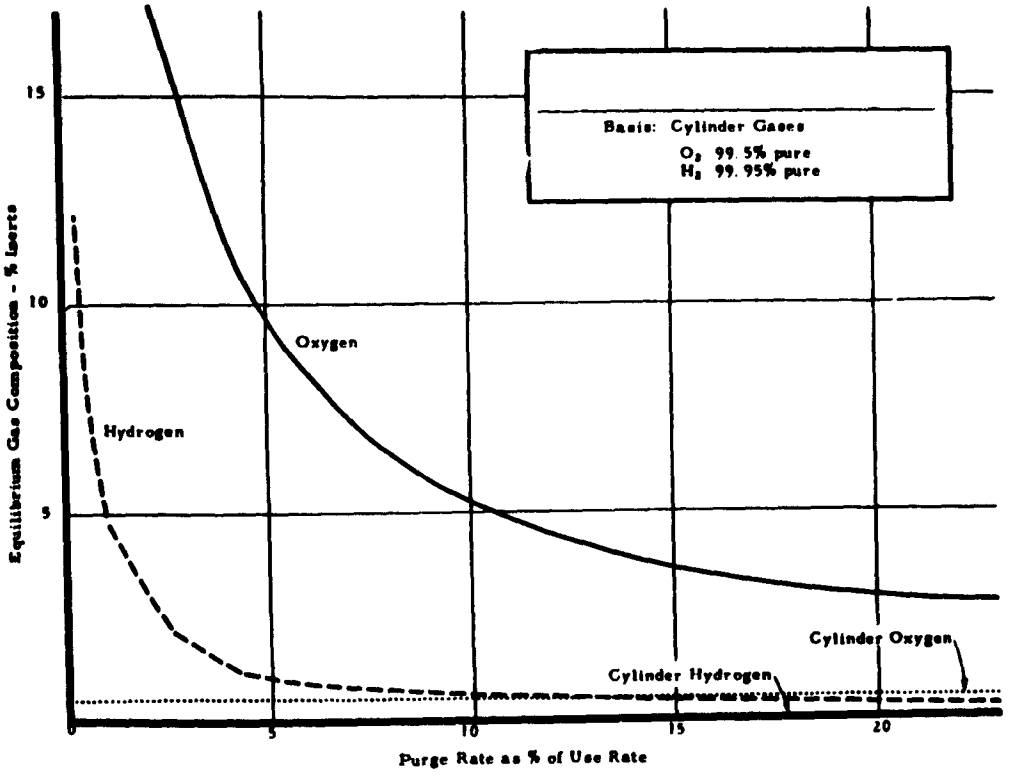

D-110

Figure 14 - Equilibrium Gas Composition vs Purge Rate

content of the cylinder gas is observed in comparing oxygen versus hydrogen. Thus to maintain the gas concentration within the cell chamber at 95 per cent purity requires a 10 per cent purge of the oxygen system and a 1 per cent purge of the hydrogen system. Nominal increase in the purge beyond these values does not markedly alter the equilibrium gas concentration, e. g. , yielding only 97 per cent oxygen and 97 per cent hydrogen at 20 per cent and 2 per cent respective purge rates. Since the output of the fuel

cell is affected by the gas concentration, it is desirable to maintain the gas purity at as high a level as feasible; equally important is the obvious fuel economy.

Commercial Bottle Gas Purge Requirement
For ASD 500 Watt Sustained Performance Test

O_2 use rate based on 9.5 ampere current through 72 cells:

By Figure 14 9.5 amps require 1.95 liters/hr - O_2/cell
9.5 amps require 3.90 liters/hr - H_2/cell

72 cell battery consumes

4.96 cu ft O_2/hr Use Rate
9.92 cu ft H_2/hr Use Rate

Assume 5 per cent inerts to be tolerable equilibrium condition in either gas.

By Figure 15 4.96 cu ft O_2/hr requires 10 per cent purge =

$$\frac{0.496 \text{ cu ft/hr}}{\substack{O_2 \text{ purge rate} \\ \text{Theoretical}}}$$

9.92 cu ft H_2/hr require 1 per cent purge =

$$\frac{0.099 \text{ cu ft/hr}}{\substack{H_2 \text{ purge rate} \\ \text{Theoretical}}}$$

3) Hydrogen Preheating

The 500 watt test battery employed preheating the hydrogen to minimize water vapor condensation at the inlet gas port in the anode gas chamber. Preheating is achieved by means of a specially constructed bayonet-type heater mounted in fixed position in the internal hydrogen manifold. This latter method permits heating the gas above the battery temperature, and offers a simple means of ensuring reasonably uniform feed temperature over the entire length of the battery.

Bench studies were conducted by constructing manifolds of plastic tubing to simulate the dimensions and geometries of the hydrogen manifolds of the cells and modules in which various heater designs were evaluated. Thermocouples were placed within the ports of the dummy manifolds to measure the temperature of the heated hydrogen. Gas flow rates were adjusted to the same rate to be used in the cells and modules 3.0 cu ft/hr. Heating elements, made by winding resistance wire around a glass rod or tube, were mounted co-axially within the feed manifold. The wire size, coil spacing, and voltage inputs were varied until test results indicated uniform heating of the hydrogen to temperature levels approximately 10-20°F above ambient.

Initial trials showed that the gas passing through the ports closest to the hydrogen input had little temperature increase, whereas temperatures

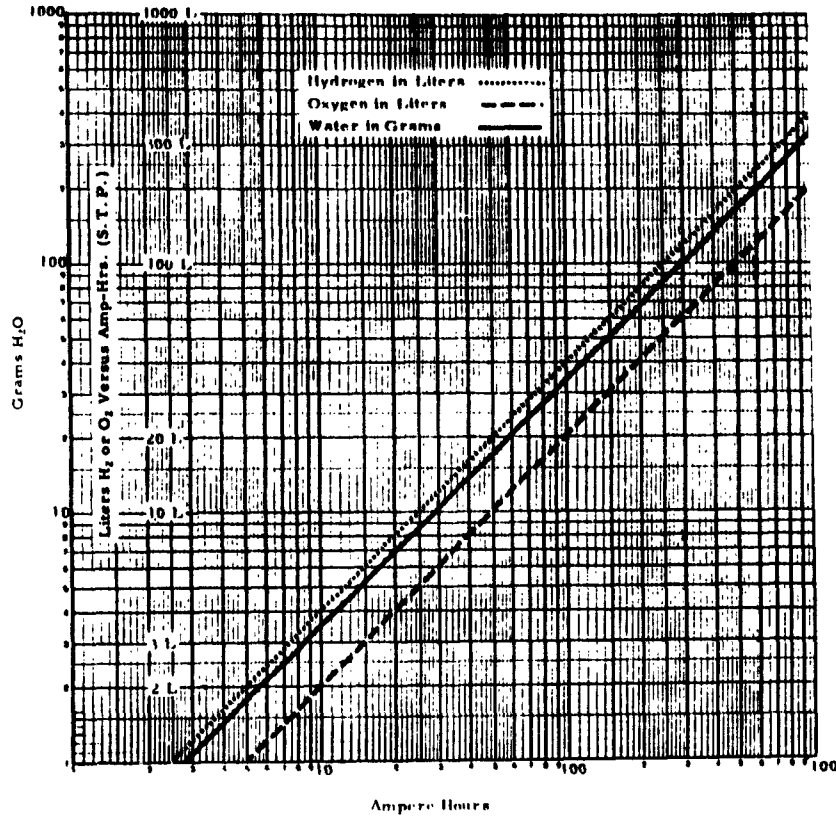

D-111

Figure 15 - Electrochemical Water Production Versus Ampere-Hour in a Single Cell (Gas Consumption Rates also Given)

recorded at the positions beyond the first port were reasonably uniform. Raising the temperatures at the first port was achieved by increasing the wattage in the first section of the heater by means of thinner, high resistance wire for the first part of the coil, in series with a thicker, low resistance wire for the last section. This method of coil construction was used in making the heaters for the 18-cell 6" x 6" modules.

The coil and the dummy manifold are shown in Figure 16, together with temperature distribution data. The test manifold and actual module manifolds were similar except that the test apparatus had 19 ports rather than 18, each port being equivalent to every port in a typical module.

Power expended to preheat incoming hydrogen to 22°F above battery temperature was 10 watts for the entire 500 watt battery.

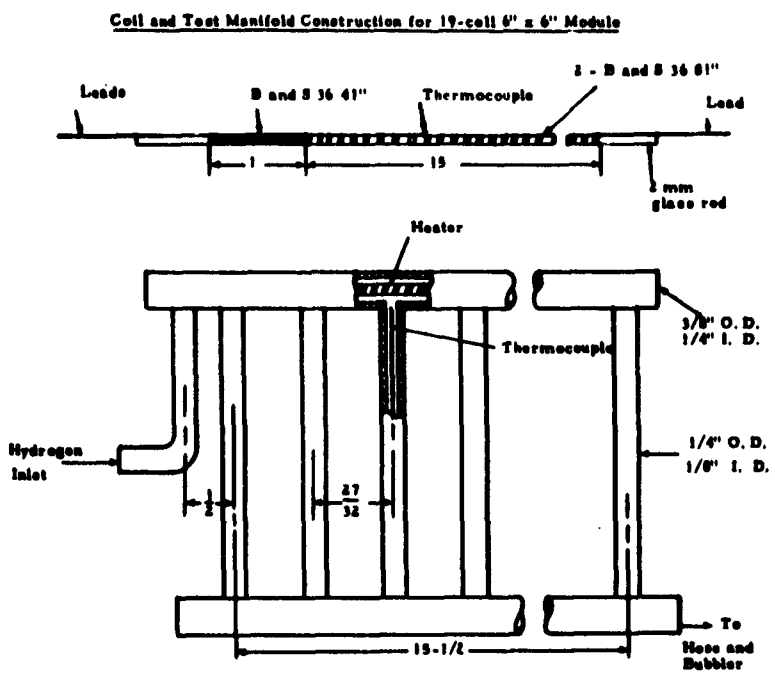

D-112

Figure 16 - Coil and Test Manifold Construction for 19-Cell 6" x 6" Module

D. Electrical System

The electrical system of the 500 watt test battery was composed of a d. c. load circuit and an a. c. control circuit. Failsafe design was imposed to prevent loss of the battery in the event of service failure. If line power was interrupted or gas supply failed, the battery was switched to open circuit.

1) D. C. Circuit

The diagram in Figure 17 shows the 28 volt d. c. circuit of the battery. The 18-cell modules are arranged in two parallel strings - each series array is composed of two modules totaling 28 volts/string. The carbon pile load resistor plus the hydrogen heaters and electrolyte pump comprised the total d. c. load across the 500 watt battery. Load protection was provided by the a. c. contactor which would open the load circuit in case

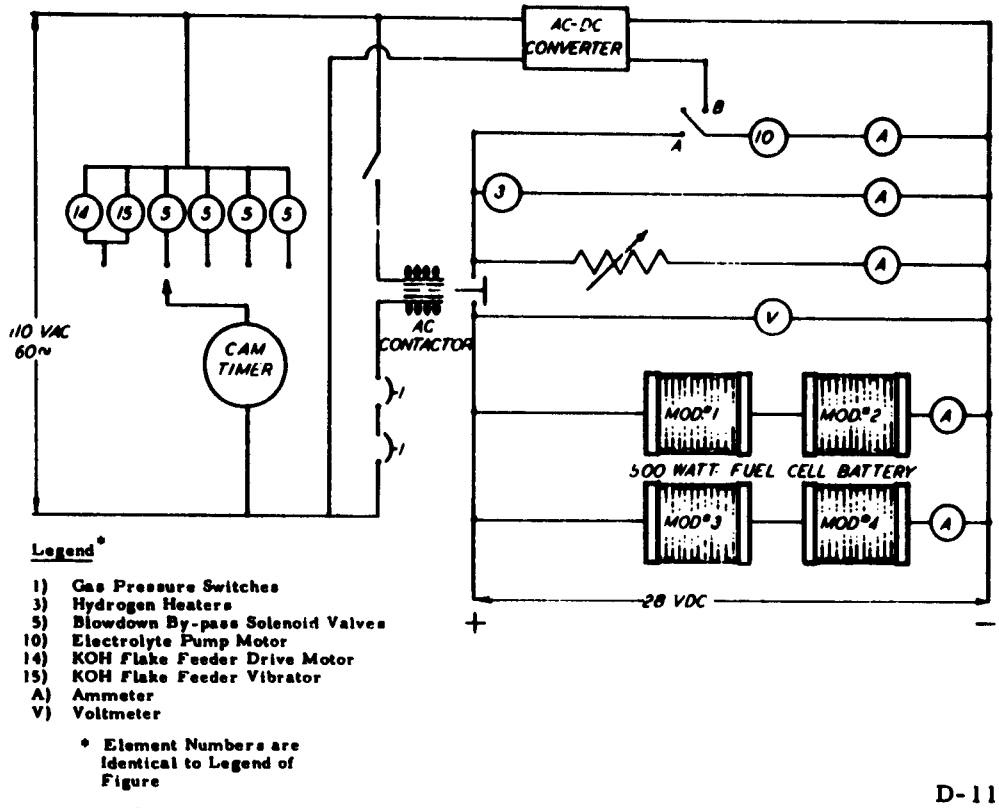

D-113

Figure 17 - 500 Watt Fuel Cell Battery Wiring Diagram

of plant power failure or less of either gas supply. A manual two-way switch is in series with the electrolyte pump motor. The pump was put on external power for system testing or to provide recirculation for pretest batteries whose voltage was below the pump motor requirements.

2) A. C. Control Circuit

The a. c. control circuit provided electrical functions which were peculiar to the sustained performance test. Some of the functions could have been provided to operate from the d. c. power of the battery but elaborate sophistication was required. It was not the purpose of the contract to do such development. Furthermore, the power required to operate the a. c. functions was of a small order and less significant because of intermittent operation. The cam-timer, driven by a synchronous motor, was used to time the KOH flake feeder and blowdown solenoid valves on cycle. The period of each function was adjusted by the dwell of the cam.

E. Data Recording

Data were gathered for the 500 watt test by means of a multiple-point continuous strip chart recorder and by visual instrument reading with manual recording.

Continuous strip chart data points were recorded of current, voltage, oxygen and hydrogen use rates and ambient temperature. Multiple temperature points were switched manually to select thermocouple positions of various fluid temperature points.

Manual-visual data were gathered at least three times daily for the following:

1) Gas tank pressure changes with time to establish by pressure-volume-temperature relationships a running account of gross gas quantities supplied to the test;

2) Amounts of purge gas vented from the test battery were accumulated by means of standard wet test meters;

3) Accumulated excess overflow of KOH liquid from reconcentration plus water dilution was collected, measured and recorded;

4) Flake KOH for reconcentration was added to the feeder hopper in 1000 gram increments and recorded;

5) Liquid pressure on the KOH system was the measured height of liquid head above a reference. By a calibration chart the KOH flow rates through the modules and heat exchanger could be estimated, and

6) Relative humidity conditions of the purge gases of the battery were measured with an electric hygrometer. Scale values were recorded and converted.

2. System Design for Water Transpiration

UNION CARBIDE Fuel Cell state-of-the-art improvement studies have been conducted over the weeks following the 500 watt - 30 day power test.

A major step forward has been taken with pure water transpiration via the gas streams of a 50 watt carbon fuel cell battery, which operated under a variety of load conditions, operating temperatures and KOH concentrations. Data in Table V show promise for sustained operation without KOH recirculation.

Generally, gas baked carbon electrodes appear to operate within a wide combination of loads, electrolyte concentrations, and temperatures and will transpire all the water of formation, seeking equilibrium conditions compatible with load.

TABLE V

WATER TRANSPIRATION TESTS

6" x 6" Plastic Framed Carbon Electrodes

Module	Anodes Type	Cathodes Type	Conc. KOH Normality	Test Duration Hrs.	Load Time Hrs.	Current Density ASF	Test Conditions for Invariant Electrolyte					Total Equil. Period Hrs.	Remarks
							KOH Conc. Normality	Temp. °F	ASF	H_2 Rate	O_2 Rate		
Mod. No. 3 Lot 8 - 7 Cells	90 PR. Cat. &W. P.	90 PR. None	8.8 - 9.43	175	71	53	9 N*	128-169	53	10x Use*	10x Use*	33	Shutdown due to malfunction from an assembly deletion.
Mod. No. 1 Lot 9 - 7 Cells	100 PR. Cat. &W. P.	100 PR. Cat. &W. P.	6.7 - 10.3	382	262	53.7 Avg.	8.3*	163-184	56-90	38-53xUse	24-41xUse	54	Malfunction due to Water Collection Receiver Overfill
							6.8	151	38	44x Use	34x Use	18	
Mod. No. 2 Lot 9 - 7 Cells	90 PR. Cat. &W. P.	90 PR. Cat. &W. P.	6.2 - 8.0	250	204	58.8 Avg.	7.7	140	53	50x Use	38x Use	4	Shutdown due to High Temp. Frame Distortion
Mod. No. 3 Lot 9 - 7 Cells	90 PR. Cat. &W. P.	90 PR. None	6.1	170	167	52	6.1	134	53	39x Use	35x Use	16	Shutdown due to Gas Supply Failure

*Nonrecirculating Gas or Electrolyte.

In operation at elevated temperature, the increased partial pressure of water vapor, resulting from increased vapor pressure of the KOH electrolyte, decreases the partial pressure or effective concentration of the reactant gases. If we were to attempt to operate a fuel cell battery at temperatures above about 50°C with stagnant (noncirculating) hydrogen and oxygen, the long path length for diffusion of reactant gases through the manifolds and cell ports to the active electrode sites would be blocked by water vapor, introducing serious concentration polarization and poor performance of the battery. Operation at high current density magnifies this effect by increasing the local temperature and by diluting the electrolyte near the anode (with a corresponding increase in vapor pressure).

In operation of a fuel cell with recirculating gases, properly designed for water transpiration, these problems can be converted into advantages. By sweeping the electrode surfaces with an excess of hydrogen and oxygen, water can be removed from the fuel cell as rapidly as it is formed, while still maintaining an adequate concentration of the reactant gases. Water vapor carried in the exit stream effectively removes heat from the battery, corresponding to the heat of vaporization of the water. Operation at high current density increases the rate of water production (i. e., the rate at which water must be removed) but also increases the temperature and vapor pressure of the electrolyte, leading to a self-regulating effect.

A. Water Transpiration Tests

Water transpiration studies have been made separately on four fuel cell modules. Each contained 7 carbon electrode cells. The testing was conducted on the same basic test skid (Figure 9) of the 500 watt sustained performance tests.

Figure 18 shows the rearrangement scheme of the 500 watt test skid for the water transpiration studies.

The first 7-cell module (Mod. No. 3, Lot No. 8) was constructed in the same manner as the 18-cell modules of the final 500 watt test except for length. It was tested on the skid under similar conditions of fluid flow and load with following exceptions: (1) gas flow rates through the battery were increased from 1/10 use rate to 10x use rate (100-fold increase); (2) battery electrolyte recirculation was stopped to force a temperature rise in the battery due to its own waste heat; (3) a condenser was added in gas lines downstream from the battery to collect water vapor transpired through the electrodes into the gas streams, and (4) battery electrolyte was more dilute (9 N).

The succeeding three battery modules (Nos. 1, 2 and 3 - Lot No. 9) were tested similarly to the above except that gas discharged from the condenser was recirculated.

Discharge curves are shown on Figure 19. Some quantitative results of the four modular invariant electrolyte tests are broadly listed in Table V. These show that:

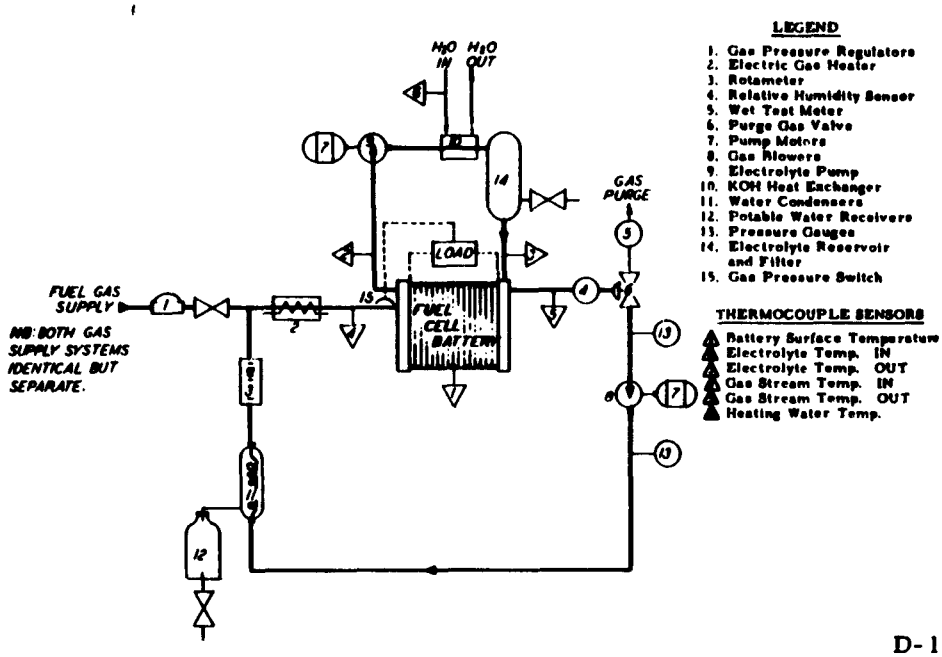

D-114

Figure 18 - 50 Watt Fuel Cell Battery
Excess Water Removed in
Gas Streams

1) The basic carbon electrode is capable of steady-state operation with complete rejection of pure water from the battery;

2) A variety of combined operating conditions can achieve an invariant electrolyte state in a carbon electrode fuel cell, and

3) System design improvements are straightforward to meet increased temperature conditions and recirculation of gases. Selection of a plastic frame material for higher temperature is well within the temperature range of the plastic family. Gas recirculation equipment can be of conventional design.

Table V lists the modules in the order tested. Module No. 8-3 operated on more concentrated KOH than the succeeding module and also in a lower temperature range. Excess gas rate through battery was less than all other modules. Less stringent conditions prevailed in the first module rather than the second because of differences in electrode porosity. The 90 PR electrodes are more porous than the 100 PR, therefore, can permit water vapor diffusion more readily.

Lower normality and higher temperature conditions necessitated high gas recirculation rates in the second module to control water vapor out

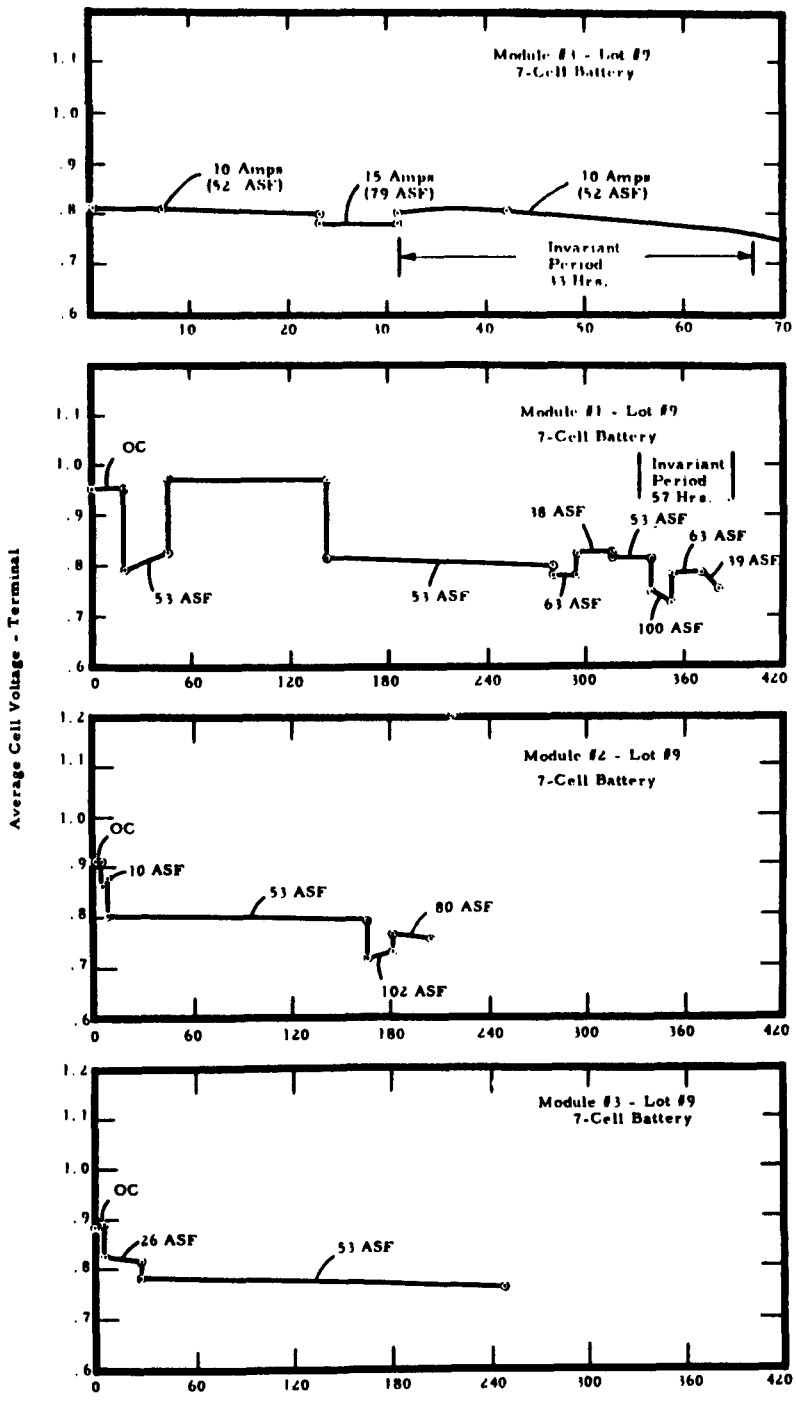

D-115

Figure 19 - Carbon Fuel Cell Voltage vs Life - Invariant Electrolyte Tests

of the electrode from drastically inhibiting inward diffusion of reactant gases causing polarization due to mass transfer.

The third and fourth modules were operated under similar conditions as module No. 9-1 to compare the electrode stock of module No. 8-3 with module No. 9-1's operating conditions. Lack of system control restricted data collection for adequate comparison.

B. Self-Regulation

The water transpiration studies conducted under the present contract have shown the UNION CARBIDE Fuel Cell to be an intrinsically self-regulating device. In the tests summarized in Table V, the electrolyte cooling loop was shut off, the gas circulation rate set at a constant value, and the fuel cell module was permitted to seek its own operating condition.

In order to analyze the operation of a fuel cell under self-regulating conditions, assume that a fuel cell is operating under steady-state conditions, i. e., the voltage, current, temperatures, flow rates are held constant and water is being removed at a rate equal to the rate of production, so that the electrolyte concentration is invariant. The system is now in a state of dynamic equilibrium, in that any change from steady-state conditions will automatically be corrected. A decrease in battery temperature, for example, increases the internal resistance, increases the polarization loss, lowers the rate of electrolyte evaporation, and lowers the ΔT between battery and heat sink lowering the heat loss. Each of these effects separately and jointly tends to increase the battery temperature back to the steady-state value.

Consider now a change in operating requirements, for example a 50 per cent increase in the output power load. The voltage will drop very slightly, and the current will increase by slightly more than 50 per cent. The rate of water production will increase in proportion to the current, tending to dilute the electrolyte. The increase in waste heat generation will increase the battery temperature until the new ΔT between battery and heat sink establishes a new steady-state temperature. At the higher battery temperature, water is removed more rapidly at the same (fixed) gas recirculation rates, aided in this tendency by the electrolyte dilution. The net effect is to establish a new temperature distribution and new electrolyte concentration at which a steady-state is maintained.

These are practical limitations on the principle of self-regulation. For completely arbitrary settings of flow rates (of gases or electrolyte) or power level, the steady-state condition toward which the system tends may be outside the permissible range of fuel cell operating parameters. For example, a call for maximum power output combined with minimal circulation rates might easily produce a new steady-state battery temperature exceeding the maximum rated temperature of the materials of construction.

There is a second important reason for designing positive controls for a self-regulating battery. The power level and rate of heat generation in the battery may be changed instantly by the closing of a switch. The resulting changes in electrolyte concentration occur relatively slowly over

a period of many minutes. Even though the initial and final steady-states (before and after the power level change) may fall well within permissible operating limits, the fuel cell in the absence of positive controls may under some possible conditions pass through a forbidden transient condition in seeking the new steady-state. Such erratic transients can be avoided by the use of fast-acting controls sensing important parameters such as output current or heat sink temperature directly. The use of positive controls also permits operation of the system for short periods of time outside the range of normal steady-state operation. For example, a heavy overload can be tolerated by preventing excessive temperature rise, even though this results in electrolyte dilution below the proper level. In subsequent operation within the normal power level range, the automatic operation of the controls will re-establish the correct electrolyte concentration.

A third reason dictating the use of positive controls originates in the desire for maximum efficiency. Some minimum recirculation rate for gases may be adequate for the maximum power level rating of the system. In operation at less than rated power, parasitic power losses can be reduced by cutting back on fluid recirculation rates, lowering the pumping power losses.

In summary, three types of control are provided for the fuel cell:

(a) The normal self-regulation of the fuel cell itself;

(b) Positive, fast-acting, continuously variable controls which operate in parallel with the normal self-regulation control, increasing the speed of response and increasing the efficiency, and

(c) Coarse-acting safety controls capable of overriding the operating controls to prevent excessive temperature rise, freeze-up, etc.

Table VI summarizes some of the self-regulating characteristics of the UNION CARBIDE Fuel Cell.

3. System Design for Vacuum Evaporation

Space vacuum evaporation is the third method of handling the water of formation in a carbon fuel cell battery operating in a space environment.

The water would be disposed in space as a vapor through the walls of porous media located in the electrolyte system of the fuel cell battery.

This method has the advantages of over-all system simplicity, invariant electrolyte and 1/3 of the waste heat is rejected by evaporation. It has the disadvantage of changing the total system weight with battery discharge. (However, in some missions this could be advantageous.)

Some work has been done on porous media through which space vacuum evaporation may be accomplished. Fuel cell system operation with vacuum evaporation has not yet been carried out in the laboratory.

TABLE VI

INTERRELATED OPERATING PARAMETERS USEFUL IN SELF-REGULATING STUDIES

Battery Temperature Increase		
Increases electrolyte conductivity	-	Less resistive losses
Decreases electrolyte viscosity	-	Less pumping losses
Decreases activation polarization	-	Higher electrochemical efficiency
Better peroxide decomposition	-	Less bubble rejection problem
Increases vapor pressure	-	Greater transpiration rate of H_2O vapor
Electrolyte Concentration Decrease	14 → 9 N	
Increases electrolyte conductivity	-	Less resistive losses
Decreases electrolyte viscosity	-	Less pumping losses
Increases vapor pressure	-	Greater transpiration rate
Gas Temperature Increase		
Increases water pickup	-	Less circulation required
Higher radiation temperature	-	Easier heat rejection
Lower Condenser Cold Side		
Dryer gas from output	-	Less recirculation required
	-	Less parasitic power required
	-	Larger radiator required
Higher Condenser Hot Side		
More efficient radiation	-	Smaller radiator required

Table VII summarizes the results of studies on the rate of transpiration of water vapor through porous Teflon. Although the finest pore structure studied (Sample A of Table VII) showed usable transpiration rates, there was considerable difficulty with leakage of KOH through occasional pinholes. As can be seen from the pore diameter range, 0.1 to 25 microns, a fortuitous combination of the larger pores can lead to weeping of liquid.

Samples of porous Teflon in sheet form were obtained from various sources and checked for total porosity and pore size distribution. Three types of tests were then made as follows:

1) A static pressure test to determine the minimum pressure (absolute) to just barely transmit free liquid through the membrane. This should provide an index of the sum of all pressures on the liquid side of a circulating system which pressure must not be exceeded to avoid bleed-through.

2) A vapor/vapor transmittance test to show the water vapor transmittance rate solely under the differential force of vapor pressure to vacuum.

TABLE VII

POROUS TEFLON

Sample	Thickness	Vendors' Rating			Determined			Test No. 1*	Test No. 2**
		Total Porosity	Pore Diameter Avg.	Range	Total Porosity	Pore Diameter Avg.	Range	Static Pressure	Vapor/Vapor Transmission
A	0.050"	Not Given	9 μ	18 μ Max.	34%	4.3 μ	0.1-25 27% 5-25 65% 0.1-4.2	340 mm	14.3 g
B_1	0.122"	~ 20%	Unknown		21%	14.0 μ	0.13-28.4 50% 15-28.4 43% 0.13-13	120 mm	15.2 g
B_2	0.126"	~ 20%	Unknown		26%	6.1 μ	0.1-21 41% 7-21 43% 0.1-6	240 mm	8.9 g
C	0.144"	59%	10 μ	30 μ Max.	62%	12.3 μ	0.9-21 57% 13-21 27% 0.9-11	140 mm	29.0 g
D_1	0.166"	25%	5 μ	--	25%	7.9 μ	0.1-21 52% 8-21 39% 0.1-7	200 mm	2.2 g
D_2	0.049"	25%	5 μ	--	25%	7.9 μ	Ditto	140 mm	4.6 g
E	0.278"	~ 50%	--	30-50 μ	62%	Not Run		100 mm	25.2 g

* Absolute pressure in mm Hg to just transmit liquid water at room temperature through the sample.

** Grams of water vapor transmitted per hour per square inch - water vapor at 59°C to vacuum. (< 2 μ) - vapor differential pressure 142 mm Hg.

3) A liquid/vapor test with liquid circulating across one face of the septum and vacuum on the opposite side.

Table VII is a summation of data on Teflon samples thus far studied. The minimum pressure to transmit free liquid (Test 1) appears to correlate in inverse relationship with average pore diameter and with membrane thickness (for a specific material - samples D_1 and D_2). The relationship of water vapor transmission to porosity and pore size is at the moment more obscure. Some of these samples have excellent vapor transmission rates although the results shown in Table VII would be reduced to about one third with 12 N KOH, for example, as a result of its lower vapor pressure at 59 to 60°C and the consequent lowered pressure differential with this liquid as compared with plain water. None of the samples would be suitable for an electrolyte evaporating system in space vacuum because of their low liquid transmittance pressure, although here the greater viscosity and specific gravity of KOH solution would at least double the values of Table VII and bring a material such as Sample A to a borderline pressure close to atmospheric. Test 3 above confirmed the unsuitability of the specimens, for example, Sample A permitted rapid leakage of water through it even when the pressure on the liquid side was reduced well below atmospheric and the total differential pressure (absolute) did not exceed 340 mm.

While there is ample reason for believing that a porous Teflon (or other plastic membrane nonwetted by KOH) could ultimately be developed with much more uniform pore structure and higher permeability than the samples tested, and which would be useful as a space evaporator membrane, such materials development effort was considered beyond the scope of the present study. Instead, effort was directed toward other media for accomplishing the same end.

Recently the literature has described studies of evaporation of liquids - specifically organic liquids - and the separation of liquid mixtures by permeation through thin plastic films with liquid phase in contact with one side of the film and reduced pressure on the opposite side. The case has been stated as follows: "... a condensable permeant may be transmitted through a membrane by exposing one face to a higher pressure of the component in the gaseous state than is maintained on the opposite face; such a process is termed vapor transmission or fixed-gas permeation (analogous to Test 2, Table VII). On the other hand, the membrane may be contacted on one face with permeant in the liquid state and the permeant transmitted through the membrane by maintaining the downstream face in contact with a gas phase below saturation in permeant vapor. Such a process may be referred to as 'pervaporation'. The pervaporative transport rate is found usually to be higher (and often far higher) than the vapor permeation rate." The polymeric plastic films used are thin - 0.001" thick or less - to obtain high permeation rates and they are nonporous, i.e., they do not contain discrete holes. Permeation requires a degree of solubility of the material in the polymer comprising the film and movement through the polymer structure by an activated diffusion process presumably following Fick's law. Data have been cited whereby a material such as n-octane (vapor pressure about half of water) has been permeated (evaporated) at 52°C through a 1 mil film at the rate of 5.3 ml per hour per square foot under a liquid/permeant pressure differential of only 400 mm Hg (760 mm on liquid side).

"Pervaporation" of this character is exactly analogous to the process objective sought for fuel cell electrolyte water removal under space environment. The thinness of the films used may permit assembly of a large surface area into a relatively compact unit. Certain available film polymers are known that have excellent resistance to strong KOH with polymer modifications having the best obtainable water vapor permeability.

Success has been achieved in preliminary experiments in transpiring water vapor through "Ethocel" film without electrolyte bleed-through or noticeable degradation of the film in service. In operation of a film separating 60°C electrolyte and high vacuum, the transpiration rate indicates that the water produced in a 500 watt fuel cell would require about 18 ft^2 of film.

IV. Test Results

1. Summary of Test Results

The 500 watt sustained performance test began May 3, 1962. Testing was completed on the last module of the original battery August 28, 1962 - more than 100 days later.

The 500 watt test battery was built up from four 125 watt modules. Module No. 1 operated for 1850 hours at rated load. Module No. 3 operated for 900 hours at rated load. At this time, it was damaged in moving it to another laboratory room, but was able to remain in operation for an additional 1800 hours at reduced load. Module No. 4 operated for 730 hours at rated load after which it developed an electrolyte leak and was removed from load. Module No. 2 was assembled improperly, with two of the metallic gas barriers contacting one of the tie rods at points of inadequate clearance. After about 70 hours on test, extremely high intercell current developed, forcing an interruption of the test. Module No. 2 was replaced by module No. 2A, which operated for 1150 hours at rated load. Although each of the four modules - 1, 2A, 3 and 4 - operated in excess of 720 hours (one month nominal), the entire battery as a system was operated for 600 hours (25 days) at rated power output.

The battery performance is summarized with respect to gross power, net power, current density, system temperature, electrolyte flow rate, current and KOH concentration in Figure 20 (A). Noteworthy events are shown by reference numbers on the graphs, Figure 20 (A) and in the following text.

After 70 hours, at reference point (1), a dead short developed across two cells - No. 13 and No. 14 of module No. 2. An estimated 7x load has been imposed on both cells for approximately two hours when the cathode of cell No. 13 failed and the cell switched from a potential supporting cell to a resistive load driven by the module current to what is termed "reversal". Its potential shifted from supporting a (0.820 volt) potential increase under 9 amp-load to a (-0.355 volt) decrease under a 5.6 amp-load.

The nature of the difficulty was an assembly fault which placed the conductive gas barrier plates (Ni-plated copper) before cell No. 13 and after cell No. 14 in contact with one of the 10 tie-rods running the battery length. The dielectric strength of the grease film on the tie-rod was sufficient to inhibit a short circuit condition against 1.6 volts for almost 75 hours, at which time the film decayed. The two cells were subjected to a short-circuit current of about 350 amp/sq ft by estimate. In retrospect, it is easy to see that a simple voltage break-down test across the tie rods to the barrier plates and electrolyte "ground" would have located and identified the fault.

Immediate steps were taken to incorporate procedures to avoid future trouble of this nature. The replacement module was assembled under the new procedure. All cells were jig-assembled and clipped together prior to module assembly in the manner shown in Figure 5 to prevent future misalignments. The gas barriers were reduced in width to provide maximum clearance between the location of the tie bolts and gas barrier edges.

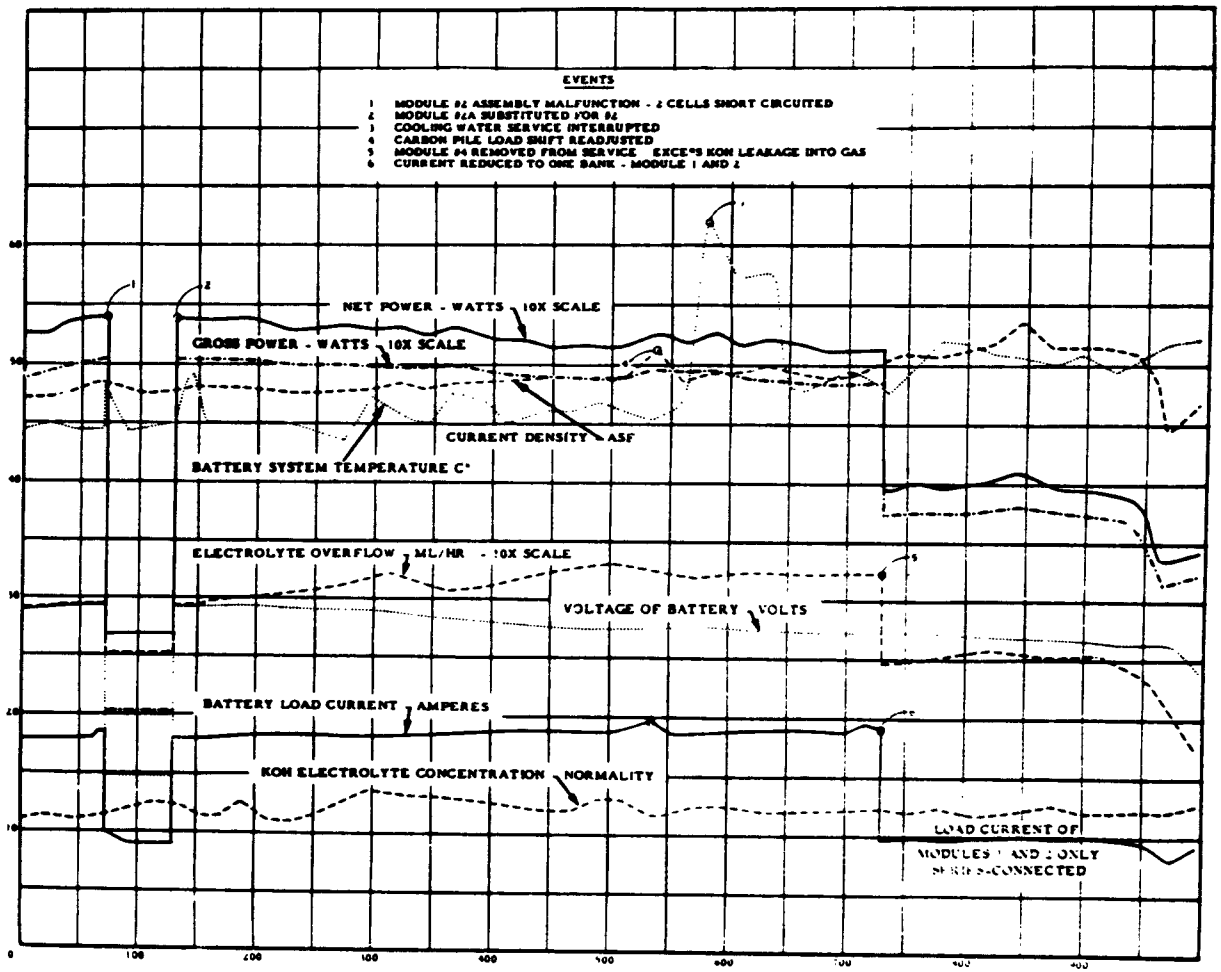

D-116

Figure 20 (A) - ASD 500 Watt Sustained Performance Test. 72-Cell Carbon Electrode Fuel Battery

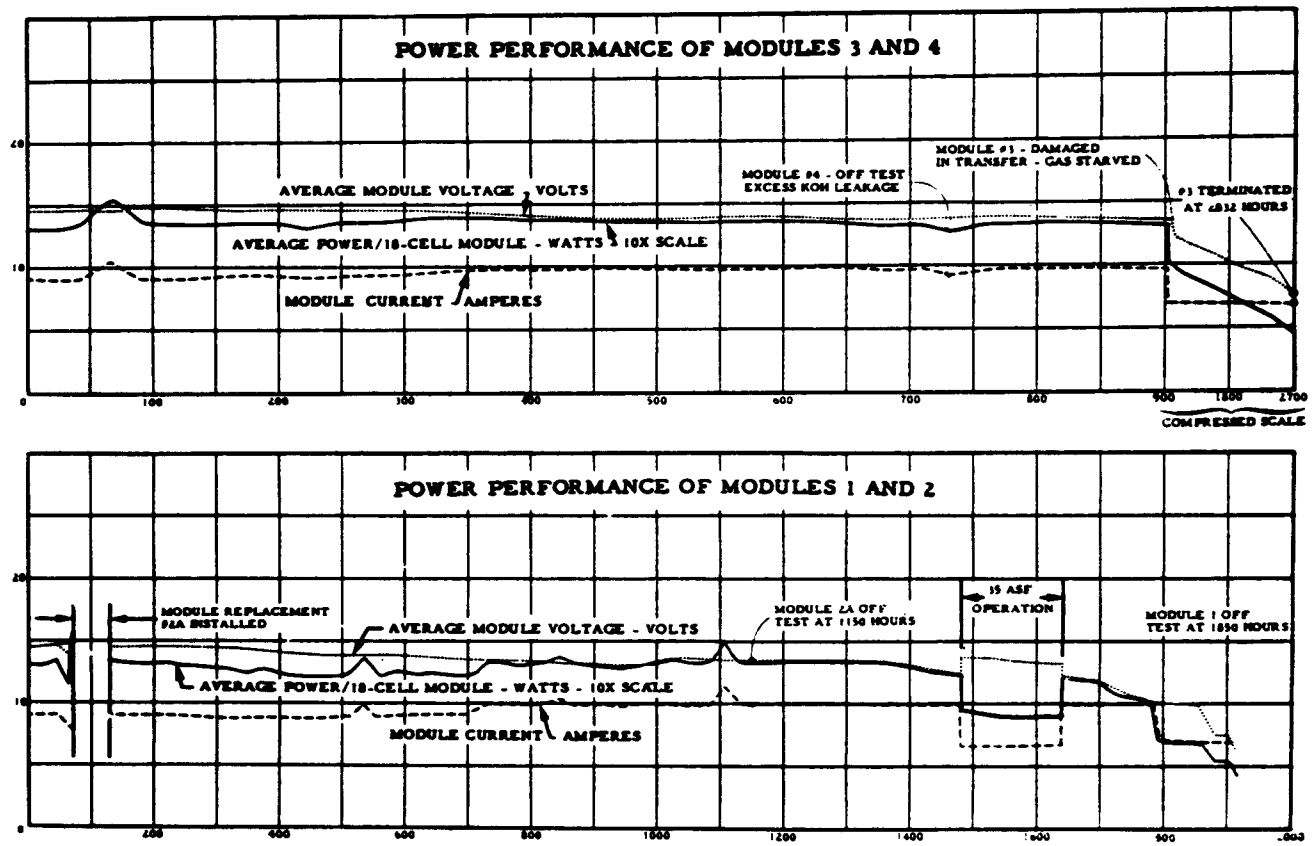

D-117

Figure 20 (B) - ASD 500 Watt Sustained Performance Test-72-Cell Fuel Battery

Module No. 2A was substituted for No. 2 at approximately 130 hours after the start of the test. (Reference point (2).) Module No. 1 (companion module to No. 2 - see Fig. 17) was idle on open circuit during the period of module replacement. Companion modules 3 and 4 were continued on rated load during the 55 hour replacement period.

Following the module replacement all modules were back in service under the original load. Approximately 200 hours after initial start of the test liquid KOH (light amber) appeared in the hydrogen gas traps and continued to accumulate in all module hydrogen traps at about the same time. KOH leakage was noted in the oxygen traps at 300 hours in all modules except No. 4.

This appearance of trace leakage early in the test was contrary to all prior experience in physical and electrochemical testing of the electrode stock, and remained a puzzle till late in the test program. After 700 hours, the leakage progressively became worse and (except for module No. 3 which was damaged in transit) was the ultimate reason for termination of the tests.

Carbon electrodes are designed to operate properly with a slight (e. g., several inches of water) positive excess of gas pressure relative to electrolyte pressure. In setting up the gas pressure balance on the pressure regulators, proper correction was made for the pressure drop due to electrolyte flow, but no correction at all was made for the static head of KOH electrolyte in the system. As a result, the electrolyte pressure in the cells was more than 10 inches W. C. higher than the gas pressure, literally forcing electrolyte into the electrodes.

Module No. 3 was still in operation on a different test stand when the difficulty was analyzed. Its gas pressure was raised from 15 inches W. C. to 35 inches W. C. which stopped the leakage. Despite gross damage in transit, this module continued on to operate for a total of 2832 hours at reduced load. Prior to this discovery of faulty gas pressure balance, it was very difficult to explain why test electrodes and cells from the same carbon stock had shown more than twice the life expectancy at more than twice the current density as observed in the 500 watt battery test. Previous examinations of cathodes in functioning batteries showed no signs of abnormal wetting, and it was thus assumed that differences on the order of 10-12 inches W. C. were insignificant. Hydrostatic tests using 48 inch liquid column against nonoperating electrodes showed no accelerated wetting effects. After the experience of arresting leakage in Module No. 3 with increased gas pressure, it is clear that anode wetting is sensitive to hydrostatic pressure, which must be controlled in future batteries.

After about 200 hours on test, a gradual but significant decrease in battery voltage was noted. Suspecting that some impurity from the flake caustic or from the system itself might be building up to a level high enough to impair electrode performance, the system electrolyte was changed at 330 hours. This electrolyte change did, in fact, stabilize the voltage.

Earlier, 3- and 4-cell test batteries had been operated at up to twice the current density of the 500 watt test battery with no evidence of this sort of voltage degradation. In these tests, however, the electrolyte had

been changed early in life (within the first 50 hours). It appears that for most stable performance, the battery should be broken in for a few hours of operation, followed by an electrolyte flush to remove any manufacturing dirt or impurities leached by KOH.

Reference point (3) on the sustained performance test chart indicates a system temperature rise when cooling water service was interrupted during a weekend period. Temperature rise had no observable ill effect (at least on short term) and some voltage improvement was observed, so temperature was reduced only partially following that incident for several days.

Reference point (4) occurred when a KOH manifold joint leaked KOH liquid onto the carbon-pile resistor upsetting its resistance making it more conductive. Readjustment corrected the problem.

At the 730 hour mark (reference point (5)), the leak rate of liquid KOH into the gas streams of module No. 4 was intolerable and caused damage to several cells in the module by interferring with normal gas service to them. After jumpering out several cells, the leak rate was still too severe and the module was taken out of service. Modules 1 and 2A remained on the test skid under the same load while module No. 3 was loaded separately for awhile (reference point (6)). Module No. 3 was removed to another test bench after 900 hours and was irreparably damaged in transit. However, it continued to display performance beyond the next 1800 hours at reduced load.

Modules 1 and 2A were removed at 1850 and 1150 hours respectively. Each was leaking badly and had suffered subsequent cell losses. In spite of the good average cell voltages of the remaining cells they were removed because the KOH leakage rate was too great to be considered normal operation.

The gross power of the 500 watt battery was nominally 535 watts initially and 520 watts at the 720 hour mark. Net power was slightly above 500 watts initially and below 500 watts at 720 hours. The difference was parasitic power - 34 watts initially and 28 watts at 720 hours.

During the sustained performance test period, current density increased proportionally as battery current - approximately an 8 per cent increase from start to 720 hours of life. Voltage decreased similarly, about 8 per cent. Average current/module changed from 9. 0 amps to 9. 75 amps.

Average cell voltage initially was 0. 820 volt and 0. 755 volt at 720 hours. This represented a change from 55. 3 per cent initial thermal efficiency to 51 per cent efficiency at 720 hours. Electrochemical conversion efficiency (based on 1. 20 volts maximum theoretical cell voltage) changed from 68. 3 per cent to 63 per cent.

2. Environmental Tests

Union Carbide gas baked carbon electrode fuel cells have successfully survived three essential dynamic environments - shock, vibration and acceleration. The cells delivered stable power without perceptible change throughout the full range of imposed conditions. These conditions were as much as a factor of 4 beyond those limits specified for the Agena B satellite.

The effect of high frequency vibration, in the kilocycle range, upon carbon electrode fuel cell performance was of chief interest. It is known that wettability of liquids change drastically under vibrational environments in the megacycle region. Aqueous KOH will "drown" porous carbon rapidly under ultrasonic conditions. It was desirable to ascertain if deleterious wetting would occur in the sonic region.

Five single baked carbon electrode fuel cells were assembled. Four live units were started and operated for at least 50 hours under a 50 amp/sq ft load with hydrogen and oxygen feed using 45°C - 12 N aqueous KOH electrolyte recirculating. All four units were fed by parallel fluid systems on the same test stand. Three of the four live cells were subjected to separate environmental tests while one remained on the test stand as a control cell. The fifth cell (unactivated) was subjected to environmental conditions in both "dry" and "wet" state.

Each of three live cells was subjected to vibration, acceleration and shock, respectively. All survived without perceptible change in the cell voltage output throughout the duration of each test. The tabulation in Table VIII shows the resistance-free voltage polarization versus load data before

TABLE VIII

COMPARISON OF RESISTANCE-FREE FUEL CELL VOLTAGES BEFORE AND AFTER ENVIRONMENTAL TESTS

Actual Cell Current Amps	Current Density (ASF)	Test Cell Voltages* - I. R. Free							
		Control		Acceleration		Vibration		Shock	
5	(26.2)	$\frac{0.905}{0.915}$	0.010	$\frac{0.900}{0.910}$	0.010	$\frac{0.905}{0.940}$	0.035	$\frac{0.920}{0.935}$	0.015
10	(52.4)	$\frac{0.875}{0.885}$	0.010	$\frac{0.855}{0.875}$	0.020	$\frac{0.880}{0.910}$	0.030	$\frac{0.900}{0.905}$	0.005
15	(78.5)	$\frac{0.845}{0.850}$	0.005	$\frac{0.820}{0.840}$	0.020	$\frac{0.865}{0.885}$	0.020	$\frac{0.885}{0.885}$	0.000
20	(104.7)	$\frac{0.825}{0.825}$	0.000	$\frac{0.790}{0.810}$	0.020	$\frac{0.850}{0.865}$	0.015	$\frac{0.870}{0.870}$	0.000

*Upper data figure taken under laboratory test bench conditions - 45°C w/ 12 N KOH electrolyte before moving to environmental test locations.

Lower figures taken under identical test bench conditions after returning from environmental test locations.

and after the specific environmental test of each cell as compared with the control cell. Most of the comparative data show slight voltage improvement following the tests, none show any decrease. Slight voltage improvements were probably due to improved surface contact of electrolyte to electrode as a result of the environmental agitations. However, except for slight voltage increases due to internal I. R. heating, such changes were not observed while the actual environmental tests were being conducted on live loaded cells. All four environmental test cells were subjected to a 50 hour 11 ampere load break-in period to stabilize voltage.

The fifth cell (unactivated) was subjected to vibration and shock in both the wet and dry conditions to ascertain (1) mechanical stability, and (2) adverse wetting of the carbon structure due to any induced increase in hydraulic pressure of the electrolyte due to the accelerating conditions.

The unactivated cell was dismantled, observed, and reassembled before and after each test. No changes were observed in either the physical cell assembly or electrolyte level maintained in a 1/4" I. D. transparent column 15" above the electrodes parallel to direction of acceleration.

A. Vibration Conditions

The vibration test cell was mounted on a base plate and bolted to the table of a Model C 10-C Exiter - M-B Manufacturing Company. The cell was positioned for the worst condition - accelerating forces normal to the electrodes.

Two model No. 2213 Crystal Accelerometers (Endeoco Corporation) were employed to monitor acceleration of the cell under vibration. The output of each accelerometer was fed into a No. 602 Unholz-Dickey dual channel linear amplifier adjusted to read a proportional output of one volt/g experienced by each accelerometer.

The "input" accelerometer was rigidly cemented to the base plate of the cell to monitor the driving vibrational input to the cell assembly. The "output" accelerometer was cemented to the center of the cell end plate opposite the mounting face to monitor the character of vibration transmitted through the assembly.

The cell was initially vibrated during a 12 minute interval. Cell load was maintained at 2 amperes while the vibration level was scanned from 380 cps to 3000 cps with a 7. 5 g acceleration input - Figure 20 (C) show a graph of the output.

Initial voltage of the cell was 0. 890 volt at 380 cps. The output accelerometer peaked to 27 g's at 560 cps; the cell read 0. 895 volt. Minutes later at 3000 cps the cell voltage still remained at 0. 895.

The frequency scan was repeated again but with a cell load of 5 amperes through a 5 minute interval. Voltage read 0. 820 at 580 cps and 0. 820 at 3000 cps.

Under an 11. 5 ampere load, the test was repeated through a 6 minute scan. Initial voltage was 0. 715 v; 0. 720 at 560 cps and 0. 720 at 3000 cps. At this point, the vibration level was increased to 5000 cps with a 10 g input and held for 30 seconds under an 11. 5 ampere load. Voltage of the cell was 0. 725 v.

B. Acceleration Conditions

A live test cell was mounted in a rotary accelerator Type G-6-B Serial No. 180 - Schaevitz Machine Works. The cell was positioned 24-3/8" from the center of rotation with the electrodes normal to the accelerating forces. The 15" liquid KOH electrolyte column was parallel to the same forces to achieve maximum liquid pressure in the electrolyte.

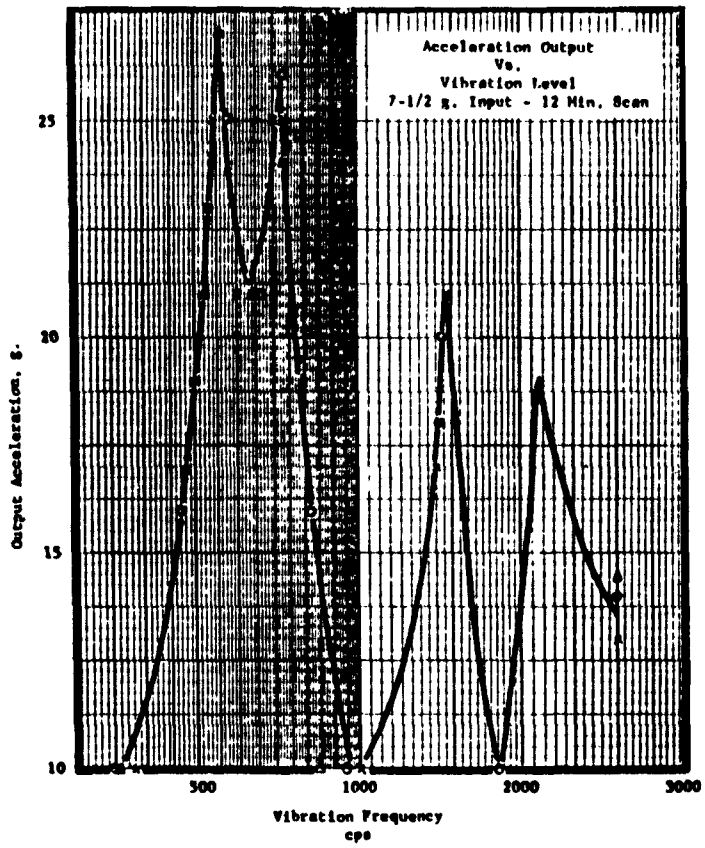

D-118

Figure 20 (C) - Fuel Cell Vibration Test

The gas supply was mounted with the cell on the opposite end of the rotating arm, exhaust gases were discharged through rotary gas connections on the rotating column of the machine. Gas pressure throughout the test was nominally 1/2 psi.

Voltage and current taps were made on the column similarly to permit variations in cell operation during rotation. Initial polarization values were:

Open Circuit Voltage	1. 050 Volts
3 Ampere load	0. 840
5 Ampere load	0. 790
10 Ampere load	0. 685
12. 3 Ampere load	0. 645

Acceleration from zero to 12 g was uniformly attained over a 4 minute period and held for a one minute interval while the cell remained loaded at 3 amperes and 0. 850 v during the entire 5 minutes. At the end of that time, polarization values were taken:

3 Amperes	0. 845 Volt
5 Amperes	0. 800
10 Amperes	0. 695
11 Amperes	0. 680

Rotation was brought to a stop after recording polarization data. Observations showed no change in the cell appearance.

With current in the cell at 11 amperes, rotation was re-started and increased to 14 g acceleration in 30 seconds. The voltage was 0. 690 at 11 amperes. These held steady for 1-1/2 minutes; rotation was brought to a complete stop one minute later. No observable changes were noted.

Rotation was re-started and attained a 20 g acceleration in 2 minutes while on open circuit (1. 06 volts). A 3 ampere load was applied initially at 30 g; one minute later the cell voltage remained steady at 0. 850 v at successively higher levels of 40 and 50 g. At this point, the gas supply was lost. A gas bottle connection broke disconnecting gas service to the cell. However, the cell suffered no observable damage, and has continued to show performance similar to the control cell although it was not restored to a gas supply for 2 hours.

C. Shock Conditions

The shock test cell was mounted in a component Shock Machine Type 20 VI - Barry Corporation. The KOH held was nominally 14" in the direction of acceleration while a nominal 1/2 psi gas pressure was maintained throughout the test. The cell polarization data before shock were:

Open Circuit Voltage	1. 065 Volts
2. 8 Amperes	0. 890
5. 0 Amperes	0. 855
10. 0 Amperes	0. 785
15. 0 Amperes	0. 735

Load on the cell was held at 11 amperes throughout three successive shock levels of:

40 g for 6 milliseconds
100 g for 3. 5 milliseconds
200 g for 5 milliseconds

The 11 ampere load was held for a 4 minute period while each shock level was attained; the cell voltage remained essentially unchanged at 0. 720 volt throughout.

No observable changes were noted in the physical appearance of the cell. Polarization data were again taken:

Open Circuit Voltage	1. 050 Volts
2. 8 Amperes	0. 880
5. 0 Amperes	0. 850
10. 0 Amperes	0. 780
15. 0 Amperes	0. 725

The cell was returned to the test bench for continued load testing to determine if any long term effects have been incurred. Lower voltage values were recorded during the environmental tests as compared to those shown in Table VIII. The recorded data during the tests were terminal voltage values taken while the cell was near room temperature.

3. Future Development Problems

Despite the successful operation of an unattended 500 watt fuel cell power supply on the laboratory bench, there remains a variety of developmental problems to be solved before the fuel cell is fully qualified as an A. P. U. for space applications. These problems are outlined below under the headings:

A. Component Development;

B. High Temperature Operation;

C. System Design and Analysis;

D. Inactive Storage and Start-up;

E. Reliability Analysis, and

F. Space Design.

A. Component Development

1) Cryogenic Fuel Supply

In operation of the 500 watt test battery, conditions of project cost and time dictated the use of hydrogen and oxygen as pressurized gases for fuel and oxidant. For space applications, high pressure storage of reactant gases is far too heavy, and supercritical cryogenic storage of H_2 and O_2 will be needed. The development of reliable tankage and controls for supercritical storage of H_2 and O_2 is considered to be a major problem requiring solution. Storage of liquid H_2 and O_2 in cryogenic tanks would offer an even lighter weight fuel supply system. This problem is considered to be longer range, since these are basic difficulties involved in handling two-phase liquid-gas systems under zero-g conditions.

2) The "Wicking Condenser"

Tests of the UNION CARBIDE Fuel Cell system in the laboratory have shown that it is possible to remove excess water vapor from a recirculating hydrogen or oxygen stream by passing the wet gas over cooled fins in contact with wicks. Water droplets condensed on the fins are drawn by capillary action into a storage tank loosely filled with a weak adsorbent. Since the wicks will draw water up against normal gravity forces, they should be usable also in zero-g conditions. Although this component, the "wicking condenser", has been subjected to feasibility tests in the laboratory, further engineering effort is required to optimize the design and prove in the performance capabilities.

3) Evaporator for Electrolyte Concentration

Water can also be rejected from the UNION CARBIDE Fuel Cell by passing warm electrolyte through a porous diffusion member which permits transpiration of water vapor but not passage of liquid electrolyte. While such evaporators have been studied on the laboratory bench, further effort is required to select optimum diffusion barriers for use with hard vacuum on the downstream side, and to design practical units based on the accumulation of further engineering data.

Although the wicking condenser and electrolyte evaporator accomplish a similar objective in removing reaction product water from the fuel cell, they have distinct further advantages and disadvantages which may dictate the use of one or the other (or both) for some particular space mission. The wicking condenser has the advantage of collecting and storing potable water, and of maintaining the system at constant mass, with minor changes if any in the center of gravity. It also transfers about 33 per cent of the waste heat generated in the fuel cell to the condenser, thus assisting in heat removal from the fuel cell battery. It has a disadvantage in that this portion of the waste heat (corresponding to the heat of condensation of water) must still be rejected from the mission via the space radiator.

The electrolyte evaporator rejects water vapor to space, so that it is not available on board. It requires the development of apposed jets to avoid interference with vehicle attitude control, or else the development of practical uses for this small reaction force. Its major advantage is that it rejects heat directly to space, without such heat passing through the space radiator, in an amount equal to the heat of condensation plus the heat capacity of the hot vapor. In a practical design, this effect could reduce the size of the space radiator by over one third. The hardware weight of the electrolyte evaporator should be considerably lighter than a wicking condenser of equivalent capacity, further reducing system weight. In operation of the electrolyte evaporator, the total system weight decreases with time. This would be an advantage in some applications, as for example a vehicle to be subjected to lunar launch after a prolonged lunar dwell.

4) Heat Exchangers

Design of future multikilowatt fuel cell power plant will require the incorporation of several types of heat exchangers for heat transfer and heat rejection. Further engineering study will be required to establish proper values for the parameters such as heat transfer coefficients, etc., used in the designs, followed by actual design and testing of the new components.

5) Electrolyte Expansion System

Since a free liquid-gas interface cannot be tolerated in space design of a fuel cell system, some provision must be made for accommodation of electrolyte volume changes in a closed liquid loop. This is visualized as an expansion bellows enclosed in a rigid tank (to avoid exposure to space vacuum forces on the bellows). Expansion of electrolyte will cause expansion of the bellows, which in turn will reduce the net free volume in the containing tank. The electrolyte volume can be related to a reference pressure generated in

the expansion tank housing, or to the linear displacement of the expansion bellows itself. Engineering effort will be required to develop a detailed design for the expansion tank system and to demonstrate quantitatively the relationship between signals generated at the expansion tank (considered as a control element) and fuel cell operating conditions.

6) Gas By-Pass Valves

Schematic diagrams for fuel cell power systems, although subject to some degree of design flexibility or ingenuity, usually contain one or more proportioning valves to control gas (or liquid) by-pass rates. Although such valve systems can be constructed according to well-established art, the exact sizes of valve and range of flow control called for require custom design for the particular fuel cell system being built.

7) Pumps

The most flexible fuel cell system design will call for both liquid pumps and gas blowers; fuel cell systems designed for a narrower range of environmental specifications may need less. Further engineering effort is required to minimize pumping power requirements, prove in pump reliability and to miniaturize with respect to weight.

8) Electrodes

The carbon electrodes used in batteries studied under the present contract will permit operation at usefully high power density, operating life and reliability. Further improvements are still possible through development of thinner and lighter electrodes and through increases in useful current density.

B. High Temperature Operation

Materials of construction, specifically the electrode framing material, limit the useful upper temperature limit for the Air Force, Aeronautical Systems Division battery to about 70°C. Still higher operating temperature would introduce numerous advantages, including:

1) The electrolyte resistivity decreases at higher temperatures, thereby reducing I. R. losses and increasing battery power output at a given current density.

2) The electrode polarization decreases at higher temperature, as a result of greater catalyst effectiveness and better ionic mobility, again leading to increased battery power output at a given current density.

3) The combined effect of items 1 and 2 above is a reduction in battery weight for a given rated power, and an even more important reduction in weight of fuel and fuel tanks resulting from lower fuel consumption in a more efficient battery.

4) Operation at higher temperature increases the rate of water transpiration into the gas streams, thereby increasing the maximum steady-state operating power of the battery for which equilibrium between

water production and water rejection can be achieved. Under normal operating conditions, greater water transpiration rates permit a decrease in the gas recirculation rates, with an attendant decrease in pumping power requirements.

5) Operability over a wider temperature range increases the overload capability of the battery, which is limited by the temperature rise which can be tolerated under overload conditions. It will thus be possible to design the fuel cell system to operate reliably over a much wider range of power outputs, and to increase the permissible time duration of excursions to peak overload conditions.

6) Operation at higher temperatures increases the efficiency of heat rejection and thereby reduces the size and weight of radiators required for space use.

7) Operation at higher temperatures increases battery efficiency, thereby reducing the total quantity of waste heat to be rejected. The important result is a further reduction in the size and weight of radiators and heat exchangers in the heat rejection system.

8) Operation at higher temperature increases the dew point of water carried in the gas streams, reducing the possibility that liquid water condensation on or in electrode surfaces can block proper diffusion of reactant gases.

Further engineering effort is required to select and prove-in new materials of construction, and to test and characterize batteries made with such materials with respect to usable power density, operating life and reliability.

C. System Design and Analysis

Much of the prior work on fuel cells has been related to the performance of components, particularly the battery component or its electrodes. Now that electrodes of reproducible quality are available, it is imperative to extend the analysis to total systems so as to include the interaction of components. In particular, it is now possible, and necessary, to study the thermal and mass transport problems involved in the design of a practical power plant. The thermal analysis or heat balance study of the system, including radiators, is essential in order to size such components as heat exchangers properly. A similar analysis is required for the control system, to define the upper and lower limits on control capability as related to assumed environmental specifications, and to predict transient responses of the total system in response to changes in power demand or changes in the environment.

D. Storage and Start-Up

Practically all of the effort on fuel cells has been related to operating systems; less effort has been devoted to problems of transportation, storage, start-up, or intermittent operation. The first fuel cell power systems to be flown will undoubtedly be well attended by senior engineers during installation

and start-up, but in the long range, it will be essential to design the system so as to permit "push-button" simplicity in start-up and shut-down.

E. Reliability Analysis

Much more testing effort is required to establish definitive measures of fuel cell reliability, not only for the battery modules but for auxiliary components and the total system. Since the reliability of the fuel cell module, for example, depends upon current density, operating temperature and other parameters such as relative humidity of the reactant gases, it is obvious that a broad testing program is required to define reliability in terms of operating conditions. A proper analysis of reliability also will require extensive environmental testing, both before and during performance tests.

F. Space Design Problems

Assuming that all of the preceding problems (items A through E) have been solved, i. e., that all components have been developed for higher temperature operation, the system design analyzed and optimized in detail, and reliability established in laboratory tests, there will still remain problems peculiar to the space environment. After completing space simulation tests, the final demonstration of utility will require testing in space. Problems which are considered specific to space include:

1) The effect, if any, of zero-g conditions on polarization; the influence of electrolyte circulation;

2) The elimination of fortuitous gas bubbles in space;

3) Operation of a cryogenic fuel supply in space;

4) Operation of a wicking condenser for water removal and storage, and

5) Validation of the radiator design.

4. Recommendations for Future Work

The itemization in Section IV, 3 , of specific problem areas requiring additional development effort can be construed as an implicit recommendation that such effort be undertaken. The following discussion suggests a logical grouping of such effort into well-defined tasks or objectives.

Further work is recommended to study the performance of the UNION CARBIDE Fuel Cell at the highest temperature for which suitable materials of construction can be found. Such work includes the selection and testing of materials for compatibility with the fuel cell environment, and the fabrication and testing of fuel cells employing such materials. It is not considered necessary to go beyond the domain of presently available materials in such a study, although in the longer range future there will be merit in basic studies designed to improve the state-of-art of materials technology related to fuel cells.

The most urgently needed effort lies in the area of system design and system testing. The present contract extension, AF 33(616)-7256 SA/5

took a long step in this direction in calling for the assembly and operation of a complete 500 watt fuel cell system. As a next logical step, it is necessary to redesign the system so as to employ a mode of operation conceptually suitable for space application. This requires, in particular, replacement of all components introduced into the present design as temporary expedients with components appropriate to space use.

Components which must be developed for space use include the following:

A. Supercritical cryogenic fuel and oxidant tankage and associated controls;

B. "Wicking condensers" for water removal and storage;

C. Lightweight pumps, blowers, valves;

D. Porous evaporators for electrolyte concentration;

E. Degasifier units for liquid-gas separation;

F. Heat exchangers and radiators, and

G. Controls, including sensors, transducers and instrumentation.

Maximum progress at minimum cost requires that such component development and testing be coordinated in a closely integrated program, with the objective of developing an auxiliary power system designed for space application. Effort would be coordinated through an over-all systems analysis, including study of heat balance, mass transport balance, and control analysis, and reliability analysis. The immediate product of such a program is a prototype power system, capable of space use and ready for space qualification testing.

Although the carbon electrodes used in the UNION CARBIDE Fuel Cell are presently capable of providing useful and reliable service in space power systems, further advances in electrode technology will broaden the range of useful application of fuel cells by providing lighter weight, longer life and higher efficiency. It is recommended that work be continued on studies to develop thinner, lighter, more uniform electrodes capable of operation at higher current density for longer periods of time.

V. Aerospace Fuel Cell Design

Based on the engineering studies of various modes of fuel cell operation conducted during the course of the contract effort, it has been possible to establish a conceptual design for a future fuel cell auxiliary power unit for space application. The optimum design and mode of operation depends upon the environmental and performance specifications. In order to permit a concrete discussion of a single design, operating conditions have been assumed as itemized below. These conditions are not to be construed as limits to fuel cell performance; performance could be extended beyond the limits indicated by appropriate changes in the design. Conversely, a simpler system would suffice if some of the operating requirements were relaxed.

Assumed Operating Conditions

Power Level Design Center	500 w to 2 kw
Mission Endurance	1 to 30 days
Fuel Supply	Supercritical Cryogenic H_2 and O_2
Load Variation and Duty Cycle	Power output variable between two times overload and minimum stand-by load, duty cycle not predetermined but under arbitrary control of mission command
Heat Sink	Any condition between "radiator facing sun" and "radiator facing black space"
Type of Control	Fully automatic response of system to both arbitrary changes in power output and arbitrary variations in heat sink effective temperature
Water Rejection	Collection and storage of potable water on board
Voltage Regulation	+0, -10% at rated load
Output Voltage	28 v d. c.
Reliability	Five 9's (0. 99999) based on minimal life support, assumed to require 75% of rated power. Four 9's (0. 9999) for full accomplishment of entire mission of 30 days, higher for shorter missions.
Environmental Specifications	As specified for Agena Satellite Program

Operation of the fuel cell power supply will be described with reference to the simplified schematic diagram, Figure 21.

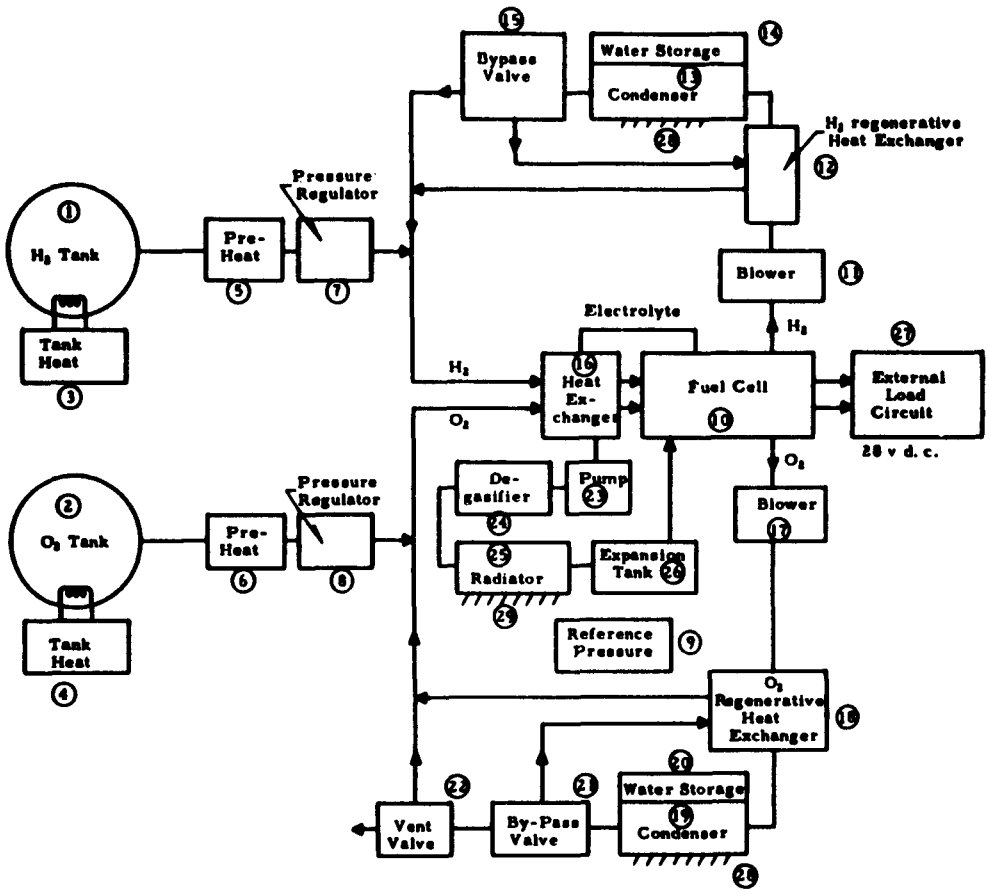

D-119

Figure 21 - Aerospace Design Schematic Diagram

A. Fuel Supply

The hydrogen supply tank is shown as item (1) in Figure 21. Supercritical cryogenic storage is chosen to avoid two-phase (liquid-gas) problems which may be associated with storage of liquid H_2 in zero-g space. A subcritical tank would be lighter (in principle) if it becomes established that pressure surges can be controlled. The hydrogen is kept at supercritical pressure by a tank heater (3) controlled by a pressure transducer located inside the tank. Exit hydrogen gas is brought to proper system temperature by a preheater (5) controlled by a temperature transducer located downstream from the preheater. Inlet pressure to the fuel cell system is controlled by pressure regulator (7) which operates as a slave regulator

controlled by pressure reference (9). Prior to launch, the H_2 tank is filled and subcooled with liquid H_2 via a fill port and vent line (not shown) and is allowed to pressurize with vents closed, by normal heat leakage. The Linde Company type superinsulation of the cryogenic tank depends upon space vacuum for full insulation capability, but will still permit about 12 hours hold time if needed during launch, without venting. If the count-down time past capping the vents exceeds 12 hours, excess pressure rise can be avoided by turning on the fuel cell power supply, which can consume fuel and oxidant at a rate greater than that required. As soon as the system is exposed to space vacuum, the heat leakage to the cryogenic fuel becomes negligible compared with normal heat input requirements supplied by tank heater (3).

The oxygen supply operates in an exactly analogous manner, except of course for differences in tank size, pressures and temperatures. Pressure regulator (8) is a slave regulator controlled by reference pressure (9) measured at the electrolyte expansion tank (26).

B. Gas Circulation System

The fuel and oxidant gas systems are similar except for the numerical values of areas, volumes, flow rates, etc., and will be described with reference to the hydrogen gas system.

Hydrogen gas passes through the fuel cell (10) via internal manifolds, picking up water and heat. It is circulated by a low velocity, low head blower (11) whose pumping rate is controlled by reference to the reference pressure (9) with provision for proper temperature compensation (to correct for net expansion of the electrolyte with temperature). The fuel cell is practically self-regulating with respect to the rate of water rejection, so that this control may be considered a safety circuit to override abnormal behavior. The H_2 gas passes through heat exchanger (12) giving up a portion of its heat, but is not permitted to drop in temperature below the dew point. The gas is further cooled in condenser (13), dropping well below the dew point and condensing water on heat exchanger fins thermally connected with the space radiator (28). Water as produced is transferred by capillary wicks to water storage tank (14) where it is stored by physical adsorption. Exit gas from condenser (13) is split into two streams by proportioning bypass valve (15), whose setting is controlled by a thermoregulator controlled by the temperature of the fuel cell (10). Gas in the bypass stream picks up heat from the regenerative heat exchanger (12) which in effect bypasses such heat across the radiator (28), permitting the temperature of the fuel cell to increase. Overriding safety circuit controls are provided to prohibit a drop in condenser temperature below the freezing point, or an increase in fuel cell temperature above the maximum design temperature. Hydrogen reenters the fuel cell through a heat exchanger (16) where it is preheated to avoid chilling the entry port region of the fuel cell. The design of this exchanger is integral with the fuel cell module, but is shown separately as it has a separate function in terms of heat balance.

The oxygen loop is similar except for a purge vent (22) to permit purging of impurities normally present in liquid oxygen. The purge frequency and amount can be pretimed by an automatic time clock, based on

oxygen purity or can be placed under operator control. Purging is not required for fuel cells operated from high purity (electrolytic) oxygen.

C. Electrolyte Ciruclation System

Hot KOH electrolyte exits from the fuel cell through the heat exchanger (16) built into the end plate structure of the fuel cell. A low velocity, low head canned rotor pump (23) whose pumping rate is controlled stepwise by preset controls based on the current to the external load (27) and the radiator temperature (28) provides coarse temperature control. Fine control on the temperature is provided by the bypass valves (15) and (21). For missions in which the heat sink temperature is relatively constant (e. g., not more than about 20° to 30°F variation) this control of pumping speed is not necessary, and a constant speed electrolyte pump will suffice. The degasifier unit (24) is physically constructed as a portion of the housing of pump (23) and operates as a centrifugal separator to eliminate any chance of gas bubbles resulting from solubility of the reactant gases in the electrolyte, or as a safety device to permit system operation despite a minor gas leak into the electrolyte system. Radiator (29) is scaled in size to prevent electrolyte freeze-up at the lowest sink temperature and lowest operating power level for which the system is rated. In order to permit reasonable tolerance in the electrolyte concentration, the radiator heat exchanger (25) must be kept above about -40°C. Expansion tank (26) provides for thermal expansion and for volume changes resulting from changes in concentration in electrolyte. The expansion tank is a completely filled bellows, whose expansion provides a means of measuring the electrolyte volume for control purposes.

D. Fuel Cell

The fuel cell battery (10) is a parallel array of 28 volt modules. Although fuel cell electrodes are available from standard production in sizes which would permit more than 2 kw to be supplied from a single 28 volt module, greater reliability can be achieved by breaking down the power supply into a number of smaller units in parallel. (Still greater reliability could be achieved where end-use requirements permit by lowering the voltage to 6 volts and increasing the number of parallel elements.) For a nominal 2 kw power supply at 28 volts, four modules in parallel each supplying 20 amperes at 28 volts would provide a nonredundant system with adequate provision for parasitic power for pumps, etc.

By inserting proper controls such as solenoid valves and relays in the parallel branches, the modules can be made completely independent with respect to any failure mode, permitting the use of binomial statistics in estimating reliability of the battery from reliability of the component modules. Based on module test data for the present state-of-art electrodes, the reliability to 200 hours life should be about 0.98, or about 0.99 to 100 hours life.

For a nonredundant system of four parallel modules, the resultant reliability to 100 hours and 200 hours respectively is 0.961 and 0.922 for the battery itself. (It can safely be assumed that the reliability of the

control and isolation circuits will not be limiting at this reliability level.) To gain a useful level of reliability, redundancy is required as shown in the following table:

Number of Modules	Redundancy	Reliability to: 100 Hrs.	200 Hrs.	720 Hrs.
4	1.00	0.961	0.922	0.748
5	1.25	0.9990	0.9962	0.9575
6	1.50	0.99998	0.99985	0.99416
7	1.75	0.9999997	0.9999947	0.9993
8	2.00	0.9999999	0.999998	0.99992

The above analysis is based on electrode failure as the only failure mode. For short periods of operation at high redundancy, it is obvious that the reliability of components other than electrodes will become controlling and require modification of the analysis.

E. Radiators

The low operating temperature of the UNION CARBIDE Fuel Cell (as compared with high temperature heat engines, for example) is a major advantage with respect to materials selection and reliability, but calls for increased radiator size at any given rate of heat rejection. In view of the high efficiency of the fuel cell, the total quantity of heat to be rejected is fortunately quite small. Based on present state-of-art for the fuel cell operating temperature, a radiator facing black space would require approximately 40 to 45 ft^2 per kilowatt (electrical) output of the fuel cell, or an assembly about 6.5' x 6.5'. A radiator facing the sun would require about 60 to 70 ft^2, or about 8' x 8'. Present engineering tests of the operation of the fuel cell at somewhat higher temperatures (e.g., 90 to 100°C) indicate that these areas can be reduced to 25 ft^2 (viewing space) or 36 ft^2 (viewing the sun) at an emissivity of 0.8 and an absorptivity of 0.2 for a 1 kw system. These radiator areas assume that the radiator must reject the total waste heat of the fuel cell to space. For a fuel cell whose electrolyte concentration is maintained constant by rejecting water (through an electrolyte evaporator which serves as an evaporative cooler) the radiator area required becomes about 18 ft^2 (viewing space) or 24 ft^2 (viewing the sun).

F. Simplified Systems

The previous analysis has discussed a complete fuel cell power system capable of fully automatic control over a wide range of power output and uncontrolled variations in heat sink temperature, operating for an extended mission at high power density. By contrast, a fuel cell power system operating at fixed load with a predetermined heat sink condition could be extremely simple in design, particularly for short missions at low power.

The electrolyte circulating pump (23), degasifier unit (24), electrolyte radiator (25, 29), H_2 and O_2 blowers (11, 17), regenerative heat

exchangers (12, 18), bypass valves (15, 21), vent valve (22), water storage tanks and condensers (13, 14, 19, 20) can all be eliminated. A modified design fuel cell (10) stores byproduct water by simple dilution of electrolyte and rejects heat by thermal conduction.

APPENDIX A

BATTERY DESCRIPTION

ASD 500 Watt Fuel Cell Test Battery Specifications:

Power (Gross)	535 Watts
Power (Net)	500 Watts
Voltage (Loaded)	28 Volts
Current (Total)	19 Amps
Number of Modules	4 Modules
Fuel	Hydrogen
Oxidant	Oxygen
Electrolyte	KOH-45%
Weight	212 lbs.
Volume	3.2 ft^3 (15" x 19" x 19.5")

Module Specifications:

Voltage	14 Volts
Current	9.5 Amps
Number of Cells	18 Cells
Weight	53 lbs.
Volume	0.8 ft^3 (7.5" x 9.5" x 19.5")

Filter-press type of assembly employing framed electrodes with a self-ported design for parallel fluid delivery to all cells.

Cell Specifications:

Electrodes	1/4" Gas Baked Carbon
Cell Area (Active)	0.191 sq. ft. (5" x 5.5")
Frame	Thermoplastic Styrene
Seals	"O" Ring-Gaskets
Gas Barrier	Ni Plated Copper
Electrolyte Cavity Thickness	1/8"
Gas Cavity Thickness	1/16"
Total Cell Thickness	7/8"
External Cell Dimensions	8-5/8" x 7-1/4"

COMPONENT WEIGHTS
500 WATT FUEL BATTERY

	500 Watt ASD Test Battery	Projected Weight, Optimized Design
4 - 18 Cell Modules	212.0	41.9
6.2 liters System Electrolyte	20.5	
Flake KOH Feeder	3.0	--
KOH Pump	0.7	40.1
KOH Pump Motor	7.0	
KOH Plumbing	15.0	
Gas Plumbing and Fittings	21.0	
Wiring and Sensors	20.0	5.0
	299.2	87.0

ASD 500 WATT FUEL CELL POWER TEST

Key to Strip Chart Record

Position	Function	Full Scale Range
1	Ambient Temperature	0 - 200°F
2		
3	Voltage of Fuel Cell	0 - 30 Volts
4		
5	Oxygen Use Rate	0 - 100*
6	Current of Fuel Cell	0 - 30 Amps
7	Hydrogen Use Rate	0 - 100*
8		
9	Thermocouple switch No. 9	0 - 200°F
10	Thermocouple switch No. 10	0 - 200°F

*Calibration curves required.

ASD 500 WATT FUEL CELL POWER TEST

Key to Thermocouple Position Code

Thermocouple Schedule	T. C. Position
Module - Electrolyte - Out	9 - 1
Module No. 4 H_2 Feed Manifold Temperature	9 - 2
Module No. 1 H_2 Feed Manifold Temperature	9 - 3
Module - Electrolyte - In	9 - 4
Heat Exchanger - Cooling H_2O Out	9 - 5
Heat Exchanger - Electrolyte - In	9 - 7
Module No. 2 H_2 Feed Manifold Temperature	10 - 1
Module H_2 Feed Gas Temperature	10 - 3
Heat Exchanger - Electrolyte - Out	10 - 5
Module O_2 Feed Gas Temperature	10 - 6
Heat Exchanger - Cooling H_2O - In	10 - 7
Module - H_2 Purge Gas Temperature	10 - 9
Module - O_2 Purge Gas Temperature	10 - 10
Module No. 3 Feed Manifold Temperature	10 - 11

ESTIMATE OF HOURLY KOH FLAKE ADDITION TO MAINTAIN 47 PER CENT AQUEOUS CONCENTRATION

Water of formation - 500 Watt Battery

No. of Cells 72

Avg. Current/Cell 9.4

Total Battery Amperes = 72 x 9.4 = 676 Amps

By Figure 15 230 g H_2O/Hr is formed by 676 Amperes - Current

$$\frac{230}{453.5} = 0.508\#\ H_2O/Hr$$

To maintain a 47% (12N) solution of KOH, x# of KOH must be added/hr to reconcentrate against 0.508#/hr water of formation.

x = weight of 100% KOH/hr

$\frac{x}{0.47}$ = weight of solution

$\frac{x}{0.918}$ = weight of concentrated flake added

0.508 = #water/hr added

$$\frac{x}{0.47} - \frac{x}{0.918} = 0.508$$

$$x = \frac{0.508}{(2.125 - 1.09)} = 0.491\#/hr \quad 100\% \text{ flake}$$

$$= 0.535\#/hr \quad 91.8\% \text{ flake}$$

Flake feeder delivers

3000 g/hr

0.535#/hr = 242.5 g/hr

$$\% \text{ on time} = \frac{242.5}{3000} = 8.1\%$$

$$= 4.86 \text{ min/hr} \xleftarrow[\text{on time}]{\text{feeder}}$$

The original 3000 g/hr feed rate of the electrolyte reconcentrator (reported in Monthly Report No. 20) was made on representative flake on hand.

Experience during the test showed that handling, weighing, supply packing, and vibrator frequency influenced the flake feed rate of the reconcentrator in the direction of higher bulk density.

The auger of the feeder delivers on a volumetric basis. Hence "on-time" of the reconcentrator was adjusted down between 50 and 60 seconds per 15 minute period or approximately 6 per cent on-time.

ASD 500 WATT SUSTAINED PERFORMANCE TEST

THERMAL BALANCE

Total heat added = Total energy out

A. Heat added based on water of formation

0. 508# water formed/hr

(0. 508#) (6760 B. t. u. /#H_2O - Heat of formation)

= 3440 B. t. u. /hr - heat added by fuel

B. Heat added by KOH flake addition

0. 535#/hr of 91. 8% flake

0. 535 + 0. 508 = 1. 043# KOH solution (specific heat = 0. 67) will undergo by Hooker Chemical brochure on caustic potash - Fig. 3, p. 15 - a 250°F temperature rise upon dilution of 90 per cent flake to a 47 per cent solution

(1. 043#) (0. 67 B. t. u. /#°F) (250) = 175 B. t. u. /hr

Total heat added = A + B

= 3440 + 175

= 3615 B. t. u. /hr ← Total Heat Added

Heat Rejected + Electrical Energy

= Total energy out

Electrical energy out = 535 watts terminal + 21 watts-leakage current power = (556) (3412 B. t. u. -hr/watt)

= 1895 B. t. u. /hr

Heat rejected = 1200 B. t. u. /hr (by water jacket heat exchanger log)

+ Heat losses due to: System conduction, Heat contents of vented gases, Overflow KOH liquid } Negligible

3615 = 1895 + 1200 + Losses

Losses = 520 B. t. u. /hr to ambient

ESTIMATE OF REQUIRED PUMPING POWER FOR KOH RECIRCULATION IN 500 WATT BATTERY SYSTEM

Pumping power for KOH recirculation in the 500 watt battery system was that required to service 4 - 18 cell modules and one heat exchanger.

4 Modules - 630 ml/min - mod - 1.5 specific gravity

1' Pressure head

Discharge through 4 - 3/16" I. D. tubes

$$\text{Pump H/Mod} = \frac{(630)(1.5)(1 + \text{Vel. Hd})}{454 \times 33,000}$$

$$\text{Vel. Hd} = \frac{V^2}{2g}$$

$$V = \frac{63 \text{ ml/min}}{6} \quad \frac{(1 \text{ cu ft})}{28320 \text{ ml}} = \underline{\text{Negligible}}$$

$$= \frac{(630)(1.5)}{454 \times 33,000} \times 4 = \frac{8.35}{3.3} \times 10^{-4}$$

$$= 2.78 \times 10^{-4} \text{ IP}$$

$$2.78 \times 10^{-4} \times \frac{746 \text{ watts}}{} = 0.2075 \text{ watt/module}$$

Heat exchanger circulation rate required was equal to that of each module but the pressure drop through the heat exchanger was 40° of liquid or 3-1/3' (3-1/3 x pumping power/module).

Therefore:

Total system pumping power = (3-1/3 + 4) x power/module

Total pump = (7.33) (0.2075 watt)

= 1.53 watts

Assuming 50 per cent efficient pump driven by a 60 per cent efficient d. c. motor

$$\text{Optimum pumping power} = \frac{1.53}{(0.5)(0.6)}$$

= 5.1 watts

ASD 500 WATT SUSTAINED PERFORMANCE TEST

ELECTRICAL LOG

Module No. 1

(Sample Data)

Total Accum. Hrs.	Total Hrs. Load	Amps	Battery Cell Number																		Total Voltage	Power
		I	E_1	2	3	4	5	6	7	8	9	10	11	12	13	14	15	16	17	18	ΣE	Watts
9	0	OC	.975	.985	.990	.980	.990	.985	.990	.995	.990	.990	.995	.990	.995	.995	.990	.980	.990	.995	17.7	0
18	0	1.0	.890	.890	.885	.890	.895	.890	.890	.890	.890	.890	.890	.890	.885	.890	.890	.895	.885	.890	16.0	32.0
40	11	9.0	.790	.805	.810	.800	.815	.810	.810	.800	.815	.815	.810	.820	.815	.815	.820	.820	.815	.810	14.70	132.30
169	79	9.05	.810	.815	.820	.815	.815	.820	.825	.815	.830	.825	.820	.830	.825	.825	.825	.825	.825	.820	14.90	134.8
217	127	9.05	.780	.805	.810	.805	.820	.815	.820	.810	.820	.810	.810	.820	.810	.810	.815	.805	.815	.810	14.70	132.7
257	167	9.25	.77	.80	.80	.80	.81	.805	.81	.80	.81	.795	.805	.805	.80	.805	.805	.79	.80	.795	14.55	134.6
303	213	9.00	.765	.800	.800	.800	.810	.810	.810	.810	.820	.805	.810	.815	.805	.810	.810	.790	.810	.800	14.60	131.4
401	311	9.0	.735	.780	.780	.785	.780	.795	.790	.800	.805	.785	.800	.795	.785	.785	.795	.760	.785	.780	14.30	128.7
449	359	8.85	.710	.760	.760	.770	.755	.780	.775	.785	.790	.770	.790	.785	.770	.765	.785	.740	.770	.760	14.00	123.9
498	408	8.82	.695	.745	.740	.760	.740	.770	.765	.770	.780	.760	.775	.780	.755	.750	.775	.730	.755	.745	13.80	121.7
546	456	8.90	.700	.755	.755	.765	.750	.775	.770	.770	.780	.760	.775	.775	.760	.755	.775	.730	.755	.745	13.80	122.8
594	503	8.8	.705	.76	.765	.77	.75	.78	.775	.78	.790	.775	.790	.785	.77	.76	.78	.735	.765	.750	13.95	122.8
640	550	9.0	.680	.745	.750	.755	.730	.765	.760	.770	.775	.760	.770	.780	.755	.740	.770	.715	.745	.735	13.70	123.3
688	598	9.15	.680	.740	.745	.750	.730	.765	.760	.760	.770	.760	.770	.775	.750	.740	.770	.710	.740	.735	13.65	125.09
729	639	9.4	.655	.730	.735	.745	.715	.755	.755	.755	.765	.750	.760	.765	.745	.730	.760	.700	.730	.715	13.45	126.4
817	727	9.9	.670	.730	.735	.745	.720	.750	.750	.740	.760	.745	.760	.765	.745	.735	.760	.705	.735	.715	13.45	133.1
889	799	9.85	.640	.710	.720	.735	.700	.740	.740	.730	.750	.735	.760	.760	.740	.720	.755	.685	.715	.690	13.15	129.3
1049	959	10.02	.680	.740	.750	.760	.730	.760	.760	.745	.770	.755	.770	.775	.755	.740	.770	.715	.740	.715	13.60	136.3
1169	1079	9.9	.665	.740	.745	.750	.725	.750	.750	.715	.760	.740	.760	.765	.750	.740	.760	.710	.745	.710	13.45	[illegible] 2
1218	1128	9.9	.670	.740	.740	.750	.720	.740	.740	.700	.745	.730	.745	.755	.745	.740	.760	.715	.745	.715	13.40	132.7
1392	1302	9.99	.690	.750	.740	.760	.720	.750	.730	.660	.725	.715	.730	.715	.745	.750	.760	.725	.765	.715	13.30	132.9
1518	1428	9.93	.625	.700	.680	.715	.660	.680	.690	.590	.670	.675	.690	.660	.685	.700	.710	.660	.730	.625	12.35	123.5
1674	1584	9.93	.620	.690	.675	.715	.640	.665	.695	.580	.660	.680	.700	.660	.690	.700	.710	.645	.730	.585	12.20	121.1
1794	1704	9.9	.590	.660	.655	.690	.600	.645	.670		.615	.665	.690	.640	.675	.680	.700		.700	.540	10.55	104.4

OC = Open Circuit
ΣE = Terminal Voltage by Meter

Module No. 2A

(Sample Data)

Total Accum. Hrs.	Total Hrs. Load	Amps	Battery Cell Number																		Total Voltage	Power
		I	E_1	2	3	4	5	6	7	8	9	10	11	12	13	14	15	16	17	18	ΣE	Watts
16	2	9.05	.815	.815	.815	.810	.815	.815	.820	.810	.830	.810	.815	.820	.815	.820	.830	.810	.825	.810	14.75	133.2
59	47	9.10	.805	.805	.805	.785	.810	.800	.820	.810	.810	.805	.795	.805	.795	.800	.810	.785	.795	.800	14.60	132.9
107	95	9.45	.81	.80	.815	.765	.815	.80	.82	.82	.82	.815	.805	.81	.795	.81	.83	.79	.805	.81	14.6	138.0
216	204	9.0	.790	.790	.800	.740	.810	.790	.815	.810	.800	.805	.770	.770	.770	.800	.805	.750	.760	.790	14.35	129.1
285	273	9.0	.785	.785	.795	.715	.805	.77	.805	.80	.795	.805	.755	.75	.76	.795	.800	.73	.745	.78	14.1	126.9
330	318	8.95	.775	.770	.785	.660	.795	.755	.800	.790	.780	.795	.735	.725	.745	.785	.780	.700	.720	.760	13.80	123.5
377	365	8.85	.780	.780	.795	.660	.800	.755	.805	.795	.780	.795	.740	.740	.750	.785	.790	.710	.730	.775	13.90	123.0
420	408	9.0	.780	.780	.790	.660	.800	.765	.805	.795	.780	.800	.750	.735	.750	.790	.790	.715	.735	.770	13.90	125.1
495	483	9.10	.780	.775	.795	.660	.800	.760	.805	.790	.780	.800	.750	.740	.745	.785	.785	.715	.730	.775	13.95	126.9
841	829	9.86	.745	.740	.775	.600	.770	.730	.780	.765	.750	.775	.725	.705	.715	.750	.750	.680	.695	.730	13.30	131.2
1041	1029	9.9	.760	.750	.780	.625	.780	.755	.780	.755	.740	.770	.730	.720	.735	.765	.765	.710	.720	.735	13.55	134.1
1240	1228	9.99	.770	.760	.795	.660	.790	.770	.755	.735	.700	.750	.720	.695	.740	.765	.750	.710	.735	.735	13.50	134.9

ΣE = Terminal Voltage by Meter

ASD 500 WATT SUSTAINED PERFORMANCE TEST

ELECTRICAL LOG

Module No. 3

(Sample Data)

Total Accum. Hrs.	Total Hrs. Load	Amps	Battery Cell Number																		Total Voltage	Power
		I	E_1	2	3	4	5	6	7	8	9	10	11	12	13	14	15	16	17	18	ΣE	Watts
24	0	2.0	.890	.890	.890	.900	.900	.900	.890	.885	.890	.890	.890	.890	.895	.890	.890	.900	.895	.905	16.1	32.2
41	11	9.0	.790	.800	.805	.810	.810	.810	.810	.805	.800	.820	.815	.810	.815	.810	.805	.810	.815	.815	14.60	131.40
136	106	9.1	.795	.805	.810	.815	.815	.820	.825	.815	.810	.820	.820	.815	.825	.820	.815	.820	.815	.810	14.60	134.66
184	152	9.25	.780	.790	.800	.800	.805	.805	.810	.810	.800	.815	.815	.810	.815	.815	.810	.810	.810	.800	14.50	135.0
224	192	9.35	.795	.800	.805	.810	.805	.810	.820	.815	.800	.815	.815	.810	.820	.820	.810	.810	.815	.790	14.70	137.4
303	271	9.25	.790	.805	.790	.805	.800	.800	.815	.810	.785	.810	.810	.810	.815	.810	.805	.810	.790	.810	14.60	135.0
392	361	9.70	.765	.785	.765	.785	.770	.760	.795	.795	.755	.780	.780	.785	.790	.790	.785	.775	.790	.745	14.20	130.2
437	405	9.9	.755	.78	.76	.78	.76	.755	.79	.79	.74	.775	.775	.78	.785	.785	.78	.765	.785	.74	14.05	139.1
473	440	9.85	.745	.770	.745	.770	.750	.740	.780	.780	.730	.765	.760	.770	.775	.780	.770	.755	.780	.750	13.85	136.4
529	496	9.85	.740	.770	.750	.770	.750	.730	.780	.780	.730	.765	.760	.770	.770	.780	.770	.755	.780	.730	13.85	136.4
593	559	9.75	.750	.77	.75	.775	.760	.740	.780	.780	.740	.770	.770	.775	.775	.785	.770	.760	.780	.740	13.95	136.0
737	703	9.75	.735	.765	.740	.760	.750	.725	.770	.770	.725	.760	.760	.770	.760	.775	.760	.750	.770	.725	13.75	134.1
838	790	9.70	.725	.760	.740	.755	.750	.725	.770	.765	.730	.760	.760	.770	.770	.780	.770	.755	.775	.740	13.80	133.9
969	935	9.70	.710	.755	.720	.755	.740	.730	.770	.765	.720	.755	.745	.760	.750	.765	.745	.740	.765	.720	13.55	131.4

ΣE = Terminal Voltage by Meter

Module No. 4

(Sample Data)

Total Accum. Hrs.	Total Hrs. Load	Amps	Battery Cell Number																		Total Voltage	Power
		I	E_1	2	3	4	5	6	7	8	9	10	11	12	13	14	15	16	17	18	ΣE	Watts
23	0.0	2.0	.900	.885	.900	.905	.900	.900	.900	.895	.900	.885	.880	.895	.890	.890	.900	.900	.900	.900		
30	1	9.0	.810	.805	.815	.820	.810	.820	.820	.815	.820	.815	.810	.820	.795	.810	.810	.820	.815	.820	14.70	132.3
71	41	9.1	.800	.800	.810	.805	.810	.810	.815	.810	.810	.810	.810	.810	.795	.800	.805	.810	.810	.810	14.70	133.8
120	91	9.1	.800	.810	.820	.810	.810	.820	.830	.820	.825	.820	.820	.820	.800	.815	.820	.820	.820	.820	14.80	134.7
165	136	9.0	.805	.800	.820	.810	.820	.825	.820	.825	.820	.815	.820	.805	.815	.815	.820	.810	.810	.810	14.60	131.40
244	215	9.35	.800	.800	.810	.805	.810	.815	.820	.815	.820	.815	.810	.820	.805	.810	.810	.805	.800	.800	14.70	137.45
328	296	9.40	.790	.800	.810	.800	.800	.810	.810	.810	.810	.810	.810	.815	.800	.805	.810	.800	.795	.800	14.60	137.24
400	369	9.75	.775	.785	.795	.790	.785	.790	.795	.795	.780	.795	.795	.805	.785	.785	.795	.785	.775	.780	14.40	140.40
412	381	9.60	.760	.770	.795	.785	.785	.790	.800	.790	.800	.790	.795	.800	.785	.785	.795	.785	.770	.780	14.30	137.3
460	428	9.80	.740	.760	.775	.760	.760	.770	.775	.770	.760	.780	.775	.785	.765	.775	.770	.760	.750	.755	13.90	136.22
528	496	9.85	.740	.760	.780	.760	.755	.765	.775	.775	.770	.780	.770	.780	.760	.760	.770	.760	.745	.750	13.90	136.92
595	563	9.75	.730	.760	.780	.755	.765	.77	.78	.760	.780	.770	.775	.780	.770	.770	.770	.760	.750	.750	13.90	135.53
648	615	9.75	.720	.745	.780	.745	.760	.775	.780	.760	.780	.775	.770	.780	.765	.765	.770	.760	.750	.745	13.85	135.04
687	654	9.75	.690	.725	.775	.725	.755	.770	.770	.755	.780	.775	.775	.775	.760	.760	.760	.755	.745	.740	13.70	132.87
736	703	9.75	.650	.720	.770	.720	.750	.765	.770	.750	.780	.770	.770	.770	.760	.760	.760	.750	.740	.730	13.65	133.09
748	715	10.1	.660	.710	.760	.715	.740	.755	.755	.740	.765	.760	.755	.760	.750	.745	.745	.740	.730	.700	13.45	135.84

ΣE = Terminal Voltage by Meter

ASD 500 WATT SUSTAINED PERFORMANCE TEST

PARASITIC POWER LOG

(Sample Data)

		Pump Motor							Hydrogen Heaters							Total
Date	Hour	E_b	- E_r	= E	x I_m	= Watts	e_1	e_2	e_3	e_4	ΣE	x I_h	= Watts	Watts
5-3-62	2400	28.85	- 6.60	= 22.25	x 1.1	= 22.30	12.4	12.2	11.9	12.9	49.40	.250	12.35	34.65
5-6-62	0050	29.10	- 6.55	= 22.55	x 1.1	= 22.61	10.95	10.90	10.45	11.45	43.75	.250	10.94	33.55
5-9-62	0000	29.2	- 6.80	= 22.40	x 1.1	= 22.44	10.35	11.30	10.55	11.55	43.75	.260	11.75	34.19
5-11-62	0812	28.80	- 6.45	= 22.35	x 1.1	= 22.39	11.20	10.20	10.30	11.35	43.05	.260	11.19	33.58
5-13-62	2100	28.80	- 6.45	= 22.35	x 1.1	= 22.39	11.20	10.20	10.30	11.30	43.0	.260	11.18	33.57
5-16-62	0035	28.80	- 6.50	= 22.30	x 1.1	= 22.33	11.20	10.20	10.35	11.40	43.15	.260	11.22	33.55
5-18-62	0915	28.65	- 5.80	= 22.85	x 1.1	= 25.13	10.90	10.00	11.20	11.15	43.25	.250	10.81	35.90
5-20-62	0045	28.30	- 5.70	= 22.60	x 1.1	= 24.96	10.00	9.85	10.00	10.95	41.60	.250	10.40	35.36
5-22-62	1810	27.60	- 6.15	= 21.45	x 1.1	= 23.60	10.50	9.60	9.70	10.70	40.50	.240	9.71	33.31
5-23-62	0910	27.70	- 8.00	= 19.70	x 1.1	= 21.60	10.55	9.65	9.75	10.75	40.70	.245	9.97	31.57
5-25-62	0930	27.75	- 9.45	= 18.30	x 1.1	= 20.13	10.60	9.65	9.80	10.75	40.80	.245	10.0	30.13
5-27-62	2110	27.90	- 10.6	= 17.30	x 1.1	= 19.03	10.65	9.70	9.85	10.8	41.10	.245	10.07	29.10
5-30-62	0020	27.65	- 10.35	= 17.30	x 1.1	= 19.03	10.60	9.70	9.75	10.75	40.80	.245	10.00	29.03
6-2-62	0915	27.60	- 10.50	= 17.10	x 1.1	= 18.81	10.50	9.60	9.70	10.65	40.45	.245	9.91	28.72

E_b = Battery Voltage E_r = Pump Motor Resistor Voltage ΣE = sum of heater voltages

$E_{motor\ voltage} \times I_m$ motor current = Pump Power I_h = the heater current

ELECTROLYTE LOG

(Sample Data)

Date	Hour	Flake Charge in Tower gms	Feeder On - Time Sec.	T. C. 9-7 °C	System Sp. Gr.	Conc. %	N	Electrolyte Overflow Tower Drained - ml/hr.	°C	Sp. Gr.	%
5-9-62	1323		24	47	1.460	47	12.4	940	163	31	1.465	46.4
5-9-62	1440	1000										
5-10-62	0930			49	1.425	44	11.3	950	311	32	1.430	43.7
5-10-62	1240	1000	52	49	1.430			960	328	31	1.430	
5-11-62	0820			44	1.430	44.2	11.4	1650	311	33	1.430	43.6
5-11-62	0900	1000		45	1.430	44.2						
5-12-62	0050	1000		44.5	1.470	47.7	12.7		327			
5-14-62	0720			44.5	1.430	44.2	11.4	2385	318	29	1.434	43.9
5-14-62	1015	1000										
5-15-62	0815			43.5	1.465	47.2	12.5	2530	338	27	1.470	46.8
5-15-62	0930	1000										
5-15-62	2000	1000		47	1.475	47.6		880	312	33	1.475	47.6
5-16-62	0055	1000										
5-16-62	0840	1000		47	1.500	50.3	13.7	2210	340	34	1.495	49.2
5-16-62	1245	1000										

ASD 500 WATT SUSTAINED PERFORMANCE TEST

HYDROGEN GAS LOG

(Sample Data)

Date	Hour	ΔT Hrs.	P*	°F Amb't	Cu. Ft.	CF/H_1 at Amb't	Purge Cu. Ft.	Purge CF/H_2	$(CF/H_1 - CF/H_2)$ at Ambient Temperature	CF/H at 0°C.	Net Use #/Hr.
5-7-62	0200	5.61	330	78	(51.2)	9.1	3.81	.68	8.42	7.66	.0429
5-7-62	0738	9.61	1950	78	(74.8)	7.8	6.48	.67	7.13	6.49	.0363
5-7-62	1715	7.33	1140	77	(56.8)	7.7	5.36	.73	6.97	6.34	.0355
5-8-62	0035	7.60	25	76	(58.1)	7.6	5.90	.78	6.82	6.21	.0348
5-8-62	0811	8.81	2170	75	(64.3)	7.3	7.17	.81	6.49	5.91	.0331
5-8-62	1700	7.33	1450	75	(47.4)	6.5	5.63	.77	5.73	5.21	.0292
5-9-62	0020	7.58	940	75	(53.4)	7.0	5.51	.73	6.27	5.71	.0320
5-9-62	0755	8.83	400	78	(81.5)	9.2	6.80	.77	8.43	7.67	.0430
5-9-62	1645	7.83	1700	77	(86.6)	11.1	5.56	.71	10.39	9.45	.0529
5-10-62	0025	8.15	770	77	(102.9)	12.6	6.65	.82	11.78	10.72	.0600
5-10-62	0834	8.43	1830	76	(97.2)	11.53	7.54	.89	10.64	9.68	.0542
5-10-62	1700	7.17	780	77	(96.7)	12.65	8.31	1.16	11.49	10.46	.0586
5-11-62	0010	7.98	1980	77	(95.8)	12.01	9.16	1.15	10.86	9.88	.0553
5-11-62	0809	8.02	930	76	(99.0)	12.34	11.29	1.41	10.93	9.95	.0557
5-11-62	1610	8.13	2130	76	(97.8)	12.03	10.20	1.25	10.78	9.81	.0549
5-12-62	0018	8.53	1100	76	(96.7)	11.34	8.74	1.03	10.31	9.38	.0525
5-12-62	0850	11.92	360	78	(160.1)	13.4	15.23	1.28	12.13	11.03	.0618
5-12-62	2045	2.92	400	78	(39.0)	13.4	4.05	1.34	12.06	10.97	.0614
5-12-62	2340	9.83	2220	78	(118.5)	12.1	12.59	1.32	10.78	9.81	.0549
5-13-62	0935	27.25	2150	78	(362.3)	13.3	58.10	1.84	11.16	10.16	.0569
5-14-62	1705	7.50	900	78	(96.8)	12.9	14.93	2.34	10.59	9.61	.0539
5-15-62*	0035	7.83	2100	75	(102.1)	13.0	14.88	1.90	11.10	10.10	.0566

*P = Recorded Tank Pressure at Indicated Time
Tank Changes not shown

OXYGEN GAS LOG

(Sample Data)

Date	Hour	ΔT Hrs.	P*	°F Amb't	Cu. Ft.	CF/H_1 at Amb't	Purge Cu. Ft.	Purge CF/H_2	$(CF/H_1 - CF/H_2)$ at Ambient Temperature	CF/H at 0°C.	Net Use #/Hr.
5-3-62	2035	28.17	1775	78	189	6.71	43.78	1.55	5.16	4.70	.418
5-5-62	0048	38.83	2330	77	250	6.44	76.97	1.98	4.46	4.06	.361
5-6-62	1535	10.34	2290	78	68	6.58	13.91	1.35	5.23	4.76	.424
5-7-62	0155	30.25	1680	78	140	4.63	45.76	1.52	3.11	2.83	.252
5-8-62	0810	13.75	400	75	106	4.46	36.61	1.54	2.92	2.66	.237
5-9-62	0755	28.50	2370	77	189	6.63	46.58	1.41	5.22	4.75	.423
5-10-62	1225	33.33	2290	76	249	7.47	57.21	1.61	5.86	5.33	.474
5-11-62	2145	26.00	2300	77	201	7.73	57.90	1.83	5.90	5.37	.478
5-12-62	2345	39.17	500	77	290	7.45	67.41	2.15	5.30	4.82	.429
5-14-62	1455	33.50	2400	78	258	8.19	82.48	1.66	6.53	5.94	.529
5-16-62	0025	24.08	2350	77	188	7.81	29.29	1.86	5.95	5.41	.482
5-17-62	0030	8.33	700	79	69	7.74	73.19	1.86	5.88	5.35	.476
5-17-62	0850	31.08	2350	79	236						

*P = Recorded Tank Pressure at Indicated Time
Tank Changes not shown

ASD 500 WATT SUSTAINED PERFORMANCE TEST

GAS TEMPERATURE LOG

(Sample Data)

Date	Time	Avg. H_2 Feed Gas T.C. 10-3 °F	Module H_2 Manifold Temperatures °F Mod. T.C.	#1 9-3	#2 10-1	#3 10-11	#4 9-2	Avg. H_2 Purge Gas Temp. T.C. 10-9	Avg. O_2 Feed Gas Temp. T.C. 10-6 °F	Avg. O_2 Purge Gas Temp. T.C. 10-10
5-9-62	1650	77		137	136	132	133	112	80	94
5-12-62	0030	79		135	134	133	132	89	80	94
5-13-62	0923	81		135	134	133	134	110	82	83
5-16-62	0905	79		137	137	135	135	100	80	94
5-18-62	0930	81		134	132	130	133	108	83	104
5-20-62	1000	83		134	132	131	134	56	84	97
5-22-62	1030	79		131	128	128	129	102	83	96
5-23-62	1730	79		132	128	130	130	123	80	95
5-24-62	0820	92		134	130	130	132	127	86	95
5-25-62	1730	80		134	130	130	132	128	82	92
5-26-62	1920	84		133	131	131	132	125	86	93
5-28-62	0749	82.5		142	137.5	138	140	112	86	95
5-29-62	0725	80		138	133.5	133.5	135	113	84	94.5
5-31-62	0815	82		139	137	136	138	122	84.5	100
6-1-62	0737	79		139	79	135	137	120	79	97
6-2-62	1000	78		139	137	137	138	121	80	96

ASD 500 WATT SUSTAINED PERFORMANCE TEST

RELATIVE HUMIDITY LOG

(Sample Data)

		Gas Temp. Thermocouples				Relative Humidity Sensors															
						Position #1-Total H_2 Purge				Position #2-Total O_2 Purge				Position #3-Mod. #1 O_2 Purge				Position #4-Mod. #1 H_2 Purge			
		H_2 In	H_2 Out	O_2 In	O_2 Out	Rel. Hum.		Temperature		Rel. Hum.		Temperature		Rel. Hum.		Temperature		Rel. Hum.		Temperature	
Date	Hour	10-3	10-9	10-6	10-10	S. R.	Actual	S. R.	Actual	S. R.	Actual	S. R.	Actual	S. R.	Actual	S. R.	Actual	S. R.	Actual	S. R.	Actual
5-4-62	0055	79	112	80	88	58	76.5	63	78.5	100+	*	66	83	100+	*	63	78.5	55	25.0	65	81.5
5-5-62	0735	78	91	78	90	66	82	65	81.5	100+	*	67	85	100+	*	64	80	62	27.9	66	83
5-7-62	0800	82	94	84	91	51	70	65	81.5	100+	*	67	85	100+	*	64	80	62	27.9	66	83
5-9-62	0025	74	86	74	92	38	60.5	63	78.5	100+	*	65	81.5	100+	*	63	78.5	38	17.5	65	81.5
5-9-62	1255	77	95	78	92	40	61.5	65	81.5	100+	*	67	85	100+	*	66	83	58	26.2	68	87
5-10-62	0027	78	92	80	91	56	75	64	80	100+	*	66	83	100+	*	64	80	60	27.0	66	83
5-11-62	0015	79	98	81	92	36	59.2	64	80	100+	*	67	85	100+	*	64	80	19	9.1	64.5	81
5-12-62	0915	79	78	80	94	44	64.2	65	81.5	100+	*	67	85	100+	*	65	81.5	35	26.1	66	83
5-14-62	0705	82	109	83	93	43	63.5	65	81.5	100+	*	67	85	100+	*	65	81.5	18	8.8	65	81.5
5-16-62	0855	79	100	81	94	39	61	64	80	98.5	52	66	83	100+	*	63	78.5	28	13.2	64	80
5-19-62	0908	84	87	84	97	31	56.7	67	85	94	48.8	69.5	89	100	*	66.5	83.5	17.5	8.5	66.5	83.5
5-22-63	0840	82	60	85	94	35	58.8	63.5	79	97	51	66.5	84	100+	*	64	80	100+	*	76	101
5-23-62	1720	79	123	80	95	31	56.7	63.5	79	88	43.7	67	85	95	49.5	65	81.5	↓	↓	↓	↓
5-24-62	1000	79	55	82	93	37.5	60.1	63.5	79	100+	*	66	83	100+	*	64	80				
5-27-62	0930	84	113	85	99	10	46.4	64.5	81	96	50.5	69	88	100+	*	66	83				
5-29-62	1710	78	74	79	98	10.5	46.6	62	77	96	50.5	67	85	100+	*	65.5	82				
6-1-62	0722	79	115	79	96	10	46.4	61	75	99	52.5	65	81.5	100+	*	63.5	79				
6-3-62	1110	79	104	79	88	15	48.8	63	78.5	100	53	66	83	100	53	64	80	↓	↓	↓	↓

*Value Indeterminate S. R. = Scale Reading

↓Sensor Damaged

ASD 500 WATT SUSTAINED PERFORMANCE TEST

HEAT EXCHANGER LOG

(Sample Data)

		Heat Exchanger KOH Rate							Cooling Water				
Date	Time	In. Head	#/ Hr.	SP. GR.	T. C. In °F 9-7	T. C. Out °F 10-5	ΔT °F	BTU/ Hr.	ml/ Min.	T. C. °F 9-5	T. C. °F 10-7	ΔT °F	BTU/ Hr.
5-10-62	0900	31	91.23	1.425	113	96	17	1039	316	92	67	25	1041.7
5-12-62	2050	28.5	88.42	1.450	114	90	24	1422	352	88	65	23	1067.7
5-14-62	0700	29.0	88.15	1.430	113	92	21	1240	400	85	65	20	1055.0
5-15-62	1940	27.5	88.59	1.475	117	89	28	1662	401	85	66	19	1004.7
5-17-62	0045	31	95.39	1.490	115	89	26	1662	495	83	64	19	1246.1
5-18-62	0930	29.75	93.11	1.485	114	90	24	1497	555	82	64	18	1317.4
5-19-62	2135	27.75	90.39	1.495	116	82	34	2059	840	74	61	13	1441.4
5-21-62	1635	34.5	99.59	1.465	110	91	19	1267	585	80	63	17	1312.7
5-22-62	0027	35.0	100.18	1.465	113	91	22	1476	505	81	62	19	1266.5
5-24-62	0015	30.5	93.77	1.480	115	90	25	1570	470	84	63	21	1298.6
5-25-62	1730	37.0	104.89	1.485	115	92	23	1616	655	79	62	17	1468.3
5-26-62	1915	36	99.98	1.440	115	90	25	1674	600	80	63	17	1345.0
5-28-62	1830	34.25	99.89	1.475	117	95	22	1472	414	86	65	21	1146.4
5-30-62	2120	37.75	103.00	1.445	120	104	16	1104	276	97	69	28	1018.9
6-1-62	1730	34.25	99.89	1.475	120	98	22	1472	338	89	64	25	1114.3
6-2-62	2100	33.75	98.91	1.475	120	100	20	1325	286	95	68	27	1052.8
							Avg. 1472 BTU/hr.					Avg. 1200 BTU/hr.	

ASD 500 WATT SUSTAINED PERFORMANCE TEST

CUMULATIVE MATERIAL RECORD

(Sample Data)

Date	Hour	Tests Hours	Hydrogen Weight: Gross Use Accum. #	Hydrogen Weight: Purge Accum. #	Hydrogen Weight: Net # Used Accum.	Oxygen Weight: Gross Use Accum. #	Oxygen Weight: Purge Accum. #	Oxygen Weight: Net # Used Accum.	Net Gas # Accum.	Power Amp Hrs. Accum.	Accum. H_2O # By Amp-Hrs.	KOH Flake Added Accum.	Total KOH Overflow #	Net # H_2O Accum. By Overflow Minus Flake
5-3-62	2100	Start												
5-8-62	0100	100	5.580	.375	5.205	49.7	10.126	39.6	44.8	55,800	41.89	46.30	92.66	46.36
5-12-62	0500	200	10.905	.868	10.037	100.2	22.677	77.5	87.5	111,708	82.67	72.76	153.66	80.90
5-16-62	0900	300	17.234	1.729	15.505	161.5	37.612	123.9	139.4	177,336	132.28	125.67	258.75	133.08
5-20-62	1300	400	23.971	3.177	20.794	224.4	53.515	170.9	191.7	243,972	185.19	178.58	360.12	181.54
5-24-62	1700	500	30.586	5.503	25.083	289.1	70.539	218.6	243.7	311,022	244.71	229.29	462.41	233.12
5-28-62	2100	600	38.266	7.331	30.935	350.4	88.024	262.4	293.3	379,062	286.60	282.20	569.16	286.96
6-2-62	0100	700	43.658	9.320	34.338	395.3	110.474	284.8	319.1	446,922	337.31	332.91	672.50	339.59
6-3-62	0700	730	45.610	9.794	35.816	411.3	115.833	295.5	331.3	467,442	348.33	346.14	691.97	345.85

APPENDIX B

ANALYSIS OF LEAKAGE CURRENTS IN FUEL CELL BATTERIES

This report contains analysis of parasitic leakage currents within the fuel cell module that are caused by having a common electrolyte system in contact with series-connected cells. The mechanical and physical parameters of the electrochemical system are translated into a mathematical and electrical model. Leakage currents of individual cells for modules up to 40 cells have been calculated by computer for 6" x 6" plastic framed electrodes used in the 500 watt sustained performance test.

Experimental data are presented that verify this theoretical analysis. Power loss in modules is discussed and presented, analyzing the electrochemical effect on individual electrodes.

Historical

Early in the development of fuel cell hardware interest arose concerning whether there may be some deleterious effects caused by having cells in series, yet having an electrolyte system common to all cells. This same condition had arisen before in other systems.

This condition was considered in the original frame design of the 6" x 6" electrode. Late in 1960, the electrolyte porting was modified to provide better flow characteristics. Again cell-to-cell electrolyte resistance was considered and the cross-sectional area of the electrolyte manifold was reduced both for fluid flow distribution and electrical resistance characteristics.

In the summer of 1960, the first mathematical analysis of fuel cell leakage currents was made. A mathematical model was made corresponding to the electrochemical and physical parameters. Refinements were made to the mathematics so that calculations could be made easily on a computer.

In May, 1962, final calculations as well as experimental confirmation were made on the 500 watt battery 6" x 6" ASD plastic frame construction in a 17-cell battery. The comparative data for a 17-cell module show:

TABLE I

Bipolar Cell Position	Leakage Current Values - Amps	
	Computed	Measured
1	0.227	0.258
2	0.333	0.357
3	0.382	0.432
4	0.405	0.461
5	0.416	0.470
6	0.421	0.447
7	0.423	0.484
8	0.424	0.491
9	0.424	0.492
10	0.423	0.487
11	0.421	0.489
12	0.416	0.489
13	0.405	0.478
14	0.382	0.458
15	0.333	0.407
16	0.227	0.304

The data are shown on the curves of Figure B-1.

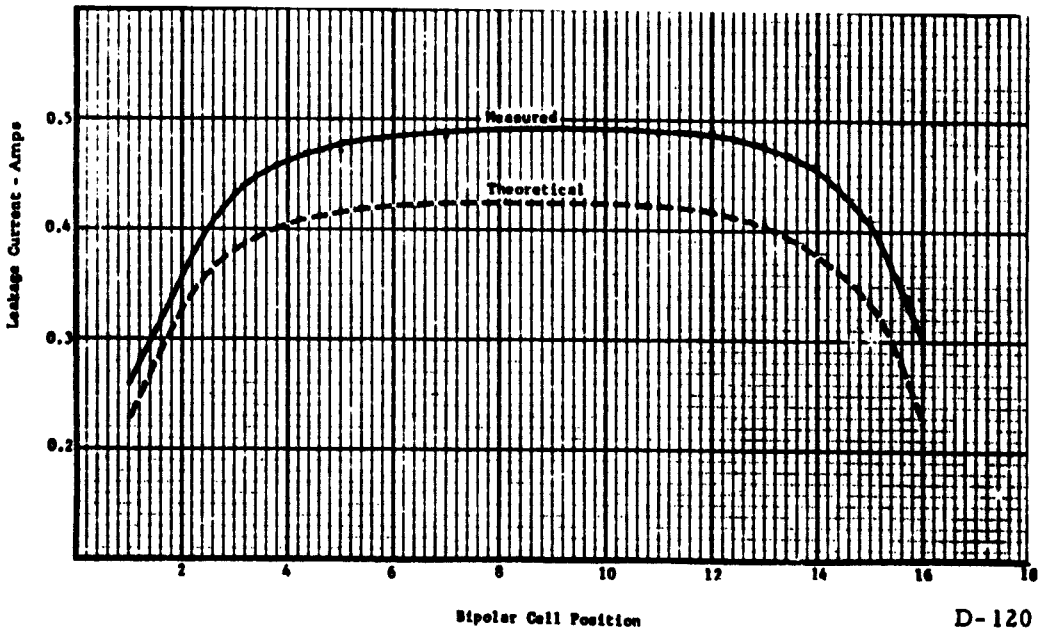

Figure B-1 - Leakage Current vs Cell Position. 17-Cell Carbon Electrode Fuel Cell Battery. 6" x 6" Plastic Framed Electrodes. Common Electrolyte.

Discussion

A. Analysis of Electrode Battery Parameters

To analyze the problem, it is important to study the physical make-up of the individual cell and follow its formation into a fuel cell module. Current within a cell normally flows through the electrolyte interim between electrodes. But since the electrolyte is a good conductor, current (ionic) will also flow to any point in the electrolyte system that has a difference in potential. There are four electrolyte accesses in each cell from the common manifolds. (See Figure B-2.) Current (ionic flow) following Ohm's Law is proportional to the potential difference and inversely proportional to the electrolyte resistance. Electron flow is counter to the conventional current flow.

With a multicell battery there are current paths to each cell from the common electrolyte manifold. Electrically the resistance from each cell to the common manifold is the same for a particular construction. Also the cell-to-cell resistance is uniform in the common manifolds.

To show a physical picture of leakage currents a sketch is made in Figure B-2 which describes the voltage and resistance arrangements within the module. A four-cell module is built up yielding cell voltages E_A, E_B,

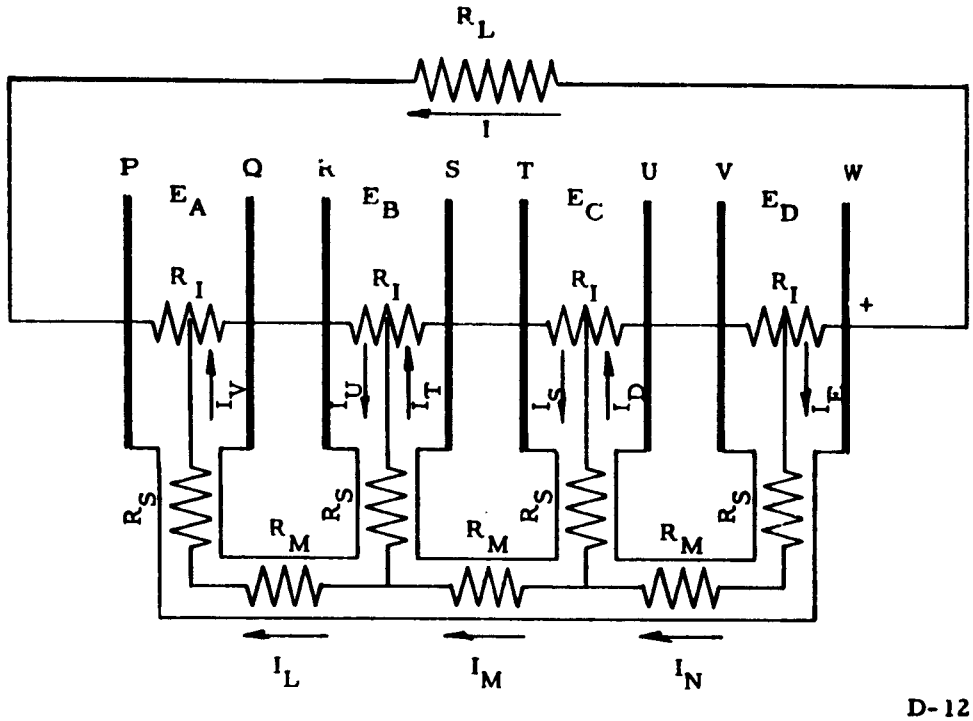

D-121

Figure B-2

E_C, E_D. Each cell has an internal resistance, R_I. One half of the internal resistance is arbitrarily attributed to each electrode. Cell-to-cell resistance in the common manifold is lumped together in R_M. Inlet resistance to each cell is lumped together as a single resistance and is described as R_S. Each individual cell contains the two electrodes P-Q, R-S, T-U, V-W.

Taking, for example, the two center electrodes S and T, we see that they form in reverse an active bipolar cell with an external (electronic) load circuit of the low resistance wire mesh and current collector. The internal (ionic) circuit provides current flow through the common electrolyte manifold (R_M) and the cell inlet orifices (R_S). This cell has a high internal resistance, and extremely low external resistance. The leakage current path is shown in Figure B-3.

This special short circuit cell satisfies the conditions required for current flow in any electrochemical system.

a) External electronics circuit.

b) Internal ionic path.

c) Two electrodes at a difference of potential.

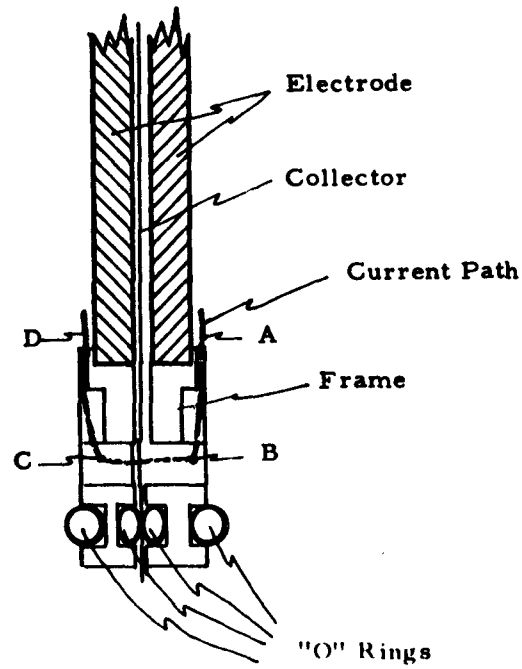

Resistance A-B	R_S	3.86 Ω
Resistance B-C	R_M	2.35 Ω
Resistance C-D	R_S	3.86 Ω

D-122

Figure B-3 - Bipolar Electrode Leakage Current Paths

In like manner, two electrodes Q-R and U-V form such cells in the four-cell module. Every electrode is under some sort of leakage current drain except electrodes P and W.

Since these cells do not have a complete electronic circuit, there can be no chemical reaction causing ionic current flow. This situation does change, however, when the battery has an external load when there is both electronic and ionic conduction at every electrode, as well as ionic conduction through the manifold electrolyte paths.

In describing the electrolyte leakage path, the resistance between the end of the electrolyte inlet and the electrode is considered negligible. Calculation would be difficult requiring extensive graphical analysis.

It is necessary to simplify the electrical circuit by superposition of the circuit elements and combination of existing bipolar electrode voltages.

As shown in Figure B-4, values of R_I are combined and placed in series with the equivalent cell voltages formed from the corresponding pairs of half-cell voltages. E_1, E_2, and E_3 are equivalent to electric potentials across Q-R, S-T, and U-V; E_4 is derived from the half-cell voltages of electrodes P-W. The various inlet resistances, R_S, and cell manifold resistances, R_M are essentially the same as shown before.

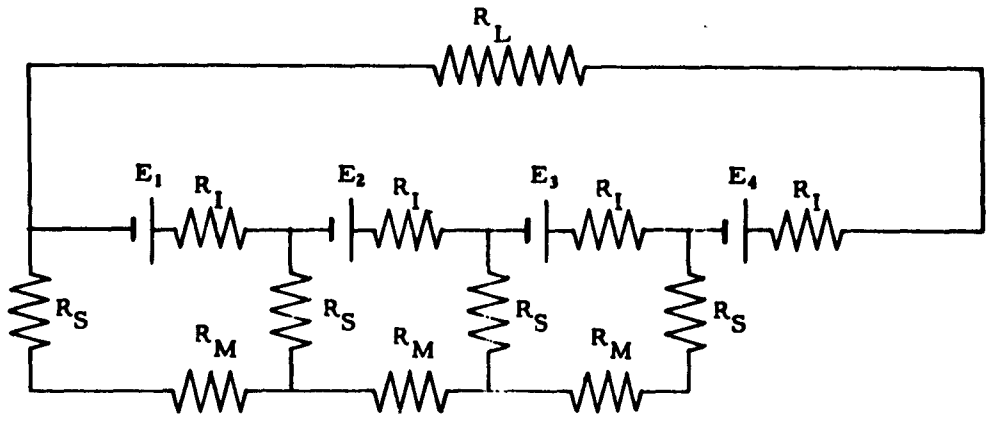

D-123

Figure B-4

We now have the mathematical model of a four-cell fuel cell module. Leakage currents entering and leaving each electrode shown in Figure B-2 or individual loop (manifold) currents in Figure B-4 can easily be derived from Kirchoff loop equations. Since there are three unknowns, three simultaneous equations result. Similarly, it follows that there are N-1 equations for a fuel cell module of N cells. Manual solution of higher order simultaneous equations becomes unmanageable (if not impossible) so computer help was sought in this problem.

Knowing what the mathematical model of the task is, the next step is to determine what the resistance constants R_S, R_M, and R_I are for the individual fuel cell frame constructions. The fundamental relationship for resistance of any material is shown in Equation (1).

Where $$R = \frac{\rho L}{A} \qquad (1)$$

R = resistance in ohms

ρ = specific resistance of material in ohm inches

L = length of conductor in inches

A = cross-sectional area in square inches.

Normal operation of fuel cell modules in recent months has used an electrolyte of 12 to 14 normal potassium hydroxide. Specific resistance of 0.618 ohm inch is used for 12 N potassium hydroxide at 60°C.

Manifold and inlet resistances were calculated by considering each as separate portions of the electrolyte stream and calculating resistance. Resistance constants for each type construction are shown below. Resistance of each inlet and manifold is combined in parallel and resolved into a single resistance R_S and R_M.

Electrolyte Single Cell Resistance

Frame Design	Resistance (Ohms) R_M	R_S
6" x 6" Type ASD Battery	2.35	3.86

The general equations and determinants were reviewed to rewrite them in a form that the digital computer could easily handle. Derivation of these equations is attached.

The results of the calculations for any number of cells from N = 1 to N = 40 are listed in Table II; computed values of leakage current for the 17-cell battery have been compared with experimental values in Table I and graphed in Figure B-1.

Solution of Leakage Currents for the Fuel Cell

Given a battery of n + 1 fuel cells:
and independent variables X_1, R, and E where

$X_1 = R_I + 2\ Rs + Rm$ (sum of loop resistances)

$R = R_s$

it is desired to find the dependent variables $I_1, I_2, I_3, \ldots, I_n$.

The following equations can be written:

$$
\begin{aligned}
E &= X_1 I_1 - RI_2 \\
E &= -RI_1 + X_1 I_2 - RI_3 \\
E &= -RI_2 + XI_3 - RI_4 \\
&\vdots \\
E &= -RI_{n-1} + X_1 I_n
\end{aligned}
$$

and in determinant form

TABLE II

Run 1 5/3/62

R_S = 3.860, xl = 10.070, E = 1.000

N	1																			
1	.09930																			
2	.16103																			
3	19454	.24844																		
4	.21140	.29243																		
5	.21956	.31372	.33982																	
6	.22344	.32383	.36232																	
7	.22526	.32859	.37291	.38519																
8	.22612	.33082	.37787	.39591																
9	.22652	.33187	.38019	.40092	.40666															
10	.22670	.33235	.38128	.40326	.41169															
11	.22679	.33258	.38179	.40436	.41404	.41672														
12	.22683	.33269	.38202	.40487	.41513	.41907														
13	.22685	.33274	.38213	.40511	.41565	.42017	.42142													
14	.22686	.33276	.38218	.40522	.41588	.42068	.42251													
15	.22686	.33277	.38221	.40527	.41600	.42092	.42303	.42361												
16	.22686	.33278	.38222	.40529	.41605	.42103	.42327	.42412												
17	22686	.33278	.38223	.40531	.41607	.42108	.42338	.42436	.42464											
18	.22687	.33278	.38223	.40531	.41608	.42110	.42343	.42447	.42487	- Theoretical leakage current - 18-.ell module - 500 watt test										
19	22687	.33278	.38223	.40531	.41609	.42112	.42345	.42453	.42497	.42511										
20	.22687	.33278	.38223	.40531	.41609	.42112	.42346	.42455	.42504	.42522										
21	.22687	.33278	.38223	.40532	.41609	.42112	.42347	.42456	.42506	.42528	.42534									
22	.22687	.33278	.38223	.40532	.41609	.42112	.42347	.42457	.42507	.42530	.42539									
23	22687	.33278	.38223	.40532	.41609	.42113	.42347	.42457	.42508	.42531	.42541	.42544								
24	.22687	.33278	.38223	.40532	.41609	.42113	.42347	.42457	.42508	.42532	.42542	.42547								
25	.22687	.33278	.38223	.40532	.41609	.42113	.42347	.42457	.42508	.42532	.42543	.42548	.42549							
26	.22687	.33278	.38223	.40532	.41609	.42113	.42347	.42457	.42508	.42532	.42543	.42548	.42550							
27	.22687	.33278	.38223	.40532	.41609	.42113	.42347	.42457	.42508	.42532	.42543	.42548	.42551	.42551						
28	.22687	.33278	.38223	.40532	.41609	.42113	.42347	.42457	.42508	.42532	.42543	.42549	.42551	.42552						
29	.22687	.33278	.38223	.40532	.41609	.42113	.42347	.42457	.42508	.42532	.42543	.42549	.42551	.42552	.42552					
30	.22687	.33278	.38223	.40532	.41609	.42113	.42347	.42437	.42508	.42532	.42543	.42549	.42551	.42552	.42553					
31	.22687	.33278	.38223	.40532	.41609	.42113	.42347	.42457	.42508	.42532	.42543	.42549	.42551	.42552	.42553	.42553				
32	.22687	.33278	.38223	.40532	.41609	.42113	.42347	.42457	.42508	.42532	.42543	.42549	.42551	.42552	.42553	.42553				
33	.22687	.33278	.38223	.40532	.41609	.42113	.42347	.42457	.42508	.42532	.42543	.42549	.42551	.42552	.42553	.42553	.42553			
34	.22687	.33278	.38223	.40532	.41609	.42113	.42347	.42457	.42508	.42532	.42543	.42549	.42551	.42552	.42553	.42553	.42553			
35	.22687	.33278	.38223	.40532	.41609	.42113	.42347	.42457	.42508	.42532	.42543	.42549	.42551	.42552	.42553	.42553	.42553	.42553		
36	.22687	.33278	.38223	.40532	.41609	.42113	.42347	.42457	.42508	.42532	.42543	.42549	.42551	.42552	.42553	.42553	.42553	.42553		
37	.22687	.33278	.38223	.40532	.41609	.42113	.42347	.42457	.42508	.42532	.42543	.42549	.42551	.42552	.42533	.42553	.42553	.42553	.42553	
38	.22687	.33278	.38223	.40532	.41609	.42113	.42347	.42457	.42508	.42532	.42543	.42549	.42551	.42552	.42553	.42553	.42553	.42553	.42553	
39	.22687	.33278	.38223	.40532	.41609	.42113	.42347	.42457	.42508	.42532	.42543	.42549	.42551	.42552	.42553	.42553	.42553	.42553	.42553	.42553
40	.22687	.33278	.38223	.40532	.41609	.42113	.42347	.42457	.42508	.42532	.42543	.42549	.42551	.42552	.42553	.42553	.42553	.42553	.42553	.42553

$$I_1 = \frac{\begin{vmatrix} E & -R & O & \cdots & & O \\ E & X_1 & -R & & & \vdots \\ E & -R & X_1 & & & \vdots \\ \vdots & \vdots & \vdots & & & \vdots \\ \vdots & \vdots & \vdots & & & \vdots \\ \vdots & \vdots & \vdots & & X_1 & -R \\ E & O & O & \cdots & -R & X_1 \end{vmatrix}}{\begin{vmatrix} E & -R & O & \cdots & & O \\ E & X_1 & -R & & & \vdots \\ E & -R & X_1 & & & \vdots \\ \vdots & \vdots & \vdots & & & \vdots \\ \vdots & \vdots & \vdots & & & \vdots \\ \vdots & \vdots & \vdots & & X_1 & -R \\ O & O & \cdots & & -R & X_1 \end{vmatrix}}$$

For simplicity, write the denominator as:

$$X_n = \begin{vmatrix} X_1 & -R & O & \cdots & & O \\ -R & X_1 & -R & & & \vdots \\ O & -R & X_1 & & & \vdots \\ \vdots & \vdots & \vdots & & & \vdots \\ \vdots & \vdots & \vdots & & & \vdots \\ \vdots & \vdots & \vdots & & & \vdots \\ \vdots & \vdots & \vdots & & X_1 & -R \\ O & O & O & \cdots & -R & X_1 \end{vmatrix}$$

and the numerator with E factored out as:

$$Y_{m,n} = \begin{vmatrix} X_1 & -R & \cdots & 1 & \cdots & & O \\ -R & X_1 & & 1 & & & \vdots \\ O & -R & & 1 & & & \vdots \\ \vdots & \vdots & & 1 & & & \vdots \\ \vdots & \vdots & & \vdots & & & \vdots \\ \vdots & \vdots & & 1 & & & \vdots \\ \vdots & \vdots & & 1 & & X_1 & -R \\ O & O & \cdots & 1 & \cdots & -R & X_1 \end{vmatrix}$$

where the m'th column is replaced by 1's. The m corresponds to the respective loop current (m = 1, 2, 3, . . . , n).

Then $I_m = E \frac{Y_{m,n}}{X_n}$ (n + 1 cells).

Computer techniques are desired in order to solve the determinants for n larger than 5. The determinants can be reduced by matrix reduction.

Three generalized equations result:

$$X_0 = 1$$
$$X_1 = X_1$$
$$X_2 = X_1 X_1 - X_0 R^2$$
$$X_3 = X_1 X_2 - X_1 R^2$$
$$X_4 = X \; X_3 - X_2 R^2$$
$$\vdots$$

(1) $$X_n = X \; X_{n-1} - X_{n-2} R^2$$

Now solving for the Y terms:

$$Y_{1,1} = 1$$
$$Y_{1,2} = X_1 + R\, Y_{1,1}$$
$$Y_{1,3} = X_2 + R\, Y_{1,2}$$
$$Y_{1,4} = X_3 + R\, Y_{1,3}$$
$$\vdots$$

(2) $$Y_{1,n} = Y_{n-1} + R\, Y_{1,n-1}$$

$$Y_{2,n} = X_1 Y_{1,n+1} + R X_{n-2} Y_{1,1}$$
$$Y_{3,n} = X_2 Y_{1,n-2} + R X_{n-3} Y_{1,2}$$
$$Y_{4,n} = X_3 Y_{1,n-3} + R X_{n-4} Y_{1,3}$$
$$\vdots$$

(3) $$Y_{m,n} = X_{m-1} Y_{1,n-m+1} + R X_{n-m} Y_{1,m-1}$$

The Royal McBee LGP 30 digital computer was programed for any given X and R. It will give results for all order systems up to N = 30 (31 cells). This program is valid only when the network takes on the symmetry where X_1 is the sum of the resistances in any loop and R is the common resistance between loops.

Table II gives results for $X_1 = 10.07$, $R = 3.860$ and $E = 1$. Because of symmetry, $I_n = I_1$, $I_{n-1} = I_2$, $I_{n-2} = I_3$, etc. Only the loop currents for one half of the battery are shown.

If $E \neq 1$, simply multiply the loop currents by the value of E to get actual current.

If there is a load current I_L, then multiply the loop currents by $E - I_L R_I$. This can be done if $R_I << X_1$.

Aeronautical Systems Division. Dir/Aero-mechanics. Flight Accessories Lab., Wright-Patterson AFB, Ohio.
Rpt Nr ASD-TDR-62-1044. CARBON ELECTRODE FUEL CELL. Interim report, Mar 63. 92p. incl illus., tables.

Unclassified Report

Experimental studies are conducted on components of a carbon electrode fuel cell system, with emphasis on problems of operation in a space environment. A 500 watt (net electrical output) fuel cell system has been operated for 25 days continuously on fully automatic control in the laboratory. The

(over)

performance is analyzed and related to the design of future flyable power systems.

1. Fuel Cells
2. Carbon
3. Electrodes

I. AFSC Project 8173, Task 817303
II. Contract AF 33(616)-7256 SA/5
III. Union Carbide Products Co., Cleveland, Ohio
IV. Aval fr OTS
V. In ASTIA collection

Aeronautical Systems Division. Dir/Aero-mechanics. Flight Accessories Lab., Wright-Patterson AFB, Ohio.
Rpt Nr ASD-TDR-62-1044. CARBON ELECTRODE FUEL CELL. Interim report, Mar 63. 92p. incl illus., tables.

Unclassified Report

Experimental studies are conducted on components of a carbon electrode fuel cell system, with emphasis on problems of operation in a space environment. A 500 watt (net electrical output) fuel cell system has been operated for 25 days continuously on fully automatic control in the laboratory. The

(over)

performance is analyzed and related to the design of future flyable power systems.

1. Fuel Cells
2. Carbon
3. Electrodes

I. AFSC Project 8173, Task 817303
II. Contract AF 33(616)-7256 SA/5
III. Union Carbide Products Co., Cleveland, Ohio
IV. Aval fr OTS
V. In ASTIA collection